Journal
International I J of Modern
M E
Engineering
ISSN: 1930-6628
www.ijme.us

INTERNATIONAL JOURNAL OF MODERN ENGINEERING

Fall / Winter 2012
Volume 13, Number 1

The Leading Journal of Engineering, Applied Science and Technology

Industrial

Electronics

Biomedical

Civil

Aerospace

Computer

Electrical

Chemical

Mechanical

ENGINEERING

THE LEADING JOURNAL OF ENGINEERING, APPLIED SCIENCE, AND TECHNOLOGY

www.ijme.us

www.iajc.org

INTERNATIONAL JOURNAL OF MODERN ENGINEERING

ABOUT IJME:

- IJME was established in 2000, and it is the first and official flagship journal of the International Association of Journal and Conferences (IAJC).
- IJME is a high-quality, independent journal steered by a distinguished board of directors and supported by an international review board representing many well-known universities, colleges, and corporations in the U.S. and abroad.
- IJME generally publishes research related to all areas of engineering, applied science, and related technology.

OTHER IAJC JOURNALS:

- The International Journal of Engineering Research and Innovation (IJERI)
  For more information visit www.ijeri.org
- The Technology Interface International Journal (TIIJ).
  For more information visit www.tiij.org

IJME SUBMISSIONS:

- Manuscripts should be sent electronically to the manuscript editor, Dr. Philip Weinsier, at philipw@bgsu.edu.

  For submission guidelines visit www.ijme.us/submissions

TO JOIN THE REVIEW BOARD:

- Contact the chair of the International Review Board, Dr. Philip Weinsier, at philipw@bgsu.edu.

  For more information visit www.ijme.us/ijme_editorial.htm

www.tiij.org

www.ijeri.org

Contact us:

Mark Rajai, Ph.D.

Editor-in-Chief
California State University-Northridge
College of Engineering and Computer Science
Room: JD 4510
Northridge, CA 91330
Office: (818) 677-5003
Email: mrajai@csun.edu

INTERNATIONAL JOURNAL OF MODERN ENGINEERING

The INTERNATIONAL JOURNAL OF MODERN ENGINEERING (IJME) is an independent, not-for-profit publication, which aims to provide the engineering community with a resource and forum for scholarly expression and reflection.

IJME is published twice annually (Fall and Spring issues) and includes peer-reviewed articles, book and software reviews, editorials, and commentary that contribute to our understanding of the issues, problems, and research associated with engineering and related fields. The journal encourages the submission of manuscripts from private, public, and academic sectors. The views expressed are those of the authors and do not necessarily reflect the opinions of IJME or its editors.

EDITORIAL OFFICE:

Mark Rajai, Ph.D.
Editor-in-Chief
Office: (818) 677-2167
Email: ijmeeditor@iajc.org
Dept. of Manufacturing Systems Engineering & Management
California State University-Northridge
18111Nordhoff Street
Northridge, CA 91330-8332

THE INTERNATIONAL JOURNAL OF MODERN ENGINEERING EDITORS

TABLE OF CONTENTS

Editor's Note: IJME Impact Factor and Indexing 3
Philip Weinsier, IJME Manuscript Editor

Electric Vehicle Energy Usage Modeling and Measurement 5
Robert Prins, Robbie Hurlbrink and Leonard Winslow, James Madison University

Piecewise n^{th} Order Adomian Polynomial Stiff Differential Equation Solver 13
Amir A. Mobasher, Alabama A&M University; Arastoo Poor Biazar, University of Alabama in Huntsville; Zhengtao Deng, Alabama A&M University

A Novel Design of a Human-Robot Finger Controller 18
Iem Heng, Andy S. Zhang and Raymond Yap, NYC College of Technology

Value of Formal Project Management to Automotive Employees 27
Muhammad Sohail Ahmed, Eastern Michigan University

Performance Improvement of MANETs with Link Lifetime 36
Merlinda Drini, Queensborough Community College/CUNY; Tarek Saadawi, City College of New York

Prediction of Chamber Pressure for a Mach 4 Supersonic Wind Tunnel 45
Z.T. Deng, Xiaoqing Qian and Dave Pett, Alabama A&M University; Dan Rodgerson, AeroLab LLC

Comparison of Time Delay Controllers for A Class of Networked Control Systems 51
Sri R. Kolla, Bowling Green State University

Performance Analysis on Multicast Feedback Control with Unsynchronized Clocks 57
Shuju Wu, Central Connecticut State University; Xiaobing Hou, Central Connecticut State University

Instructions for Authors: Manuscript Submission Guidelines and Requirements 66

EDITOR'S NOTE:
IJME IMPACT FACTOR AND INDEXING

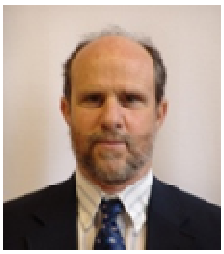

Philip Weinsier, IJME Manuscript Editor

IMPACT FACTOR AND INDEXING

Faculty publication in academic journals is a key criterion for appointment, tenure and promotion at most universities. Furthermore, many universities weigh the publications according to the quality, or impact, of the journals. But what metrics do authors use in choosing a journal? And, how do we, as fellow researchers and/or readers in search of journal articles, find what we're looking for? Yes, doing an Internet search generally produces results; but such results just as often are so watered down with what we are not looking for that we waste valuable time or get frustrated and give up. For the savvy readers, though, they join indexing or abstracting service organizations. Here, one can find articles focused into discipline-specific topics. Examples of such organizations include ChemAbstracts (chemistry) and PubMed/Medline (medicine).

The most well-known of these abstracting and indexing organizations are Google and Thomson Reuters/ISI, which cover a broader mix of disciplines. Here, readers and researchers alike are able to home in on what they need, while at the same time receive a measure of the relative quality of the source journal. Google provides information about journal articles cited by other articles; information that can give researchers a sense of value in terms of how other researchers are using the studies published there. Thomson Reuters/ISI, for its part, provides a ranking of journals by what it calls its impact factor (IF). For years, the scientific community has used this as a measure of the average number of citations to articles published in a given journal. It has also become a common practice to use IF as a means of ranking the relative importance of a journal.

The Thomson Reuters/ISI Web of Knowledge is a larger platform that includes multiple databases and tools such as the Web of Science—which also covers the Science Citation Index—and the Journal Citation Reports (JCR), which reports all related analytical information as well as impact factors. The Web of Knowledge indexes more than 11,000 science and social science journals. What you may not know is that besides ISI's impact factor, there are numerous other methods for ranking journals such as:

- Google Journal Metrics (using Google Scholar)
- Eigenfactor Search
- H-Index (available from Scopus and SCImago Journal Rank)
- Citations (available from Microsoft Academic Search)
- SCImago Journal Rank (SJR)

IJME: THE NUMBERS

The most popular ranking organization is Google Scholar Metrics (GSM), which is also available free to the public. According to GSM, the impact factor of IJME, since its first issue in the fall of 2000, is 1.63 (with no self citation), placing it among the top 100 engineering journals worldwide. It is also the #1 visited engineering journal website, according to the National Science Digital Library (NSDL), one of the world's largest libraries funded by NSF.

As noted above, impact factor of a journal is but one measure of its quality; another is indexing. While almost all journals seek indexing in indexing organizations, on rare occasions the major indexing organizations approach high-quality journals on their own to sign indexing contracts. We are proud that IJME and its sister journals, IJERI and TIIJ, have been invited to join EBSCO, one of the largest leading indexing organizations.

IAJC, the parent organization of IJME, has also taken an aggressive approach to index the journal with other major indexing organizations in order to maximize its exposure and improve its quality and impact factor. At the time of this publication, IJME is indexed by 21 major indexing organizations and under review by several more—visit our website (www.ijme.us) for a complete listing.

Editorial Review Board Members

Listed here are the members of the IAJC International Review Board, who devoted countless hours to the review of the many manuscripts that were submitted for publication. Manuscript reviews require insight into the content, technical expertise related to the subject matter, and a professional background in statistical tools and measures. Furthermore, revised manuscripts typically are returned to the same reviewers for a second review, as they already have an intimate knowledge of the work. So I would like to take this opportunity to thank all of the members of the review board.

If you are interested in becoming a member of the IAJC International Review Board, send me (Philip Weinsier, IAJC/IRB Chair, philipw@bgsu.edu) an email to that effect. Review Board members review manuscripts in their areas of expertise for all three of our IAJC journals—IJME (the International Journal of Modern Engineering), IJERI (the International Journal of Engineering Research and Innovation) and TIIJ (the Technology Interface International Journal)—as well as papers submitted to the IAJC conferences. Please watch for updates on our website (**www.IAJC.org**) and contact us anytime with comments, concerns or suggestions.

Jessica Buck	Jackson State University (MS)
Shaobiao Cai	Penn State University (PA)
Rigoberto Chinchilla	Eastern Illinois University (IL)
Raj Chowdhury	Kent State University (OH)
David Domermuth	Appalachian State University (NC)
Mehran Elahi	Elizabeth City State University NC)
Verna Fitzsimmons	Kent State University (OH)
Nitish Gupta	Bhagwan Parshuram (INDIA)
Mohsen Hamidi	North Dakota State University (ND)
Youcef Himri	Safety Engineer, Sonelgaz (ALGERIA)
Xiaobing Hou	Central Connecticut State University (CT)
Charles Hunt	Norfolk State University (VA)
Pete Hylton	Indiana University Purdue (IN)
Ghassan Ibrahim	Bloomsburg University (PA)
John Irwin	Michigan Technological University (MI)
Sudershan Jetley	Bowling Green State University (OH)
Reza Karim	North Dakota State University (ND)
Pete Klein	Ohio University (OH)
Ognjen Kuljaca	Brodarski Institute (Croatia)
Jane LeClair	Excelsior College (NY)
Guoxiang Liu	University of North Dakota (ND)
Basile Panoutsopoulous	Central Connecticut State University (CT)
Thongchai Phairoh	Virginia State University (VA)
Huyu Qu	Honeywell International, Inc.
Desire Rasolomampionona	Warsaw University of Technology (POLAND)
Sangram Redkar	Arizona State University-Poly (AZ)
Marla Rogers	Wireless Systems Engineer
Anca Sala	Baker College (MI)
Li Tan	Purdue University North Central (IN)
Phillip Waldrop	Georgia Southern University (GA)
Liangmo Wang	Nanjing University Science & Technology (CHINA)
Tom Warms	Sam Houston State University (TX)
Biao Zhang	US Corp. Research Center ABB Inc.
Chongming Zhang	Shanghai Normal University (CHINA)

ELECTRIC VEHICLE ENERGY USAGE MODELING AND MEASUREMENT

Robert Prins, Robbie Hurlbrink and Leonard Winslow, James Madison University

Abstract

Although electric vehicles show significant promise as a viable means of transportation [1], technical and societal challenges remain. One of the largest consumer concerns related to electric vehicles is their perceived lack of range. Although range estimates for particular vehicles are available, these estimates may be unreliable, especially if the vehicles will experience duty cycles that are dissimilar to standard test duty cycles. Speed, load and topography all play a significant role in the real range of an electric vehicle. Although vehicles produced by large manufacturers are well characterized by their manufacturer, highly detailed information is seldom shared. Vehicles from smaller manufacturers (such as utility vehicle manufacturers) may not be as well characterized. Fleet managers and other potential owners do not have a reliable way to estimate vehicle range along their routes prior to purchase and operation. This study explored an energy usage modeling approach that could be applied by fleet managers and other owners to help them make appropriate decisions regarding electric vehicle deployment. This paper describes an experiment in which road load calculations, vehicle efficiency and route data (route elevation and travel speed profiles along a specified route) were used to model the energy requirements of an electric utility vehicle. Road testing of an electric utility vehicle was performed along the specified route to validate model predictions. Results show that the total energy required along the route by the test vehicle was 0.50kWh, while the model prediction was 0.58kWh.

Introduction

The primary goal of this effort was to accurately model energy usage along potential routes of travel in order to predict energy usage for a vehicle that is scheduled to travel a known route. Of particular interest were the energy requirements of electric vehicles since these vehicles are the subject of "range anxiety" and because of the current sparseness of recharging facilities. Although electric vehicles that come from large manufacturers are well characterized and provide range estimate updates to their operator, the underlying model that is used to provide this information is typically proprietary. Furthermore, vehicles such as the test vehicle that do not come from large manufacturers are less well characterized so that comprehensive energy usage data is unavailable. One current approach to energy usage prediction is based on fixed duty cycles such as SAE J1711 [2] or Federal Urban Driving Schedules [3] which can be run on dynamometers. Results from such tests provide a way to compare different vehicles under identical conditions. While comparative data are valuable, the duty cycles applied during the tests may not be well correlated to the duty cycle that a particular vehicle will experience when it is deployed. The primary advantages of the approach described herein are that it accounts for vehicle road loads along the specific route that the vehicle will be deployed along, and it is based on vehicle parameters that are readily available.

The approach to energy usage modeling described here requires knowledge of driveline efficiency and the external and inertial forces that are aligned with the direction of travel. The forces aligned with the travel direction are used to predict the tractive force required; these forces depend on both route-specific and vehicle-specific parameters. The route parameters required by the model are vehicle speed and road gradient. In tests, vehicle speed and road gradient were determined using two different sources: Global Positioning System (GPS) tracking devices and the United States Geological Survey (USGS) database. The vehicle parameters required by the model were either directly measured or supplied by book values. For instance, vehicle weight was directly measured, while drag coefficient was based on a book value.

The approach was applied to model an electric utility vehicle on a route on the campus of James Madison University (JMU) in Harrisonburg, VA. Road testing along the chosen route was also performed in order to validate model results. The test vehicle was a Vantage [4] EVX1000 utility truck with a 72V x 192Ah lead acid battery pack, a Curtis controller and a High Performance Electric Vehicle Systems AC-50 three-phase electric motor. Although this system supports regenerative braking, regenerative braking was suppressed during tests to simplify modeling. During road tests, battery pack voltage and current were monitored to provide a running tally of energy usage.

Methodology

Prediction of energy usage requires a model of the vehicle and the route that the vehicle will travel. After the model was developed and a prediction obtained, the predicted energy usage was compared to the measured energy usage along the route. A measure of energy usage along the route was obtained by monitoring battery energy output while driving the route. This section describes the vehicle model, route model, energy usage prediction and energy usage measurement.

Vehicle Model

The vehicle model used in this study was based on the external and inertial forces acting on the vehicle that are aligned with the direction of travel as described by Gillespie [5]. These external forces are in equilibrium with the tractive force applied by the wheels:

$$F_T = F_R + F_D + F_G + F_A \quad (1)$$

where,

F_T = tractive force
F_R = rolling resistance force
F_D = force due to drag
F_G = force due to gravity
F_A = force due to acceleration in the direction of travel

Rolling resistance addresses forces related to contact between tire and road surfaces, drag is due to wind resistance, the force of gravity accounts for the force required to change elevation, the acceleration force accounts for the force required to change speed. Equation 1 can be expanded to show the terms associated with each force:

$$F_T = W f_r + (1/2) \rho c_d A v^2 + W \sin\theta + (W/g) a \quad (2)$$

where,

W = weight of loaded vehicle
f_r = rolling resistance coefficient
ρ = air density
c_d = drag coefficient
A = frontal area
v = air speed
θ = angle of road
g = acceleration due to gravity
a = acceleration in direction of travel

Determination of Rolling Resistance Force

The force of rolling resistance is due to the deformation of tires rolling along the road surface. Rolling resistance is affected by factors such as tire pressure, pavement characteristics and tread conditions. During road testing, tire pressure was maintained at a consistent level while variation in road surface and tread conditions were noted to be negligible. The weight of the loaded vehicle was measured using a drive-on scale at a local lumber company; the measured weight was 14,055N (3,160lb). The rolling resistance coefficient was determined from coast-down tests. In a coast-down test, the vehicle is driven at a constant speed and then allowed to "coast down" to a stop [6]. Vehicle speed is recorded at known time intervals during the coast-down period so that deceleration can be calculated. If the road is flat and the speed is relatively low, gravitational force and drag force and can be neglected and all of the deceleration can be attributed to rolling resistance. As a perfectly flat test surface was not available for this effort, coast-down tests were performed in two directions on a reasonably flat test surface in order to determine the rolling resistance coefficient. The results from each direction were used to provide a two-way average of deceleration. Using this approach, the rolling resistance coefficient was determined to be 0.014, which lies within typical values reported by Gillespie [5].

Determination of Drag Force

The force due to drag accounts for wind resistance and is dependent upon the density of air, the shape of the vehicle, the frontal area of the vehicle and the air speed of the vehicle. Air density was determined based on temperature, pressure and humidity conditions as provided by a handheld weather station at the time of testing. Drag coefficients can be directly measured in wind tunnels or determined from high-speed coast-down tests. The vehicle speed was limited to ~11.5m/s (25MPH), which was determined to be too slow to get reliable coast-down data for drag force. A book value of 0.45 associated with similarly shaped pickup trucks [5] was used for modeling purposes. The frontal area was determined by direct measurement of the vehicle to be 2.16m^2. Testing was done in calm conditions so that air speed could be well approximated by ground speed. Ground speed along the route was determined by a GPS tracker and verified by comparison to wheel speed, as shown in Figure 1.

The wheel speed shown in Figure 1 was determined by monitoring the motor speed signal from the controller while traveling the route. A combination of the motor speed with known driveline ratios and tire size results in wheel speed. Figure 1 shows that the GPS-tracker-based speed and the wheel speed compare well along the route.

Table 1. Road-Load Variables, Values and Sources

Label	Variable	Value	Unit	Source
W	weight of loaded vehicle	14055 (3160)	N (lb)	drive-on scale
f_r	rolling resistance coefficient	0.014	N/A	coast down test
r	air density	varies	kg/m^3	equation based on parameters measured at time of test
c_d	drag coefficient	0.45	N/A	book value for similar vehicle
A	frontal area	2.16	m^2	measurement of vehicle
v	air and ground speed	varies continuously	m/s	route model
q	angle of road	varies continuously	degrees	route model
g	acceleration due to gravity	9.81	m/s^2	book value
a	acceleration	varies continuously	m/s^2	route model

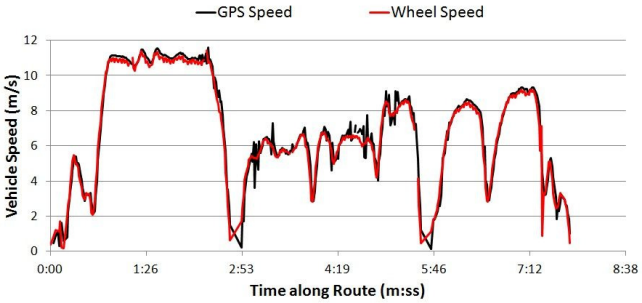

Figure 1. Comparison of GPS-Speed Measurement to Wheel-Speed Measurement

Determination of Gravitational Force

The force due to gravity accounts for changes in elevation and is dependent upon vehicle weight and change in elevation. The weight of the loaded vehicle was measured as described above; the road angle was based on sequential GPS measurements of position and elevation.

Determination of Force Due to Acceleration in the Direction of Travel

The force due to acceleration in the direction of travel accounts for changes in vehicle speed and is dependent on vehicle mass and change in travel speed. The weight of the loaded vehicle was measured as described above; changes in travel speed were based on sequential GPS-tracker-based speed measurements. Table 1 indicates the values of the variables in Equation (2).

Table 1 shows that a book value was relied upon for one variable (drag coefficient) while values for the other variables were measured. Some of the variables remained constant during testing while vehicle speed, road angle and acceleration varied continuously. The continuous variables were measured at a frequency of 1Hz which is the collection rate of the GPS trackers used in this study.

Route Model

The route model consists of the elevation profile of the path of travel as well as an expected speed profile of the vehicle along the path. The elevation profile of the JMU route used in the energy calculations came from two sources: GPS trackers and the USGS database. The source of the speed profile was again the GPS trackers.

Determination of Elevation Profile

For this study, GPS trackers and USGS data were the sources of elevation data. In order to determine the elevation profile of the path, four different methods were used which were then compared. The four methods were:

- Raw elevation data from Trimble Geo XH GPS tracker
- Raw elevation data from Garmin eTrex Vista GPS tracker
- Post-processed (differentially corrected) elevation data from the Trimble Geo XH GPS tracker
- Elevation data from USGS database

The GPS-tracker-based elevation data were collected by traveling the route with two active GPS trackers, which provided elevation data at 1Hz intervals. The GPS trackers used to conduct this study were a Trimble Geo XH and a Garmin eTrex Vista. The Trimble Geo XH is survey grade, while the Garmin eTrex Vista is recreational grade. The Garmin eTrex Vista produces lower accuracy position data but has a built-in barometric pressure sensor which allows relative elevation readings to be taken without relying on satellites.

The Trimble GPS data were also post-processed using differential correction to provide a third set of elevation data. Differential correction methods remove anomalies due to issues in the interaction between satellites and GPS receivers (typically due to atmospheric conditions) based on readings from nearby GPS receivers that are in a fixed location [7]. Because the Trimble tracker is survey grade, differentially corrected route data from the Trimble tracker is considered to be the most reliable source of route model data used in this study.

The fourth set of elevation data was sourced from a USGS database. The USGS has image-based digital elevation models (DEMs) published online that have a resolution of 10 meters. This means that in an image, every 10-meter by 10-meter pixel is assigned an elevation value [8]. For the case described here, the route was entered into ArcMap (geospatial analysis software) and the elevation data for points along the route were extracted from the appropriate DEM.

Elevation data from each of the four methods were processed to provide elevation relative to a start point. Figure 2 shows the relative elevation profiles resulting from the application of the four methods discussed above**.**

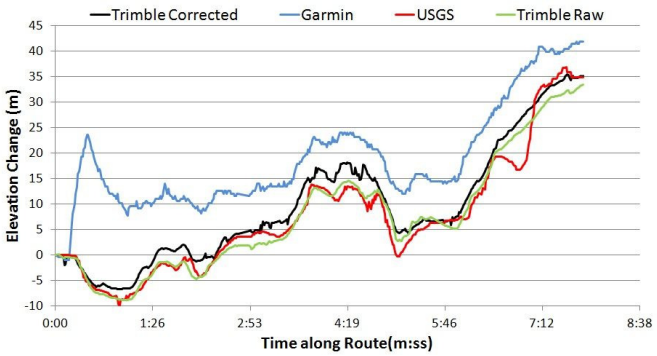

Figure 2. Elevation Profiles from Four Methods

Figure 2 shows that the Trimble raw, Trimble corrected and USGS elevation data are similar in value and shape. The Garmin elevation data display a ~25m jump near the beginning of the run, but then follow a similar shape to the others. One potential problem with relying on USGS data is observed as a dip near the 7:00 minute mark. The USGS DEM has 10-meter resolution which is not small enough to resolve a bridge that was part of the route. In this case, the USGS DEM provided elevation data for the ravine that the bridge crosses.

Determination of Speed Profile

The speed profile of the route was determined by traveling the route at typical speeds with an active GPS tracker. The GPS trackers provided position data at 1Hz intervals, vehicle speed was calculated from the difference in position between sequential position points. The speed profile for the route is shown in Figure 1. The speed profile used in this study is based on differentially corrected route data from the Trimble tracker.

Energy Usage Prediction

The goal of this effort was to predict the amount of energy that must be supplied by the battery pack. The amount of energy required from the battery pack is a function of the amount of energy required at the wheel and vehicle drivetrain efficiency. Energy requirements at the wheel are based on tractive force predictions while drivetrain efficiency is based on RPM-specific values published by the motor manufacturer.

Predictions of energy usage at the wheel are based on the tractive force model as calculated in Equation (2). Since some of the tractive force parameters (speed, road angle and acceleration) change with each successive time interval, the energy calculation addresses a single interval. In order to use tractive force to determine energy usage for a given interval, the distance across which the tractive force is applied during the interval must be known, as shown in Equation (3):

$$\Delta E_{wheel,i} = F_{T,i}\Delta d_i \tag{3}$$

where,

$\Delta E_{wheel,i}$ = energy usage at the wheel to travel the interval distance Δd_i
$F_{T,i}$ = tractive force during interval i
Δd_i = distance traveled during interval i

Equation (3) can be rewritten in terms of speed, as shown in Equation (4):

$$\Delta E_{wheel,i} = F_{T,i} v_i \Delta t_i \tag{4}$$

where,

$\Delta E_{wheel,i}$ = energy usage at the wheel to travel for the interval time Δt_i

$F_{T,i}$ = tractive force during interval i

v_i = average speed along path during time interval i

Δt_i = length of time interval i

Equation (5) is an expansion of Equation (4) and shows the tractive force terms from Equation (2). In Equation (5), terms that are updated for each time interval are given the interval subscript i.

$$\Delta E_{wheel\ i} = [W f_r + (1/2) \rho c_d A v_i^2 + W \sin(\theta_i) + (W/g)(v_i - v_{i-1})/\Delta t_i] v_i \Delta t_i \quad (5)$$

The amount of energy required from the battery pack depends on the energy required at the wheel as well as vehicle drivetrain efficiency. In order to determine the energy required from the battery pack, an efficiency factor based on published data from the motor manufacturer that correlates efficiency to motor RPM at peak load was applied. Motor RPM was determined from vehicle speed and known drive ratios; motor RPM is continuously variable so that drivetrain efficiency must be updated for each time interval, as shown in Equation (6):

$$\Delta E_{battery\ i} \times \eta_i = \Delta E_{wheel\ i} \quad (6)$$

where,

$\Delta E_{battery\ i}$ = energy provided from battery pack during interval i

η = drive efficiency during interval i

$\Delta E_{wheel\ i}$ = energy required at wheel during interval i

This method results in a prediction of the incremental energy provided by the battery pack for each time interval; the total energy provided by the battery pack along a particular route is predicted by the summation of the $\Delta E_{battery\ i}$ values from all of the intervals.

Road Tests

In order to validate the energy usage predictions of the model, vehicle energy usage was monitored (measured at the battery pack) while traveling along the route. This was done by logging battery pack voltage and current at 1Hz time intervals along the route. The amount of energy removed from the battery during each time interval is the product of the battery pack voltage, current and time interval, as shown in Equation 7.

$$E_{measured,i} = V_{measured,i} I_{measured,i} \Delta t_i \quad (7)$$

where,

$E_{measured,i}$ = energy removed from battery pack during interval i

$V_{measured,i}$ = battery pack voltage during interval i

$I_{measured,i}$ = battery pack current during interval i

Δt_i = length of time of interval i

This approach results in a measurement of the incremental energy provided by the battery pack for each time interval; the total energy provided by the battery pack along a particular route is the summation of the $\Delta E_{measured\ i}$ values from all of the intervals.

Results

The results of this effort include the raw speed and elevation data used to construct the route model, battery energy usage predictions based on tractive force prediction, and measured energy usage from road testing.

Figure 3 shows a typical set of elevation and speed profile data for a particular route along with the corresponding energy usage prediction (based on differentially corrected Trimble tracker elevation data). Energy usage is graphed as cumulative energy usage so that the final point on the graph represents the total energy prediction for the route. The dependency of energy usage predictions on route elevation and speed profiles can be seen in Figure 3. For instance, note that near the 2:50 minute mark, the vehicle speed is near zero and there is little elevation change which suggests that little energy input is required. The cumulative energy graph is nearly flat at this point, which indicates little predicted energy usage at that time. On the other hand, note that near the 7:00 minute mark, the road increases in elevation while speed is maintained at a constant ~9m/s (20MPH), which suggests that significant energy input is required. The cumulative energy graph has a steep slope at this time which indicates high predicted energy usage.

Recall that four different methods were used to determine elevation in the route model. Each method results in a different route elevation profile, as shown in Figure 2. The elevation profile variation affects energy usage predictions, as shown in Figure 4.

The energy values in Figure 4 are graphed as cumulative energy usage so that the final points on the graph represent the total energy predictions for the route. Figure 4 also includes the measured energy from road testing for comparison. It can be seen that the lines representing the four energy usage predictions are similar in shape and value to the line that represents measured energy usage. The prediction

with the worst agreement is the one that relies on the Garmin GPS tracker for elevation profile. All predictions over-predicted the energy usage required for the entire route, although not at all points along the route. Table 2 summarizes the predictions of energy usage along the route from the four methods, as well as their variation from the measured energy usage.

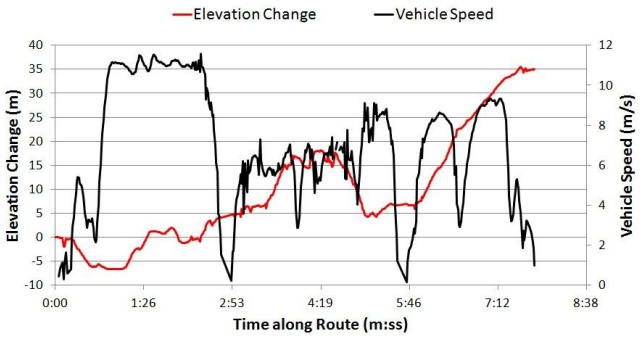

(a) Elevation and Speed Profiles of Route

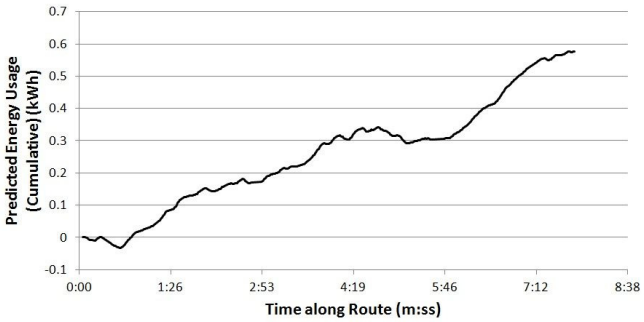

(b) Prediction of Energy Usage along Route

Figure 3. Energy Usage Prediction along Route and the Underlying Elevation and Speed Profiles

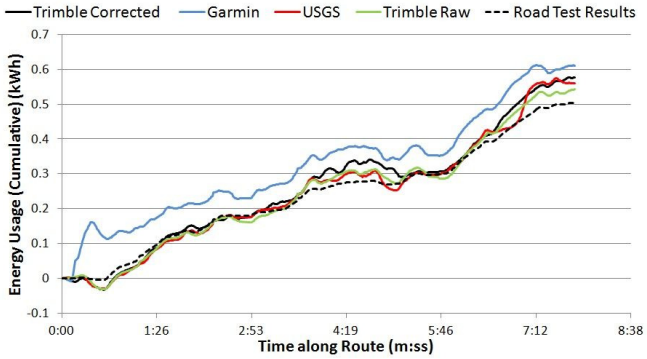

Figure 4. Energy Usage Prediction and Road Test Results

Table 2. Total Energy to Travel Route

Data Source	Total Energy to Travel Route (kWh)	% Variation from Road Test
Trimble (corrected)	0.577	+ 14.8
Garmin	0.611	+ 21.4
USGS	0.560	+ 11.3
Trimble (raw)	0.542	+ 7.9
Road Test	0.503	-

Table 2 shows that variation between energy usage measured during the road test and energy usage predictions varies from 8% to 22%. The major contributor to variation is the source of the elevation model used to predict energy usage. The Garmin tracker, which reported an elevation profile dissimilar to the Trimble tracker and the USGS model, is the source of the elevation model that varies by nearly 22% from the road test values. Although the raw Trimble tracker data show the lowest variation (8%) relative to road test data, the differentially corrected output from the Trimble tracker (Trimble corrected) is likely a better source of elevation data.

Figure 4 demonstrates that the model over predicts the measured energy usage. At the end of the route, the total energy usage predicted by the most reliable model (Trimble corrected) was 0.58kWh in comparison to a measurement of 0.50kWh; this represents a variation of ~15%.

Discussion

The selected route included ~20m total descent and ~55m total ascent, which is representative of typical routes traveled on the campus of JMU. It can be seen from Figure 4 that energy usage predictions and measured energy usage exhibit similar form although differences do exist. If the variation between predicted and measured energy usage is characterized as ~14% (the average variation), different conclusions could reasonably be drawn. For some purposes, 14% variation may be considered acceptable in which case an avenue for future work would be to further test and validate the current approach on other routes and with other vehicles to gain confidence that the approach is universally reliable. For other purposes, 14% variation may be considered unacceptable in which case further refinement of the model would be in order.

Efforts directed at model refinement could begin with a comparison of Figures 4 and 3a which suggest that while in

general the energy usage models tend to over predict energy usage, this is especially noticeable from 3:45 - 4:40 minutes (minimal elevation change combined with varied speeds) and from 6:20 - 7:47 minutes (extended deceleration while making an ascent). While such observations provide some insight, it would be ill-advised to make adjustments to the model in order to better match the measured energy usage without understanding the interactions between vehicle model parameters and route model parameters. This suggests that an avenue for further work would be to continue to work with the test vehicle under controlled conditions of slope, speed and payload in order to scrutinize the model.

The main strength of using a GPS-tracker approach to developing a route model is that elevation measurements along the route are made directly. This means that the model does not depend on DEMs from the USGS which may not resolve critical route features. The main weakness of using the GPS-tracker approach is that the route must be driven while collecting tracker data. For relatively long routes, the effect of route features that are not properly resolved by DEMs may not be significant, in which case predictions of total energy usage should be reasonably close to actual energy requirements. This suggests that another avenue for further work would be development and validation of USGS-based route models with the intent of developing a reliable prediction of energy usage that does not require physical presence along the route.

Conclusions

An energy usage model that accounts for the route of an electric vehicle was applied to a small, electric-powered utility vehicle traveling a route with significant elevation variation. A model of tractive force as well as elevation and speed profiles of the route provided energy usage predictions along the route. The predictions were validated by a road test in which the route was traveled while energy usage from the battery pack was monitored. At the end of the route, the total predicted energy usage varied from the measured energy usage by ~15%.

Paths for future work include continued testing of the current model along other routes and with other vehicles, refinement of the model, and further development of USGS-based route models.

Acknowledgements

The authors thank Kelly Sites of James Madison University Facilities Management - Transportation for use of the electric vehicle and the Alternative Fuels Vehicle Laboratory (AFV) for providing work space; Dr. Carole Nash, Assistant Professor in the Department of Integrated Science and Technology at James Madison University, for sharing her expertise in geospatial sensing and modeling; and Ed Thurnau, electrical engineer with GE Intelligent Platforms, for sharing his expertise in signal conditioning and processing.

This research was supported in part by the 'Shenandoah Valley as a National Demonstration Project Achieving 25 Percent Renewable Energy by the Year 2025' under U.S. Department of Energy Grant #DE-EE0003100. The views expressed are those of the authors and do not necessarily reflect those of the sponsors.

References

[1] Larminie, James, and Lowry, John (2012). *Electric Vehicle Technology Explained*. (2nd ed.). West Sussex, United Kingdom: John Wiley and Sons, Ltd.

[2] Society of Automotive Engineers Surface Vehicle Recommended Practice, *SAE J1711 – Recommended Practice for Measuring Fuel Economy of Hybrid-Electric Vehicles*, Society of Automotive Engineers Publication, Issued March 1999.

[3] Testing and Measuring Emissions. (2011). Retrieved March 3, 2011, from http://www.epa.gov/nvfel/testing/dynamometer.htm

[4] Vantage Electric Vehicles. (n.d.). Retrieved October 14, 2012, from http://www.vantagevehicle.co.

[5] Gillespie, T. D. (1992). *Fundamentals of Vehicle Dynamics*. Warrendale, PA: Society of Automotive Engineers.

[6] White, R. & Korst, H. (1972). The Determination of Vehicle Drag Contributions from Coast-Down Tests. *SAE Technical Paper 720099*.

[7] Chivers, Morag. (2003). Differential GPS Explained. Retrieved September 25, 2011 from http://www.esri.com/news/arcuser/0103/differential1of2.htm

[8] Blackwell, P.R., & Wells, G. (1999). DEM Resolution and Improved Surface Representation *Esri International User Conference*. San Diego, CA.

Biographies

ROBERT PRINS is an Assistant Professor of Engineering at James Madison University in Harrisonburg, VA. He earned his B.S. degree (Mechanical Engineering, 1993) from Michigan Tech, M.S. (Mechanical Engineering, 1996) from The University of Virginia, and Ph.D. (Mechanical Engineering, 2005) from Virginia Tech. Dr. Prins' interests are development and testing of electric vehicles as well as

project-based engineering education. Dr. Prins may be reached at prinsrj@jmu.edu

ROBBIE HURLBRINK is a junior in the engineering program at James Madison University. Mr. Hurlbrink is interested in electric propulsion and intends to pursue graduate work in mechanical engineering. Mr. Hurlbrink can be reached at hurlbrrw@gmail.com

LEONARD WINSLOW is a recent graduate of James Madison University where he earned his B.S. degree (Geographic Science, 2012). Mr. Winslow can be reached at winslolf@dukes.jmu.edu

PIECEWISE NTH ORDER ADOMIAN POLYNOMIAL STIFF DIFFERENTIAL EQUATION SOLVER

Amir A. Mobasher, Alabama A&M University; Arastoo Poor Biazar, University of Alabama in Huntsville;
Zhengtao Deng, Alabama A&M University

Abstract

A piecewise nth order Adomian polynomial solver for initial value differential equations capable of solving highly stiff problems is presented here. This powerful technique which employs Adomian polynomials is shown to obtain nearly exact solutions for the benchmark cases studied. The high accuracies at reduced computational cost is obtained by varying the integration time and the order of the polynomials. The time step in the current solver is on the order of 10 to 30 times larger than those used by other standard techniques such as fourth-order Runge-Kutta. It was found that the piecewise continuous polynomials increases the time-step requirements as the order of polynomials increases. The current algorithm utilizes high-order Adomian polynomials to advance the solution within the stiff region with relatively large time steps. The algorithm was validated against a first-order system with and without large stiffness and a second-order, non-linear flame propagation. Results were compared with exact solutions using the Lambert W-function and fourth-order Runge-Kutta methods. Good agreement was obtained for the flame-propagation prediction. It was found that while obtaining relatively large time steps, accuracies on the order of 10^{-15} were obtained.

Introduction

A number of applications in science and engineering demand solutions of stiff differential equations. Stiffness is generally defined as the solution space that contains (very) large gradients. Such examples include problems in chemical kinetics, atmospheric sciences, biochemistry, electronics and automatic control systems, to name a few. In flame propagation, concentration of chemical species can decay at different rates; thus, a kinetic-reaction differential equation describing the species concentration usually has a broad range of time constants. The solution to this system of ordinary differential equations is dominated by the species that have the shortest time constants [1]. The stiffness of the problem requires that the error introduced during the computation be damped by the algorithm. The step size has to be extremely small. Larger step sizes may cause numerical accuracy and stability problems. In general, stiff problems may be solved by some differential equation solvers if the computational cost is not an issue. For large-scale engineering problems involving flame propagation [2], the solution of stiff problems becomes a matter of efficiency.

Currently, many elaborate schemes for the solution of stiff differential equations exist [3]. Perhaps the most widely accepted technique is the Gear [4] method. Other methods such as the Sin-Cos-Taylor-Like [5] method and the Multi-step Runge-Kutta method [6] have been used by other authors. Commercial software programs such as Matlab [2] use modifications to Runge-Kutta to address stiffness. Until recently, one overlooked approach is the method proposed by Adomian for the solution of non-linear and linear ordinary differential equations [7-11]. This approach was also employed to address a classic fluid-dynamics problem with high accuracy [12], [13]. A number of other physical problems have been recently solved by this methodology [14-16]. The Adomian Decomposition Method requires term-by-term differentiation and integration of the basic differential equations. Although this approach produces highly accurate solutions to non-linear differential equations, it has some drawbacks: 1) It requires laborious work by the user, due to successive differentiation and integration of the resulting Adomian Polynomials; 2) For stiff problems, the solution can only be partially convergent [12]; and 3) the approach is problem-specific [7].

The goal of this current study was to formulate an algorithm that would address the aforementioned issues. The authors refer to the current formulation as "Piecewise nth order Adomian Polynomial Differential Equation Solver" or, in short, Adomian Differential Equation Solver (ADES). The word "piecewise" means to break up the domain into sub-domains in order to obtain a series solution in each sub-domain utilizing Adomian polynomials of a specified order. Here, a new methodology for the solution of stiff differential equations will be presented. It will be shown that the current technique will obtain nearly exact solutions while maintaining large Δt's (as much as 30 times larger than the standard fourth-order Runge-Kutta technique). The current technique was validated against three test examples with a highly stiff nature and it was found that the solution obtained via this technique was highly accurate while the time required to obtain the solution was minimal.

Methodology

Consider the differential equation system of the form

$$\dot{u} = f(t,u) \tag{1}$$

where $f(t,u)$ is any linear or non-linear function of order n. Adomian polynomials are employed to construct the solution space for u as:

$$\begin{aligned} u &= u_0 + L^{-1}(f) \\ L^{-1} &= \int_{t1}^{t} (\cdot)dt \end{aligned} \tag{2}$$

where L^{-1} is the integration operator. The solution of the system of differential equations in Equation (1) is then expressed as:

$$u = \begin{bmatrix} u_1 \\ u_2 \\ \dots \\ u_n \end{bmatrix} = \begin{bmatrix} \sum_{i=0}^{\infty} u_{1,i} \\ \sum_{i=0}^{\infty} u_{2,i} \\ \dots \\ \sum_{i=0}^{\infty} u_{n,i} \end{bmatrix} \tag{3}$$

where $u_{i,0} = u_i\ (0)$ is the prescribed initial conditions and $u_{i,j+1} = L^{-1}(A_{i,j}(u_{i,0}, u_{i,1}, \dots, u_{i,j})$ is the $j+1^{th}$ term of the i^{th} equation and $A_{i,j}$ is the Adomian Polynomial [7].

This method, proposed by Adomian, integrates the Adomian polynomials from $t = 0$ to $t = \infty$. For stiff problems, the solution is valid only up to a certain time after which the solution begins to diverge. In practical terms, polynomials of order 100 and higher are needed to approximate the solution in the high gradient region. Obviously, this is beyond computational means and efficiency. To address this situation, the current technique divides the domain to m sub-domains—hereafter referred to as Piecewise Adomian Polynomials. The solution advances by inserting the end-conditions at each sub-domain as initial conditions for the subsequent sub-domain. The solution within each sub-domain is approximated by lower-order Adomian polynomials (typically orders of 2 to 20).

Results and Discussions

In this section, three well-defined problems that are highly stiff and have been referenced by other authors in benchmarking stiff differential equations will be examined.

Example 1: First-Order Linear Systems

This example considers a first-order stiff system with no non-linear terms. This problem has been examined by Ahmad [5] and is referenced here again in Equation (4).

$$\begin{cases} \dot{u} = -100u + 99v \\ \dot{v} = -v \end{cases} \quad \text{with} \quad \begin{pmatrix} u_0 \\ v_0 \end{pmatrix} = \begin{pmatrix} 0 \\ 1 \end{pmatrix} \tag{4}$$

Adomian polynomials take the form of

$$\begin{cases} r_0 = u_0 = 0 \\ s_0 = v_0 = 1 \end{cases} \tag{5}$$

Subsequent values of r and s are presented in Equation (6),

$$\begin{cases} r_{i+1} = -100\,r_i + 99\,s_i \\ s_{i+1} = -s_i \end{cases} \tag{6}$$

with the solution u, v presented in Equation (7).

$$\begin{cases} u = \sum_{n=0}^{\infty} r_n \dfrac{t^n}{n!} \\ v = \sum_{n=0}^{\infty} s_n \dfrac{t^n}{n!} \end{cases} \tag{7}$$

Table 1 compares the relative error for three different techniques of fourth-order Runge-Kutta (RK4), Sin-Cos-Taylor-Like (SCTL) solutions and the current formulation of the Adomian Differential Equation Solver (ADES). As shown in Table 1, RK4 generates relative errors in the range of 10^{-3} to 10^{-4} within the stiff region and SCTL generates errors of 10^{-5} to 10^{-12}, while ADES generates errors of order 10^{-12}. It must be noted that the current technique uses a Δt of 0.3, which is 30 times higher than those of RK4 and SCTL.

Table 1. Comparison of Relative Error for Three Techniques

Time(s)	Exact	RK4	SCTL	ADES
0	0	0	0	0
0.1	0.90479201811	10^{-3}	10^{-5}	10^{-12}
0.2	0.81873075102	10^{-4}	10^{-9}	10^{-12}
0.3	0.74081822068	10^{-6}	10^{-12}	10^{-12}
0.4	0.67032004604	10^{-5}	10^{-12}	10^{-12}
0.5	0.60653065971	10^{-6}	10^{-12}	10^{-12}
0.6	0.54881163609	10^{-8}	10^{-12}	10^{-12}
0.7	0.49658530379	10^{-8}	10^{-12}	10^{-12}
0.8	0.44932896412	10^{-9}	10^{-12}	10^{-12}
0.9	0.40656965974	10^{-10}	10^{-12}	10^{-12}
1.0	0.36787944117	10^{-11}	10^{-12}	10^{-12}

Example 2: First-Order Systems with large Stiffness

This example also considers a linear problem, though with large stiff regions. The ordinary differential equation (ODE) system can be described as

$$\begin{cases} \dot{u} = 998u + 1998v \\ \dot{v} = -999u - 1999v \end{cases} \tag{8}$$

To obtain the ADES solution, the initial conditions were set equal to vectors r_0 and s_0.

$$\begin{cases} r_0 = u_0 \\ s_0 = v_0 \end{cases} \tag{9}$$

Since all coefficients of r can be factored out, the general expression for r and s, as in Equation (10), can be written as:

$$\begin{cases} r_{i+1} = 999r_i + 1998s_i \\ s_{i+1} = -999r_i - 1999s_i \end{cases} \tag{10}$$

And the solution u, v is given by Equation (11).

$$\begin{cases} u = \sum_{n=0}^{\infty} r_n \frac{t^n}{n!} \\ v = \sum_{n=0}^{\infty} s_n \frac{t^n}{n!} \end{cases} \tag{11}$$

Table 2 compares the relative errors between RK4 and ADES. The relative error generated by RK4 within the stiff region is in the range of 10^{-3} to 10^{-5}, while the current method generates errors of order less than 10^{-15} in all the regions.

Example 3: Flame Propagation

The final example in this section considers the problem of "Flame Propagation", which is also solved by the Matlab differential equation solver RK4. The problem is described here again for reference in Equation (12)

$$\begin{cases} \dot{u} = v - uv \\ \dot{v} = 2v(u - v) \end{cases} \quad \text{with} \quad \begin{pmatrix} u_0 \\ v_0 \end{pmatrix} = \begin{pmatrix} \delta \\ \delta^2 \end{pmatrix} \tag{12}$$

where $\delta = 0.001$.

The exact analytical solution to the flame model is given by

$$v(t) = \frac{1}{1 + W(a\, e^{a-t})} \tag{13}$$

where $a = \frac{1}{\delta} - 1$ and the function $W(z)$ is the Lambert W function.

Table 2. Comparison of Relative Error Between RK4 and ADES

Time (s)	Exact	RK4	ADES
0	0	0	0
0.001	1.63012155849531	10^{-3}	$< 10^{-15}$
0.002	1.86066871409805	10^{-3}	$< 10^{-15}$
0.003	1.94422192263888	10^{-3}	$< 10^{-15}$
0.004	1.97370033979925	10^{-4}	$< 10^{-15}$
0.005	1.98328701138628	10^{-4}	$< 10^{-15}$
0.006	1.98555717593120	10^{-4}	$< 10^{-15}$
0.007	1.98513700390092	10^{-5}	10^{-14}
0.008	1.98372836704622	10^{-5}	10^{-14}
0.009	1.98195734774168	10^{-5}	10^{-14}
0.010	1.98005426756857	10^{-6}	10^{-14}
0.020	1.96039734455236	10^{-10}	10^{-14}
0.030	1.94089106709692	10^{-14}	10^{-14}
0.040	1.92350141829273	$< 10^{-15}$	10^{-14}
0.050	1.90436225939701	$< 10^{-15}$	10^{-14}
0.060	1.88541353831420	$< 10^{-15}$	10^{-14}
0.070	1.86665336015640	$< 10^{-15}$	10^{-14}
0.080	1.848079848890170	10^{-14}	10^{-14}
0.090	1.82969114714890	10^{-14}	10^{-14}

Unlike cases 1 and 2, this example involves second-order non-linear terms. The construction of Adomian Polynomials for this problem is shown in Equations 14-17.

$$\begin{cases} r_0 = u_0 \\ s_0 = v_0 \end{cases} \tag{14}$$

$$\begin{cases} r_1 = s_0 - r_0 s_0 \\ s_1 = 2s_0(r_0 - s_0) \end{cases} \tag{15}$$

$$\begin{cases} r_2 = s_1 - r_0 s_1 - r_1 s_0 \\ s_2 = 2s_0(r_1 - s_1) + 2s_1(r_0 - s_0) \end{cases} \tag{16}$$

$$\begin{cases} r_3 = s_2 - r_0 s_2 - r_1 s_1 - r_2 s_0 \\ s_3 = 2s_0(r_2 - s_2) + 2s_1(r_1 - s_1) + 2s_2(r_0 - s_0) \end{cases} \tag{17}$$

And the general form of the above equations is represented in Equation (18)

$$\begin{cases} r_{i+1} = s_i - \sum_{j=0}^{i} r_j s_{i-j} \\ s_{i+1} = 2\sum_{j=0}^{i} s_j \left(r_{i-j} - s_{i-j}\right) \end{cases} \tag{18}$$

with the solution shown in Equation (19).

$$\begin{cases} u = \sum_{n=0}^{\infty} r_n \frac{t^n}{n!} \\ v = \sum_{n=0}^{\infty} s_n \frac{t^n}{n!} \end{cases} \tag{19}$$

Figure 1 depicts the solution for this problem with h=1.5. It is shown that at t =1000, the solution undergoes a very steep gradient. Table 3 compares the solution of the flame-propagation problem with three different methods: the Piecewise Adomian (PAP) solver, the exact solution obtained by Maple software with Lambert W-function and fourth-order Runge-Kutta method. The solution time domain listed in Table 3 is from 1000 to 1018 seconds, where the stiff region exists in this time domain. For n=5, it can be seen that the relative error is within acceptable computational limits and the solution quickly converges to a nearly exact solution with the Lambert W-function.

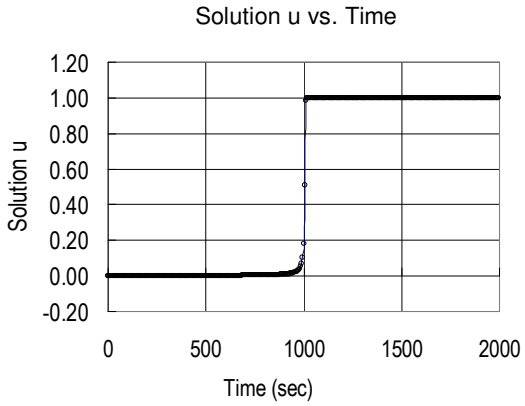

Figure 1. The Solution for the Flame-Propagation Problem with h=1.5

Conclusions

In this paper, a robust, accurate new technique was presented for the solution of stiff differential equations. The algorithm is based on the Adomian polynomials. It was shown that Δt's as much as 30 times higher than those of standard techniques of fourth-order Runge-Kutta can be used to obtain nearly exact solutions to highly stiff differential equations. One characteristic of the current algorithm is this ability to vary the order of polynomial to be used to increase the accuracy.

Table 3. Comparison of Relative Errors for Different Orders of Adomian Polynomials

Time (sec)	Exact With L-W Function	PAP (n=5)	RK4
1000	0.1840	0.1839	0.1845
1001	0.2164	0.2156	0.2164
1002	0.2592	0.2580	0.2592
1003	0.3181	0.3163	0.3180
1004	0.3999	0.3976	0.3997
1005	0.5118	0.5116	0.5115
1006	0.6519	0.6520	0.6515
1007	0.7945	0.7986	0.7940
1008	0.9006	0.9057	0.9001
1009	0.9583	0.9615	0.9579
1010	0.9838	0.9842	0.9834
1011	0.9940	0.9945	0.9937
1012	0.9978	0.9979	0.9976
1013	0.9992	0.9992	0.9991
1014	0.9997	0.9997	0.9997
1015	0.9998	0.9998	0.9999
1016	0.9999	0.9999	1.0000
1017	0.9999	0.9999	1.0000
1018	0.9999	0.9999	1.0000

References

[1] Kuo, K. K., (1986). *Principles of Combustion*. John Wiley.

[2] Moler, C. (n.d.). Stiff Differential Equations, http://www.mathworks.com/company/newsletters/articles/stiff-differential-equations.htm

[3] Biography for Stiff Differential Equations. (2003). Retrieved from http://math.fullerton.edu/mathews/n2003/stiffde/StiffDEsBib/Links/StiffDEsBib_lnk_3.htm

[4] Gear, C. W., & Petzold, L. R. (1984), ODE systems for the solution of differential algebraic systems, *SIAM Journal on Numerical Analysis*, *21*, 716-728.

[5] Ahmad, R., & Yaacob, N. (2005). Sin-Cos-Taylor-Like Method for Solving Stiff Differential Equation. *Journal of Fundamental Sciences, 1*, 34-43.
[6] Chapra, S. C., & Canale, R. P., (2010). *Numerical Methods for Engineers*. (6th ed.). McGraw Hill.
[7] Adomian, G. (1989). *Nonlinear stochastic Systems Theory and Applications to Physics*. Kluwer Academic.
[8] Adomian, G. (1983). *Stochastic systems*. Academic Press, London.
[9] Adomian, G., (1984). A new approach to non-linear partial differential equations, *Journal of Mathematical Analysis and Apolications, 102*, 420-434.
[10] Adomian, G. (1991). A Review of the decomposition method and some recent results for nonlinear equations, *Computers & Mathematics with Applications*, *21*, 101-127.
[11] Adomian, G. (1994). *Solving Frontier Problems of Physics: The decomposition Method*. Kulvar Academic, Boston.
[12] Mobasher, A., Oviedo, R. R., & Vu, B. (2001). *Application of Method of Decomposition to Classical Fluid Dynamics Problems*. Fifth Mississippi State Conference on Differential Equations & Computational Simulations. Starkville, MS.
[13] Wang, L. (2004). A new algorithm for solving classical Blasius equation, *Applied Mathematics and Computation*, *157*, 1-9.
[14] Babolian, E., Biazar, J., & Vahidi, A. R. (2004). A new computational method for Laplace transforms by decomposition method. *Applied Mathematics and Computation*, *150*, 841-846.
[15] Dehghan, M. (2004). Application of Adomian Decomposition Method for two dimensional parabolic equation subject to non-standard boundary specifications, *Applied Mathematics and Computation*, *157*, 549-560.
[16] Luo, X., Wu, Q. & Zhang, B. (2006). Revisit on Partial Solutions in the Adomian Decomposition Method: Solving Heat and Wave Equations, *Journal of Math. Analysis and Applications*, *321*, 353-363.

Biographies

AMIR A. MOBASHER is an Associate Professor of Mechanical Engineering at Alabama A&M University. Dr. Mobasher may be reached at amir.mobasher@aamu.edu

ARASTOO POOR BIAZAR is a senior research scientist of the Department of Atmospheric Sciences at University of Alabama in Huntsville. Dr. Biazar may be reached at biazar@nsstc.uah.edu

ZHENGTAO DENG is a professor of Mechanical Engineering at Alabama A&M University. Dr. Deng may be reached at zhengtao.deng@aamu.edu

A NOVEL DESIGN OF A HUMAN-ROBOT FINGER CONTROLLER

Iem Heng, Andy S. Zhang and Raymond Yap, NYC College of Technology

Abstract

Over the years, robots have been used in many areas of our lives. Robots are used for assistance at home, office, hospital, industrial plant, educational institution and waste disposal facility, among other places. Many of these working robots are either self-guided without human interference (autonomous) or human-operated with a remote controller (tele-operated). Many of these robots do not have dual operational modes that allow effective human-robot interactions. The objective of this study was to provide a unique and novel perspective for designing and building a human-robot finger controller that has dual operational modes for controlling the robot. The finger controller is a custom-made controller that is capable of controlling the robot using only two fingers on the left hand and two fingers on the right hand. Commands are communicated wirelessly to control a robot through an Arduino microcontroller and an XBee shield.

In this paper, the authors present three applications of robots controlled by the custom-made finger controller with an emphasis on the Finger-Controller's wireless communication from the transmitter to a receiver and vice versa. The three robotic applications are: Flexible Robot, Line-Following Robot and Solar Rechargeable Robot.

Introduction

Robots have evolved over the years to help people perform repetitive and dangerous tasks, which humans prefer not to do or are unable to do due to size limitations. For instance, robots have provided assistance in performing under extreme conditions and in dangerous environments such as the deep sea and in outer space. However, these robots do not collaborate with humans. In the proceedings of the 2009 4th ACM/IEEE International Conference on Human Robot Interaction, Astride Weiss stated that "effective collaboration between robots and humans is not only a question of interface design and usability, but also of user experience and social acceptance" [1]. This shows that humans are fine with the idea of working with a humanoid robot, as long as there is a clear distinction between the human and the robot in terms of tasks and working procedures.

Many human-robot interactions are done in either tele-operated or autonomous mode. In the tele-operated mode, many robots are either controlled by joysticks, keyboards, virtual GUI (graphical user interface) screens, through voice recognition or Microsoft Kinect motion-capture systems. Unlike these commonly used controllers, the finger controller is a custom-made human-robot controller that is capable of controlling many different robots. It is performed by two fingers on the left hand and two fingers on the right hand. It offers the flexibility of switching from tele-operated to autonomous mode or vice versa. Thus, the finger controller provides a unique and novel design of human-robot interactions that will help to enhance the collaboration between human and robot.

Sensors and the Finger Controller

The human hand has five fingers. The names of the five fingers are defined in Figure 1.

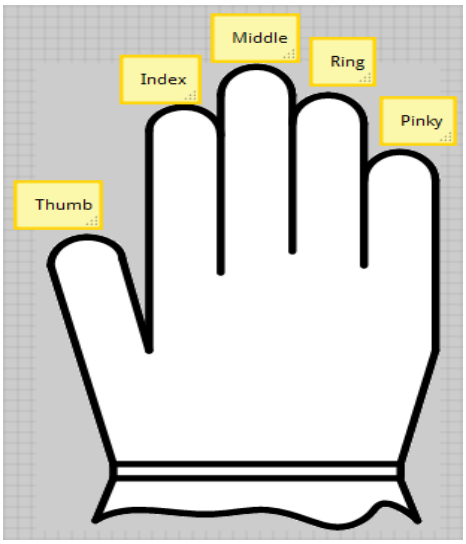

Figure 1. Right Hand

The index and middle fingers from the left and right hands are used as part of the finger controller. To make the finger controller flex with the real human fingers, the 4.5-inch flex sensor [2] would be an ideal scenario for this application. As the flex sensor is bent and flexed, as shown in Figure 2, the resistance across the sensor increases.

Figure 2. 4.5-inch Flex Sensor

If the flex sensor is flat, the nominal resistance is at 10K Ohms. When the flex sensor is bent, it has a range of 60K to 110K Ohms with a tolerance of ±30%.

Figure 3 illustrates the finger controller that contains the flex sensors on the index and middle fingers of the left-hand and right-hand gloves. The use of the flex sensors is a unique way for human-robot interactions because it is the first step to haptic robotics. Haptic means tactile feedback or physical feedback from a device or a robot [3]. For instance, the haptic feedback in a Sony Playstation 2 console has a vibrating remote controller in a shooting game. It sends feedback to the user that an event (in this case, shooting) is triggered. It is a step toward a more humane robot. In the case of the finger controller, it provides tactile feedback to the user for controlling different robotic applications.

The finger controller is designed to control a combination of two DC motors, such as Tetrix DC motors, Servo motors or CIM motors. It is designed to be used as a transmitter to send the data to the receiver. For instance, depending on the robotic application, the flex sensors on the two index fingers are controlled by the forward and backward motions of the robot. And the two middle fingers are controlled by the left and right turns of the robot.

Finger Controller and Wireless Communication

As illustrated in Figure 3, the finger controller has four flex sensors. Each hand has two flex sensors connected to the index and middle fingers. Also, each hand has one microcontroller. This is to prevent the congestion of data between the XBees and wireless data transmission interference. Also, the two XBees provide better redundancy against failure. Each flex sensor connects to the analog pin of the Arduino microcontroller [4]. The analog values from the flex sensors are based on a voltage divider between two resistance values. These values then transmit two one-way communications wirelessly to the receiver. The wireless Xbee communication radio transmits information byte by byte [5]. Each byte consists of 8 bits or 2 nibbles. All of the standard ASCII characters can be sent byte by byte. A byte looks like this, in binary, 00000000 which represents 0 in decimal or 0x00 in hexadecimal. The highest decimal possible in a byte is represented 0xFF in hexadecimal, 255 in decimal and 11111111 in binary [6]. Thus, the wireless communication can send information in numerical or character form from 0 to 255.

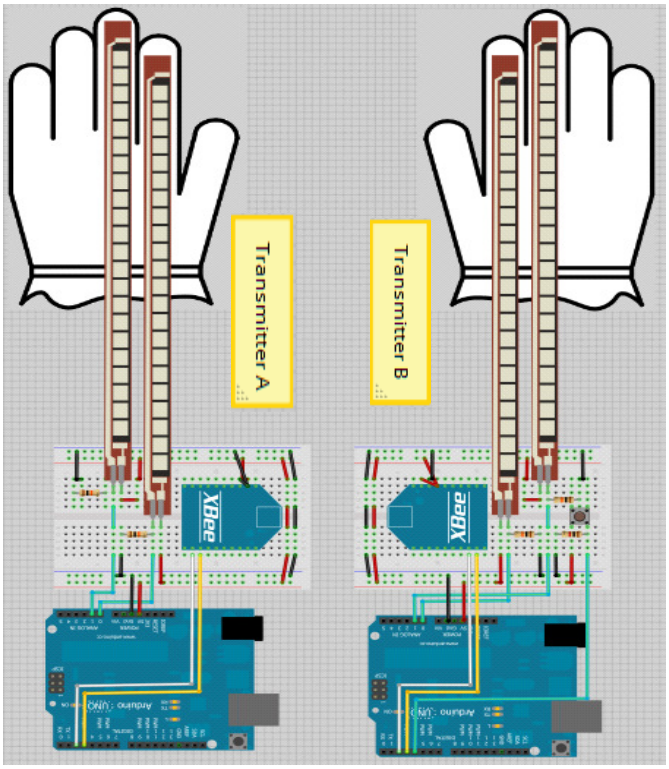

Figure 3. 3D Finger-Controller Layout

In addition to the flex sensors integrated with the finger controller, a push-button switch is implemented on the right hand of the finger controller. The push-button switch allows the user to alternate from tele-operated to autonomous mode and vice versa. Each time the user pushes the switch, the switch produces either a HIGH or a LOW signal. This HIGH or LOW signal transmits one byte (either 11111111 or 00000000) to the receiver. Thus, the finger controller is a unique and novel controller for human-robot interactions.

Prototyping of the Finger Controller

Based on the 3D layout shown in Figure 3 and 2D schematic shown in Figure 4, the design of the finger controller can be seen in Figure 5. Note that the schematic of Figure 4 is a duplicate of Figure 3. However, Figure 4 provides a clear schematic layout as a guide to complete the Finger-Controller circuit in Figure 5.

Robotic Applications

Three robotic applications are presented in this section; the Flexible Robot, Line-Following Robot and Solar Rechargeable Robot. All three robots have different characteristics and are controlled by the finger controller. To make the finger controller adapt to different robotic tasks, the high-level programming source codes were created and uploaded to the Arduino microcontroller. The source codes were developed using the following software flowchart.

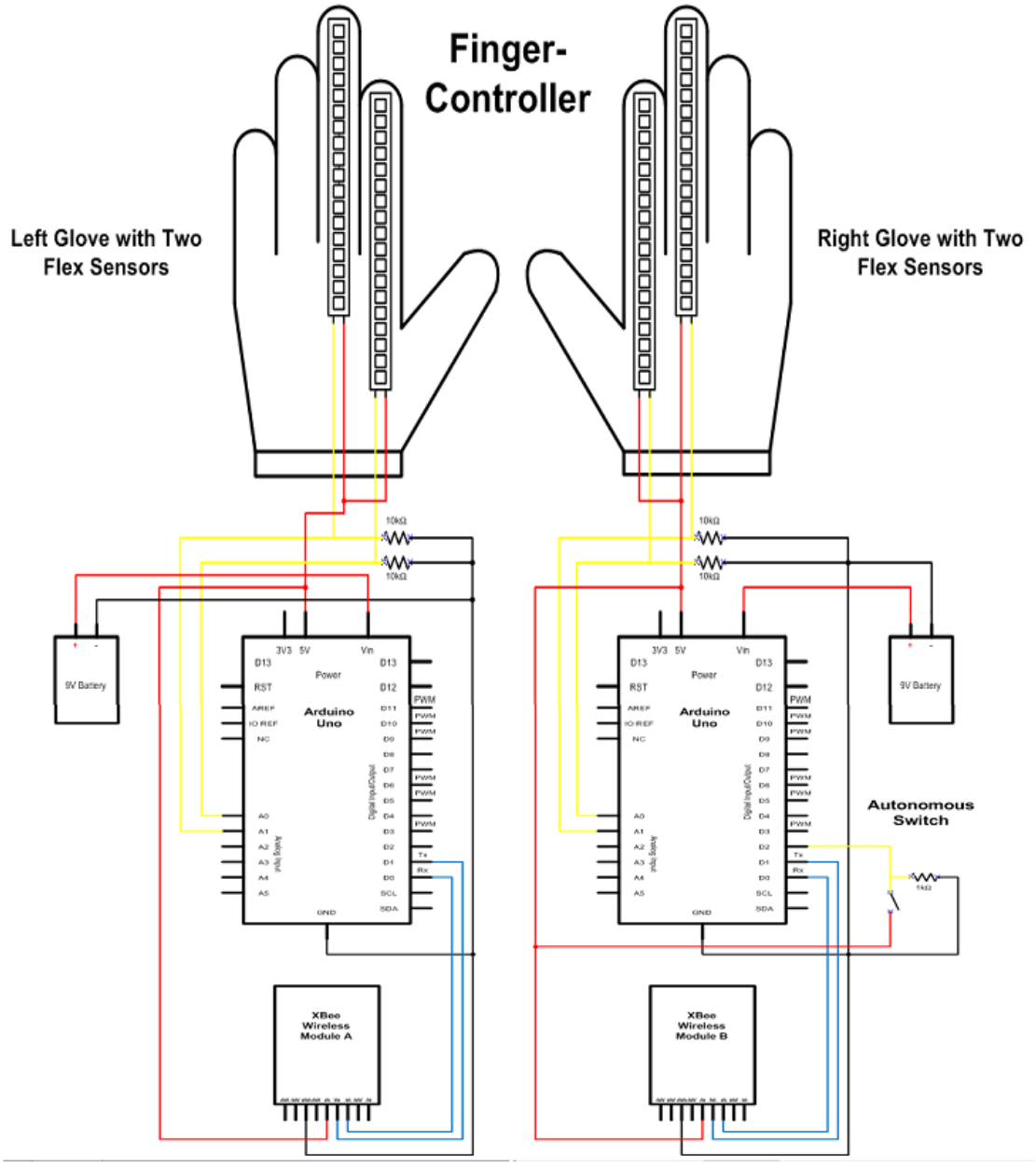

Figure 4. 2D Schematic of the Finger Controller

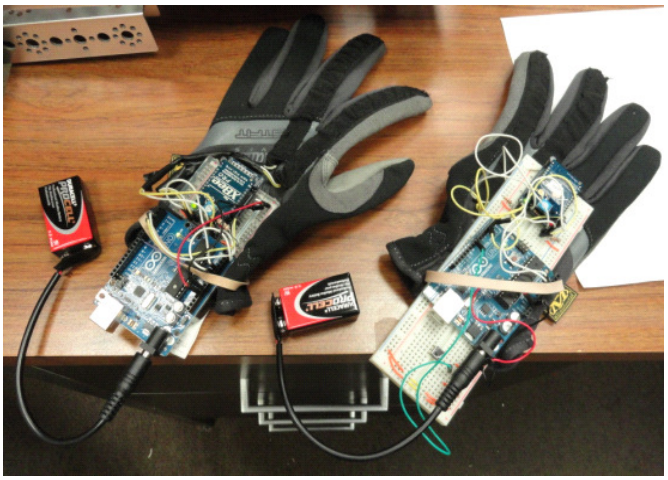

Figure 5. Prototype of the Finger Controller

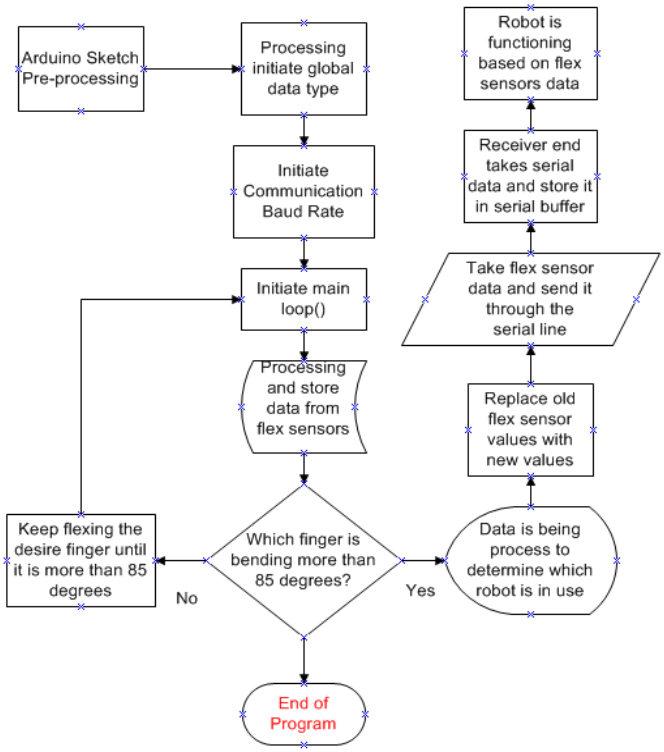

Figure 6. Finger-Controller Software Flowchart

Figure 6 is a software flowchart that is used to create the source codes for the finger controller. The user has to decide which robot is going to be used. Then, the user has to bend one of his or her four fingers (left middle, left index, right index or right middle) more than 85 degrees to select the desired robot. Each finger represents one robot application, as seen in Table 1. After the selection has been made, the robot is now controlled by the finger controller, either in tele-operated or autonomous mode.

Table 1. Robot Applications

Left Middle	Left Index	Right Index	Right Middle
Not In Use	Flexible Robot	Line Following Robot	Solar Rechargeable Robot

Note that the receiver end of the finger controller can be set up with different robotic wheel configurations and different drive systems.

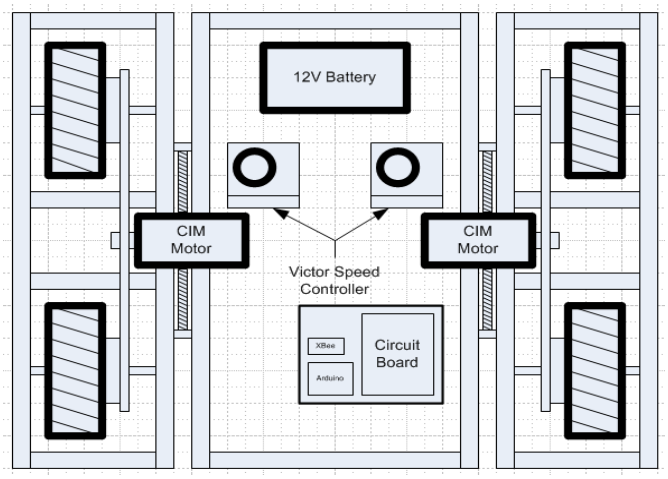

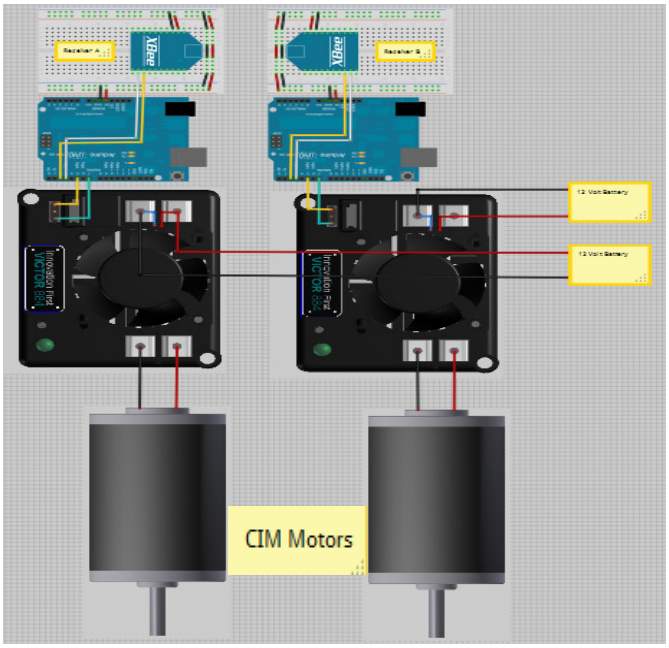

Figure 7. Conceptual Design and Schematic Layout of the Flexible Robot

Flexible Robot

The Flexible Robot has unique and innovative features for unconventional means in mobility through different environments. The concept is essentially a robot that can be controlled wirelessly through tele-operated or autonomous mode with a programmable microcontroller. At the same time, the mechanical design of the Flexible Robot has the capability of moving effectively over rough terrain that would otherwise stop conventional robots.

The Flexible Robot is a tank-drive robot that runs on four wheels. Each set of two wheels runs on a single CIM motor [7]. Therefore, there are two CIM motors for the entire four-wheeled robot. Figure 7 shows the process of conceptual design to build the electrical schematic layout.

Figure 8 shows the prototype of the Flexible Robot and the preliminary testing of the Flexible Robot controlled by the finger controller. The CIM motors in Figures 7 and 8 are controlled and powered by a Victor 884 [8] speed controller. There is one speed controller for every CIM motor. This Victor 884 speed controller can control the speed and direction of the motor. The left finger controller on the transmitter controls the left set of wheels, while the right finger controller controls the right set of wheels. The index fingers of the finger controller control the forward motion of the robot, and the middle fingers control the reverse motion of the robot. The variation of speed and direction are dependent on how much the flex sensors are bent.

Line-Following Robot

The Line-Following Robot has a unique feature of following lines when the robot is either in autonomous or tele-operated mode. The lines must be formed by using black electrical tape. For instance, the robot can follow any pattern of unknown mazes that are designed using the electrical black tape.

Unlike the Flexible Robot, the Line-Following Robot runs on two small DC motors that use a lower voltage supply of 5V. It does not use the Victor 844 speed controller but rather a low-cost, 16-pin Quadruple Half H-Bridge Driver (SN754410) IC [9]. The internal circuit setup of the H-Bridge Driver is similar to the Victor 844 speed controller. The single chip Quadruple H-Bridge IC can control two DC motors of the Line-Following Robot. Figure 9 shows the process of conceptual design to build the electrical schematic layout of the Line-Following Robot. Based on the information of Figure 9, the prototype was made and is illustrated in Figure 10.

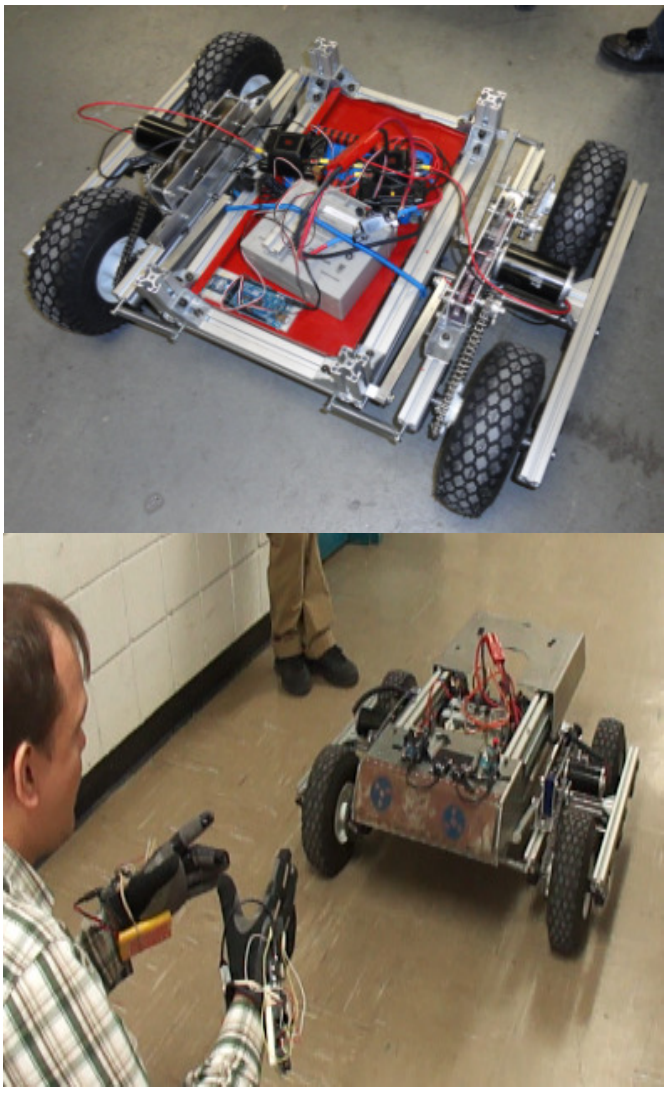

Figure 8. Flexible Robot and Finger Controller

The Line-Following Robot in Figure 10 can operate either in autonomous or tele-operated mode to follow any pattern of lines that are made out of pieces of black electrical tape. When it is in the autonomous mode, the robot has five infrared sensors activated to follow the lines of tape. The infrared sensors are off when it is switched to tele-operated mode by pressing the push-button switch on the transmitter side of the finger controller. Thus, this is an innovative feature of the finger controller for controlling the Line-Following Robot.

Solar Rechargeable Robot

The objective of the Solar Rechargeable Robot is to have the solar panel collect energy from the sun and store it in the

rechargeable battery. This rechargeable battery provides the entire power source to run the Solar Rechargeable Robot during night time and on cloudy days. In other words, the robot itself functions through the power source from the solar panel during sunny days while at the same time it can charge the rechargeable battery. This rechargeable battery can then be stored for later use during night times and on cloudy days.

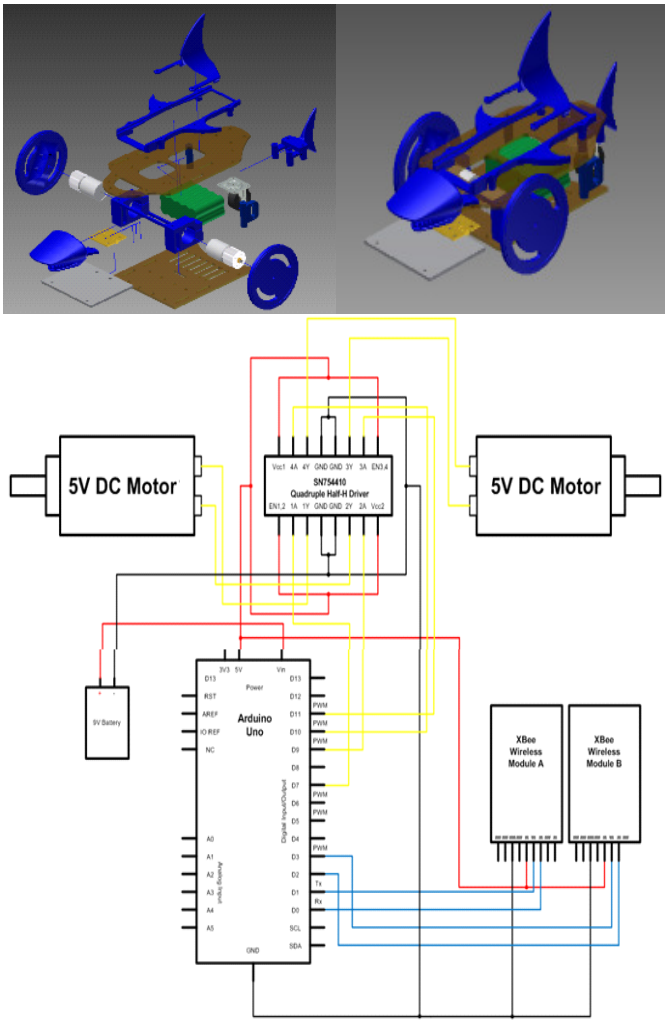

Figure 9. Conceptual Design and Schematic Layout of the Line-Following Robot

The Solar Rechargeable Robot is different from the previous two robots. Figure 11 shows a complete layout of the robot with the finger controller. It uses a steering system instead of a tank drive. The steering system is controlled by the Servo motor [10]. The Servo motor can control how much the motor turns but does not control speed. Also, the Servo motor has different variations such as 90-degree turns, 180-degree turns or full 360-degree turns.

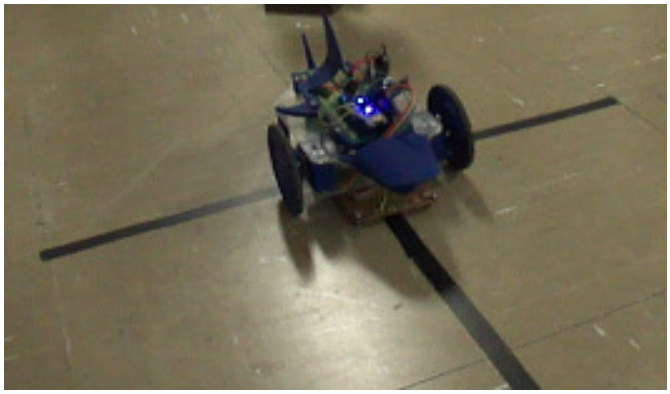

Figure 10. Prototype of the Line-Following Robot

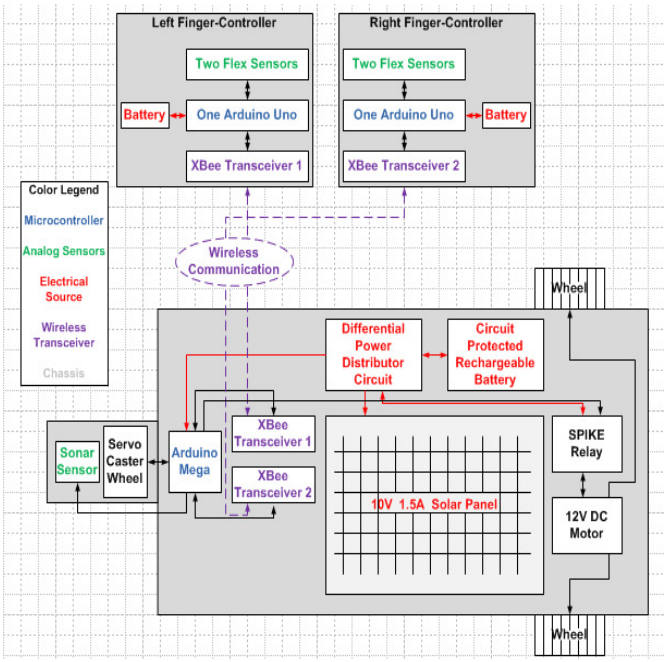

Figure 11. Layout of Solar Rechargeable Robot and Finger Controller

As seen in Figure 11, the left finger controller controls the steering while the right finger controller controls the forward and reverse rear wheels. For the rear drive system, a differential was also implemented to compensate for the turning when the steering is used. The rear drive system is a single 12-Volt Tetrix DC motor [11] controlled by a SPIKE [12], which is a device similar to a relay. The SPIKE logic can be seen in Table 2. The difference between a SPIKE and a speed controller or an H-Bridge Driver IC is that the SPIKE does not control speed, only direction. Although a speed controller can be used, the SPIKE was used to show that the finger controller can be used to only trigger the device on or off given certain thresholds.

Table 2. SPIKE Logic

Logic Signal One	Logic Signal Two	Direction
0	0	Stop
0	1	Forward
1	0	Reverse
1	1	Stop

Based on the information of Figure 11, the significant components of the Solar Rechargeable Robot are the Servo and Tetrix DC (with SPIKE) motors. The schematic layout for these components is shown in Figure 12. The Servo motor connects to the Arduino and receives 5 volts from the Arduino. Unlike the Servo, the Tetrix motor receives 12V from the external source. In addition, the Tetrix motor requires the use of SPIKE for power safety and to prevent damage to the Arduino. Also, both Servo and Tetrix motors work based on the data received from the finger controller through the XBee wireless communication system.

Figure 13 provides a complete schematic circuit of the Solar Rechargeable Robot. Note that the Ping sonar sensor is included for obstacle detection when the robot is in the autonomous mode. Also, while the robot is running by solar power, the power is then simultaneously charging the rechargeable battery. This makes the Solar Rechargeable Robot more energy efficient. The preliminary tests of the Solar Rechargeable Robot with the finger controller were successful. The finger controller was able to control the robot in tele-operated or autonomous modes. Additionally, the solar power provides the source to run the robot while it is charging the rechargeable battery. Figure 14 illustrates the preliminary tests of the Solar Rechargeable Robot and finger controller.

Since the solar power is important and crucial for running the Solar Rechargeable Robot, the voltage data were recorded before and after each preliminary test. Figure 15 shows the process of recording the data from the solar panel [13] to the rechargeable battery. Based on the preliminary data, the charging rate from the solar power to the rechargeable battery is approximately 0.05V per 30 minutes, while the robot is in use. If the robot is sitting still and not in use, the charging rate is about 0.5V per 30 minutes. The preliminary data did not take into account the temperature and intensity of the solar energy from the sun.

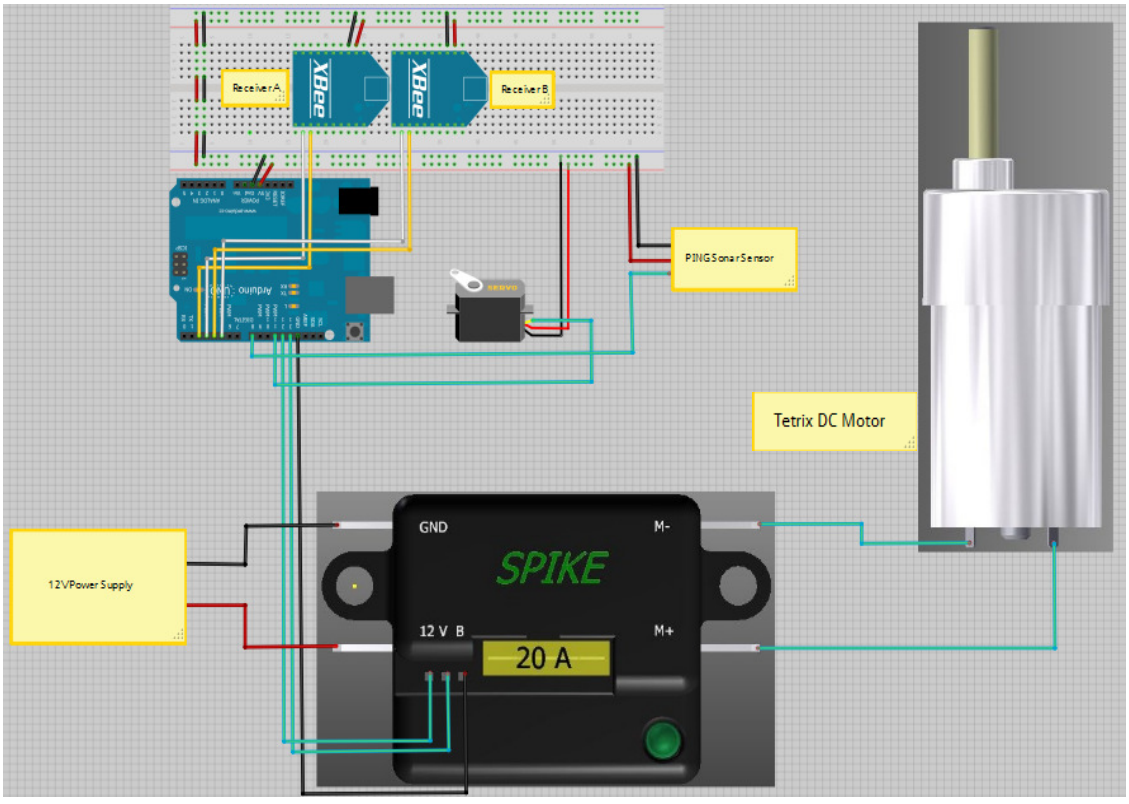

Figure 12. Schematic Layout of Servo and Tetrix motor, SPIKE, and Sonar Sensor

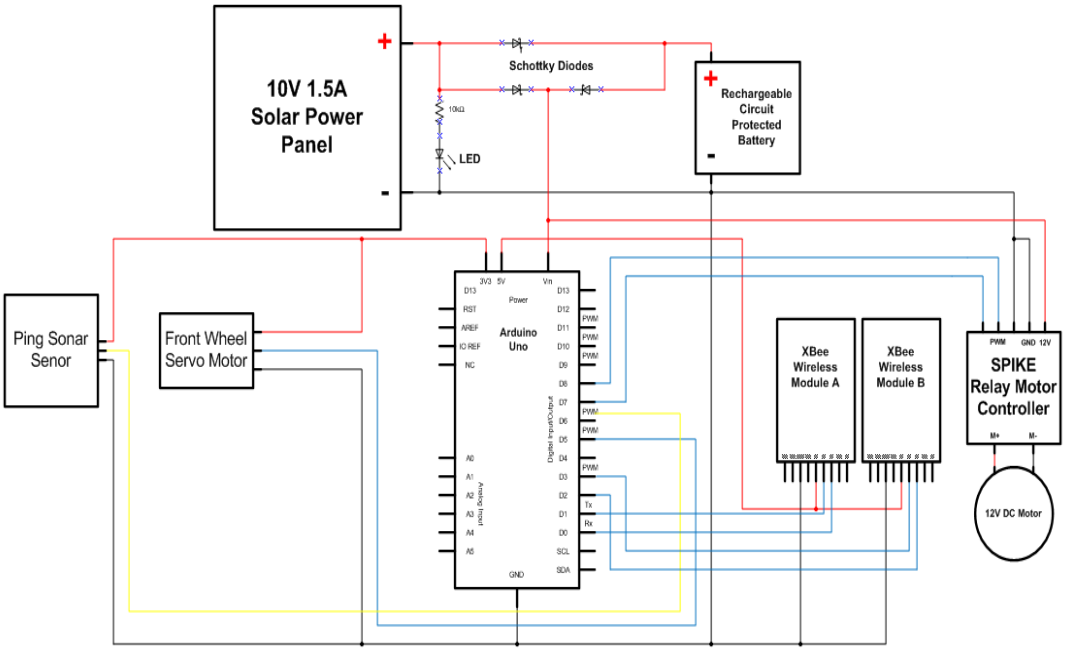

Figure 13. Schematic Circuit of Solar Rechargeable Robot

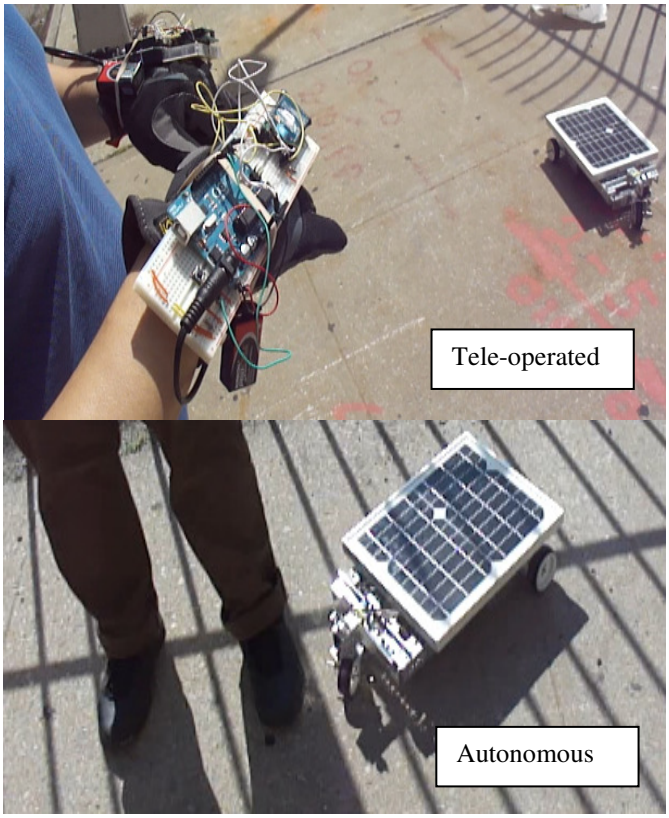

Figure 14. Testing Solar Rechargeable Robot with the Finger Controller

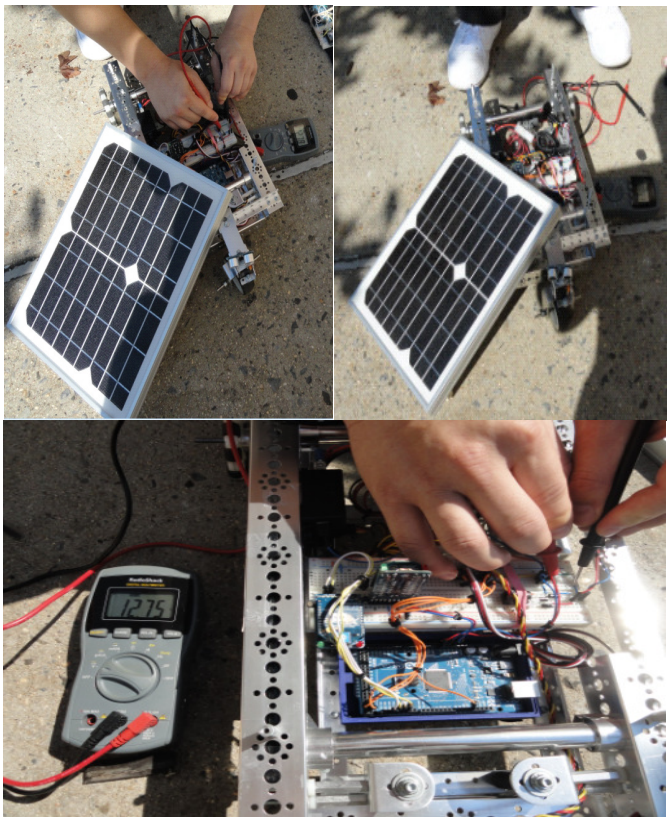

Figure 15. Solar-Power Data

Conclusion

The goal for this research project was to develop a custom -made finger controller capable of controlling (either in tele-operated or autonomous mode) different robotic applications. Three robotic applications have been discussed and have been integrated with the finger controller. The finger controller provides an enhancement of collaboration between human and robot interactions. Further, the finger controller provides the hands-on multidisciplinary activities in learning to work together as a team. For future research work, the authors plan to redesign the finger controller so that it is flexible and capable of controlling mechatronic devices such as mobile devices, appliances, TV, laptop, desktop and others. Currently, the finger controller is powered by two non-rechargeable 9-Volt batteries. Future plans include using solar power to recharge the finger controller.

Acknowledgements

This collaborative research work among the faculty members in the Mechanical Engineering Technology and Computer Engineering Technology departments is funded by a National Science Foundation Advanced Technology Education Division (NSF ATE No 1003712) grant awarded to our college. The authors would also like to thank all of the students who were involved in the research projects.

References

[1] Weiss, A., Wurhofer, D., Lankes, M., & Tscheligi, M. (2009). Autonomous vs. Tele-operated: How People Perceive Human-Robot Collaboration with HRP-2. *Proc. 4th ACM/IEEE on International Conf. on Human Robot Interaction*, San Diego, CA, 257-258.

[2] Flex Circuit Technology. (n.d.). Retrieved September 2, 2012, from http://www.spectrasymbol.co.

[3] Hikiji, R. and Hashimoto, S. (2000). Hand-Shaped Force Interface for Human-Cooperative Mobile Robot. *Proceeding of First International Workshop on Haptic Human-Computer Interaction*, Glasgow, UK, 113-118.

[4] Banzi, M. (2009). *Getting Started with Arduino*. (First ed.). Sebastopol, CA: O'Reilly Media, Inc.

[5] McRoberts, M. (2010). *Beginning Arduino*. (First ed.). New York City, NY: Apress Publisher.

[6] Heng, I., Zhang, A. & Harb, A. (2011). Using Solar Robotic Technology to Detect Lethal and Toxic Chemicals. IEEE Xplore Digital Library, (pp. 409 – 414). ISBN: 978-1-61284-634-7.

[7] Andy Mark. (n.d.). Retrieved July 1, 2012, from http://www.andymark.com/CIM-motor-FIRST-p/am-0255.ht

[8] Robot Marketplace. (n.d.). Retrieved July 12, 2012, from http://www.robotmarketplace.com/products/IFI-V884.htm

[9] Texas Instruments. (n.d.). Retrieved Jun 10, 2012, from http://www.ti.com/lit/ds/symlink/sn754410.pd

[10] Servo Motor. (n.d.). Retrieved Jun 15, 2012, from http://en.wikipedia.org/wiki/Servo_moto

[11] LEGO Education. (n.d.). Retrieved Jun 25, 2012, fromhttp://www.legoeducation.us/eng/product/tetrix_dc_drive_motor/161

[12] VEX Spike H-Bridge. (n.d.). Retrieved July 15, 2012, from http://www.vexrobotics.com/217-0220.htm

[13] Sparkfun Solar Panel. (n.d.). Retrieved August 17, 2012, from https://www.sparkfun.com/products/975

Biographies

DR. IEM HENG earned his bachelor's degree from Providence College (Providence, RI) with double majors in Pre-Engineering Program and mathematics. In addition, he earned another bachelor's degree from Columbia University (New York, NY) in mechanical engineering and master's in applied mathematics from Western Michigan University (Kalamazoo, MI); his Ph.D. in computational and applied mathematics from Old Dominion University (Norfolk, VA). Before joining the EMT/CET department at City Tech in fall of 2007, he was a faculty member and chair of the CET department at DeVry Institute of Technology (Long Island City, NY). He worked as a researcher for NASA Langley Base in Hampton, VA, for two years.

DR. ANDY S. ZHANG earned his Master's in mechanical engineering from the City College of New York in 1987 and his Ph.D. in mechanical engineering from the Graduate Center of the City University of New York in 1995. Prior joining the Mechanical Engineering Technology department at City Tech in 2000, he served as an engineering instructor for the JUMP, an engineering training program sponsored by the New York State Department of Transportation. Professor Zhang's research area includes materials testing, composite materials, CAD/CAE, robotics and mechatronics.

MR. RAYMOND YAP earned his Associate in Applied Science in Electromechanical Engineering Technology in 2007 and his Bachelor of Technology in Computer Engineering Technology in 2010 and is employed in New York City College of Technology as a Research Technician for the Research Foundation of CUNY. Research interests include electrical control systems and implementation of software programming to different types of microcontrollers.

VALUE OF FORMAL PROJECT MANAGEMENT TO AUTOMOTIVE EMPLOYEES

Muhammad Sohail Ahmed, Eastern Michigan University

Abstract

Formal project management is now an essential part of major automotive companies. Researchers report project management maturity in the automotive industry and reference several studies about the advantages and value added by project management. Most research shows the value that project management brings to an organization. In this current study, the objective was to determine the value that project management provides to employees. Eight Detroit automotive companies were surveyed. Using principal component analysis and descriptive statistics, it was found that when formal project management is applied, both companies and their employees benefit, though the values they gain are different. Employees gained value in terms of higher job satisfaction, better employment options and greater visibility within their company, including promotions. The study also outlines essential aspects for project managers and company leadership to encourage creativity and innovation among automotive employees.

Introduction

The continued survival and profitability of a corporation is dependent upon the ability to meet its economic and social purpose, most often to develop and distribute sufficient wealth or value to ensure that each group—customers, employees, suppliers, community residents and the environment—continues as part of the corporation's stakeholder system. The emphasis is on the value that can be created by interactions between firms and primary stakeholders. This interaction is generally relational rather than transactional, since transactional interactions can be easily duplicated and thus offer little advantage over the competition. In order to develop a relationship, both parties must invest time [1]. There have been several studies that indicating that a company's effectiveness depends upon the success of its projects and implementation of project management [2], [3]. These studies outlined, in detail, the tangible and intangible value that project management brings to organizations. These outcomes show a direct impact on the organization, but fail to describe how stakeholders benefit from such project management initiatives.

The United States automotive industry plays a significant role in the nation's overall Gross Domestic Product (GDP). From World War II until the present, the development of project management has radically changed structures and processes within the domestic automotive industry. Formal project management techniques have now been implemented at OEM (Original Equipment Manufacturers) and supplier levels, with some suggesting that techniques have reached maturity levels [2]. Studies directed towards the value of project management within the automotive sector are completed with no references directed to stakeholders. Thus, it is important to study how stakeholders benefit from interactions due to the implementation of formal project management. The automotive industry has a complex product development and manufacturing process which makes it one of the most knowledge-intensive industries. Similarly, the automotive supply chain stretches through various levels of suppliers to OEMs.

Given the significance of the automotive industry, this study identifies the benefits to automotive companies and, by extension, employees from the implementation of formalized project management systems. The benefit that the workforce obtains from this implementation can be more subjective and, therefore, is often overlooked. Too many times the company as a whole is treated as the primary beneficiary of any project management improvements, and the value to employees is ignored.

Project Management in the Automotive Industry

Similar to the invention of the airplane, the emergence of automobiles has had a profound effect on everyday lives. The design and manufacturing of an automobile is a complicated process. It not only must satisfy engineering criteria, but also needs to fulfill environmental, social and political aims such as minimizing waste and deposition, satisfying recycling targets, respecting health and safety regulations, reducing emissions and saving resources. Thus, the automotive industry is considered to be a highly capital- and labor-intensive industry [4].

The United States automotive industry is a critical component for economic growth, with extensive interconnec-

tions across the industrial and cultural fabric of the nation. The industry has historically contributed 3–3.5 percent of the overall GDP, while employing over 1.7 million people [5]. Not surprisingly, it is the subject of a great deal of study, largely due to its importance as the single largest industrial sector in the world economy. A typical automobile has 15,000 to 20,000 parts/components and currently takes around 18 months to design and develop. Production of these large numbers of differentiated parts, from design to marketing, is a direct result of following some systematic processes. Almost every automotive OEM has a product development process with milestones and quality gates. These development processes utilize techniques such as simultaneous engineering, robust engineering, Design for Manufacturing (DFM), Design for Assembly (DFA), Design Failure Mode and Effects Analysis (DFMEA) and Process Failure Mode and Effects Analysis (PFMEA). The assimilation of managerial techniques by the automotive industry—Total Quality Management (TQM) and Just-In-Time (JIT), for example—has certainly transformed the way in which production is managed in car plants [5].

In 1996, Keenan [6] wrote, "Program Management, (PM) is the way automotive components and systems will be developed from now on, picking up where simultaneous and robust engineering leave off. The PM trend is spawning a new management specialty, one that requires less engineering knowledge and more organization, communications and people skills." In the past, suppliers were mostly independent and have only recently formed strategic alliances and partnerships. Recently, car producers are increasingly turning to their first-tier suppliers to develop standardized components [7]. Midler & Navarre [4] traced the evolution of auto industry project management through four stages:

> 1. From the postwar period up to the 1970s, when there was no differentiation between the ''product strategies'' of carmakers in North America and Europe. Disciplined management of projects was not a core component in competitive strategy.
> 2. During the 1970s and 1980s, the gradual saturation of markets changed the competitive environment radically. Japanese carmakers succeeded in breaking into the North American market using (novel) product proliferation strategies, and the direct consequence of this business model was an explosive increase in the number of projects to be managed. The management of projects for new vehicles now assumed strategic importance.
> 3. In the late 1980s and early 1990s, manufacturers radically reorganized their approach to the management of projects for new products in order to develop more quickly and at lower cost, a greater number of products of increasingly high quality.
> 4. By the late 1990s, to 2003, the effects of the reorganization in the industry along with the second wave of reorganization of manufacturers made the new vehicle project management more complex. The issue was however, worsened by new challenges, namely: alliances, market globalization, and innovation. To find new values for differentiation, firms went down the road of innovation policies that were far more radical in terms of both engineering and styling. (pp. 1369-1370)

By the end of the 1990s, a formal approach towards project management began making its way into industry. Ellison et al. [8] demonstrated that Western carmakers had very much caught up with the Japanese, according to various metrics they had defined as being most indicative of project management performance levels, including product launch time, quality, etc. [4].

However, at the start of the new millennium, the automotive industry chose to implement innovation policies that were far more radical in terms of both engineering and styling. This high-risk process was not suited for ''heavyweight'' types of automotive project organization, with no cross-functional and cross-product project existing to address, coordinate and control these learning tracks on radical innovative features and technologies [4], [9]. By the early 2000s, a new form of project organization was gradually being put in place to guide exploration upstream of vehicle projects [9]. The climate of acquisition and partnership that followed included pairings such as Renault-GM, GM-Fiat and Daimler-Chrysler. It also created a cooperative project culture with its own problems, as compared to traditional automotive culture [4], [10].

In the future, networked organizational structures, decentralized product development and virtual development teams will form an increasingly significant part of product development in the automotive industry. This change will result in the shift of interfaces in the product development process and an increase in integration complexity [4]. The new forms of collaboration between project partners are necessary. The OEM will have a new function as a network manager linking internal processes with those of suppliers, in order to efficiently coordinate collaboration activities [11].

Project management, thus, plays a vital role in the innovation, design and development of automobiles. Although the auto industry was a latecomer to project management, compared to military equipment or the construction business,

these sectors are now working to transform their project management traditions and adopt the practices developed in the late 1980s and 1990s in the automotive sector [4].

Problem Identification

In today's competitive industry, project management is a proven tool to streamline projects and add value to the company's portfolio. Project and product success are kept aligned with the performance criteria set by individual stakeholders. It is, therefore, important to define the "value" of project management: What is valuable to organizations, and how is it measured? The application of the Value Focused Thinking (VFT) technique includes some important steps for achieving this measurement, including: i) the identification of key stakeholders; ii) the identification of stakeholder values; and, iii) converting values to objectives. An objective is thus characterized by three features, a decision context, an object and a direction of preference. This means explaining the objective within its context based on the nature of the problem, and finding out exactly what the stakeholder is trying to achieve [12].

Return on Investment (ROI) is one of the most widely used value-driven measures. Several researchers demonstrate significant challenges with the availability, reliability and defensibility of data, to perform the calculations of financial value that would be required to arrive at an ROI measure [13]. Thomas & Mullaly [14] point out that limiting ROI to financial "value" ignores all of the intangible benefits of a particular topic of discussion. The idea of value has been discussed at length in the work of the "Researching the Value of Project Management" project [14]. Researchers outline the value framework for project management; the value is organized into two major categories, tangible and intangible.

Tangible values consist of cost savings, revenue increases, customer retention, increased customer share, greater market share and reduced write-offs or rework. Intangible values include improved competitiveness, new product/ service streams, greater social good, improved quality of life, more effective human resources, higher staff retention, superior reputation, better overall management, enhanced corporate culture and improved regulatory compliance [14].

Hurt & Thomas [15] identify three main ideas for determining the value of project management. First, they discuss how the Project Management Office (PMO) created a center for knowledge of all the projects that a company has completed, are in process and are for the future. Next, they focus on the importance of having the proper leadership and staff within the PMO to ensure that all projects run according to the businesses goals and objectives. Finally, they focus on the importance of formal project management for creating an overall culture of discipline within the company.

Within automotive project management there is much research related to case studies, team/cross-cultural teams and innovation efforts [16]. Global mergers and acquisitions in the automotive industry have left fewer companies offering a greater variety of brands. Shorter product lifecycles have increased the number of product launches for each brand, raising the number of new product projects for companies. Automotive companies apply innovative management methodologies, such as project management, in order to achieve rapid and continuous improvements in their operation [17]. Beaume [18] argues that within automotive firms, innovation management no longer deals with introducing radically and totally new products, but rather with applying innovative features within a regular stream of products and platforms. He outlines an analytical framework that addresses the resulting interplay between innovative features and new products.

Methods aimed at improving the project management performance of automotive cross-company projects have been developed. Collaborative strategy maps and integrated measures for project control based on key performance indicators (KPIs) are identified as an essential step for successful project management with a collaborative project scorecard [11]. Without specifically targeting the value of project management, researchers suggest that the platform strategy adopted by automotive firms in a multi-project context reduces lead-time and development costs, enhances reliability, allows mass customization and increases manufacturing flexibility [19].

From the above research, it is easy to show how a company's bottom line is increased through the implementation of a formalized project management plan. However, the benefits that employees obtain from this implementation can be more subjective and therefore overlooked. Too often, the company as a whole is viewed as the primary beneficiary of any project management improvements, and the value to employees is outright ignored.

Problem Statement

This study suggests that one reason a company benefits so heavily from the implementation of a formalized project management system is directly related to the value that the employees obtain, thus creating a win-win situation. However, there is little research solely devoted to this conclusion. Therefore, the objective of this study was to demonstrate that the benefit companies obtain from the reorganiza-

tion of their project management system is directly related to the increased value their employees obtain from such efforts. This study was intended to target the automotive industry in general, and provide insight about the value project management offers.

Nature and Significance of the Problem

When organizations implement a formalized plan, they are taking a decisive approach to run their project management portfolio to reflect the best interests of the company's overall business goals and objectives. This decision can have a direct effect on the bottom line, including increased market share and expanded product lines. However, implementing these changes has a much further reaching effect than just the company's profit. When choosing to proceed with a formalized project management system, employees are also directly impacted. This study explored the benefits received by the automotive industry's workforce from this implementation.

To understand this issue, one must understand the difference between formal and informal project management systems. Formal project management involves project planning as well as implementation and control [20]. When formal project management is followed, the company uses proven processes and lessons learned to leverage internal strengths and ensure the best possible results. It also utilizes project management software or techniques to ensure that company resources are applied in an efficient manner. Larger aspects of formal project management include assessing where the money has been spent, and comparing the data to the work that has been completed in order to gauge whether the project will finish on schedule and within budget or not.

On the other hand, informal project management is concerned more with running projects based on intuitive judgments and relationships between individuals [21]. Informal project management relies heavily on the experience of company employees in order to plan, implement and control projects. This puts pressure on the project manager to ensure that he/she has the right people performing the correct roles. Most often, this placement is based on personal experience and best-judgment calls. This is all reliant on which individual the company has appointed to manage and organize the project portfolio.

Based on a literature search on the same topic, it was fairly clear that there is an increase in value to the company when adopting a formal project management approach. This study argues that companies often overlook the impact on employees when implementing project management plans because of the belief that anything that helps to improve the way projects are planned will be beneficial to all groups involved. To a large extent, this idea is true. When the projects are planned and implemented in a more organized manner, the effect on the employee should be mostly positive.

However, it is argued that there could be some negative repercussions if the company implements the plan without consulting employees on the improvement efforts. One such negative effect is the increase in paperwork that tends to come with formalized project management plans. If employees are not properly trained to handle this influx of paperwork, it could be cumbersome to handle and, ultimately, not be processed. A PMO's effectiveness and success depends on choosing which functions to implement, then adapting and adjusting them to fit the organization's needs [21].

Research

The research approach used in this study followed a five-step process including: identifying variables, reviewing assumptions, developing survey questions, collecting data and performing statistical analyses in order to achieve accurate results.

Step 1: Identify Variables

A literature review was performed to extract variables needed to define the value of project management for companies and employees. The purpose of this literature review was to build internal validity, raise theoretical levels and sharpen construct definitions. The collected data were used to developed hypotheses and questionnaires for steps two and three. Project management value is defined as process, organization, technology, metrics, culture and leadership, along with tangible and intangible values.

Step 2: Review Assumptions

- It was assumed that survey respondents would have a good understanding of formalized project management systems.
- It was also assumed that the respondents would respond fairly and honestly, without bias for the subject.
- It was further assumed that the responses would be based on a standard and error-free questionnaire.

Step 3: Develop Survey

Using variables collected in Step 1, hypotheses and survey questions were developed. The survey was tested by three senior automotive project managers and incorporated a list of questions that included demographic, gender and education. The remaining survey questions used the following Likert scale: 5 points = Strongly Agree; 4 points = Agree; 3 points = Undetermined; 2 points = Disagree; and, 1 point = Strongly Disagree.

There were two major subsets of questions. The first was based on the benefit/value that the employee receives, and the second focused on the benefit/value that the company receives from formalized project management. The survey questions were designed to collect data from a number of key stakeholder perspectives, including senior and junior project managers, project team members/organizational employees, and tier one and two suppliers. Senior project manager input was essential for capturing data regarding project cost, schedule and success. This type of data, in most cases, is sacred to an organization. Thus, the biggest concern was the accuracy of the information. Also, individuals tend to score higher when they critique themselves [22]. To avoid this and obtain accurate data, respondents were reminded about the importance of the survey and being a candidate. The survey for each stakeholder involved between 20 and 55 questions, and was expected to take approximately 30 minutes to complete.

Step 4: Data Collection

After being tested by five PM practitioners for clarity and to ensure construct validity, the questionnaire was piloted in an Advanced Project Management graduate class with 15 project managers as participants. Data were then collected through the online survey tool, LimeSurvey, from a group of project managers currently employed in two major Detroit automotive OEMs and six of their suppliers. The names of the companies are withheld for privacy. The primary utilization of projects within these companies focused on design, development and manufacturing. The survey was administered between October and December, 2011, and was distributed via Email to various managers, senior managers and vice presidents of the companies for their input. A target of 150 responses was set and by the end of the day 122 responses were received, out of which 106 were found valid.

Step 5: Statistical Analyses and Results

SPSS and Minitab were used to analyze the data. The two subsets of data were analyzed separately. Principal Component Analysis (PCA) was first used to identify components that showed the value of Project Management for the company and employees, followed by the descriptive statistics. PCA involves a mathematical procedure that transforms a number of (possibly) correlated variables into a (smaller) number of uncorrelated variables called principle components. The first principle component accounts for as much of the variability in the data as possible, and each succeeding component accounts for as much of the remaining variability as possible. The objective of PCA is to discover or to reduce the dimensionality of the data set and to identify new and meaningful underlying variables.

Step 5.1: Principal Components Analysis Results

A PCA analysis of data representing the value of project management for companies yielded three PCA components that explained 66.7% of the variation. Table 1 illustrates the Minitab results.

Standardized Business Process was identified as the first component and explained 39.7% of the variation with an Eigen value of 11.36. This component involved the presence of a project management office, success of the project with respect to cost and timing, following standard processes, utilizing project management tools including quality and statistical tools like Six Sigma, collaboration, continual improvement, employee training, customer focus, problem-solving techniques, and having a well-defined goal and objectives.

Organization Culture was identified as the second component, and explained 18.3% of the variation with an Eigen value of 4.6. This component involved the presence of innovation appreciation, customer focus, professionalism, training, collaboration, well-defined goals and objectives, and employees benefiting from project success. There was a significant negative effect from employee workload, risk-takers and politically charged environments.

Project Manager Capabilities, or leadership, was identified as the third component and explained 8.7% of the variation with an Eigen value of 2.4. This component involved the presence of teamwork, conflict resolution, addressing customer needs, collaboration, professionalism, decision making and problem solving. A similar PCA analysis of data representing the value of project management for em-

ployees also yielded three PCA components that explained 57.1% of the variation. Table 2 illustrates the Minitab results.

Table 1. Principal Component Analysis Results for the Value Project Management Brings to Companies

Variable	PC1	PC2	PC3
Presence of project management office	0.386	0.002	0.001
Success of project	0.542	0.357	0.024
Follow standard process	0.468	0.000	0.084
Utilizing project management tools	0.369	0.002	0.024
Continual improvement	0256	0.001	0.011
Employee training	0.325	0.512	0.051
Customer focused	0.341	0.462	0.246
Using problem-solving techniques	0.398	0.017	0.354
Well-defined goals and objectives	0.215	0.586	0.036
Innovation appreciative	0.002	0.514	0.001
Professionalism	-0.003	0.458	0.458
Collaboration	0..472	0.358	0.472
Workload	0.002	-0.572	0.001
Risk-takers	0.003	-0.275	0.006
Politically charged environment	0.012	-0.324	0.001
Teamwork	0.004	0.016	0.471
Conflict resolution	0.005	0.021	0.527
Decision making	0.001	0..012	0.541

Personal Satisfaction was identified as the first component and explained 33.6% of the variation with an Eigen value of 10.46. The components defined employee satisfaction with the company based on the success of projects in which they participated. It was heavily weighted by job satisfaction, teamwork and availability of training/education funds. Other variables included years of service, education, project management experience, well-defined job responsibilities, use of project tools, management encouragement and ability to innovate. Having searched for a job in the previous six months was the only negative variable. Most of the factors in this component were intangibles, with the exception of promotion and cash incentives offered by certain tier-two suppliers.

Table 2. Principal Component Analysis Results for the Value Project Management Brings to Employees

Variable	PC1	PC2	PC3
Success of project	0.021	0.357	0.381
Follow standard process	0.004	0.267	0.024
Utilizing project management tools	0.219	0.002	0.034
Employee training/ educational funds	0.525	0.421	0.317
Well-defined job Responsibilities	0.215	0.001	0.016
Innovation appreciation	0.329	0.005	0.018
Collaboration	0.022	0.358	0.001
Workload	0.002	-0.332	-0.027
Risk-takers	0.033	0.015	0.286
Politically charged environment	0.017	-0.324	0.001
Teamwork	0.464	0.017	0.021
Conflict resolution	0.004	-0.321	0.009
Job satisfaction	0.658	0.001	0.005
Years of service	0.312	0.482	0.001
Employee education	0.284	0.002	0.007
Project management experience	0.347	0.007	0.421
Encouragement	0.365	0.001	0.047
Open communications	0.004	0.328	0.008
Looked for a job in last six months	-0.244	-0.324	0.421

Loyalty was identified as the second component and explained 14.3% of the variation with an Eigen value of 8.32. This included seniority, direct benefit from project success, and availability of training/education funds, open communication, structured processes, and collaborative environments. The component showed a negative relationship with workload, politically charged environments, conflict resolution and not looking for a job. This was a surprising result. After 2008, financial collapse within Michigan's automotive industry resulted in layoffs of hundreds of thousands of engineers and related workers. Most of the engineers have since left the state and have acquired jobs in the medical

product industry, aerospace, etc. During mid and late 2011, the automotive industry in Michigan faced an acute shortage of product designers, manufacturing engineers and program managers. It was a common belief that those engineers would not come back to the automotive industry. Based on this perception, it was thought that employee loyalty towards a company would be low. The only negative effect came from the employees who paid for their own training or education.

Exposure and Employability was identified as the third component and explained 9.2% of the variation with an Eigen value of 3.12. This component explained how working on projects improved workforce employability in other industries and/or provided greater exposure within their current company. It is very common for a tier-one automotive project manager to receive offers from OEMs based on their work habits and project management experience. This component included training/education funding, project management experience, risk taking, searching for a job in the past six months and benefits from project successes. It was interesting to note that employee exposure with the company increased with high project success rates even though they may not have worked on many projects.

Step 5.2: Descriptive Statistics

This study concentrated on the value formal project management brings to an organization and employees. As shown under problem identification, several research studies exist on the value formal project management brings to companies. Thus, this study concentrated on the employee side, as outlined below.

Demography: There were 106 valid surveys, with 75.5% male and 24.5% female participation. Interestingly, this is consistent with the BLS population survey of 2011 that reported 25.9% of jobs in the motor vehicle and motor vehicle equipment manufacturing industry were held by women in 2011 [23]. Also from that study, 65% of responses were from OEMs and 35% were from suppliers. Additionally, 52.8% of the respondents had 4-year college degrees, 45.3% had graduate degrees, and 1.9% had a 2-year diploma. On average, respondents had managed 35-50 projects. Wright [24] reports that project managers in the North American automotive segment work on 17 projects a year. Lastly, 65% of the respondents had been with their company for 5-8 years, while only 26% had been with their company for more than 8 years. This suggests that employees need some motivation to remain loyal to their companies.

Formal Project Management: Since early 2000, it has been reported that the automotive industry is on its way to project management maturity [2]. Studies identified the presence of PMOs in the major automotive companies, and 73.6% of the survey respondents either agreed or strongly agreed with the presence of a formal PMO in their organization. Moving forward, the group of respondents who agree or strongly agree to a question will be referred to as group X in this study. There were five questions in the survey to specifically investigate the effect of PMOs within an organization. From group X, 84.9% reported that their company followed some sort of formal project management; 90.5% of the same group indicated that they did follow some systematic project management processes; and, 85.5% received some sort of project management training. From Table 3, it can be concluded that automotive companies have been following systematic/ formal project management, enabling them to adopt project planning and coordination in a uniform manner. Furthermore, automotive companies are taking initiatives to provide training to their employees, utilize definite monitoring processes, ensure effective team participation, and employ project managers to act as leaders in managing products and in conflict resolution.

Table 3. Project Management Office in Automotive Companies

Question	% Respondents agree (4) or strongly agree (5)
When working on projects, the projects goals and objectives are clearly defined at the start of the project	81%
When working on projects, project managers clearly establish team members' roles and responsibilities	78%
When working on projects, project managers have definite and structured project monitoring processes	78%
When working on multiple projects, I don't see any difference in the overall project management process followed by various project managers	82%
The project management team in my company has become more effective	84%
Project Managers in my company are well versed in managing projects	84%
Project Managers in my company provide leadership and conflict resolution	86%

Value for Employee: Most (79%) respondents reported gaining significant experience by participating in projects. Almost the same percentage (81%) agreed or strongly agreed that their experience in project management had increased their employability; 84% believed that working on projects had given them more visibility in the company;

and, 72% agreed that following standard project management tools and processes increased their chances for promotion. Employee loyalty towards their companies increased with the number of successful projects they participate in. Additionally, 85% of respondents agreed that every successful project increased their value within the company, and 85% valued any training or education funding their companies provided. The loyalty of this group of students was significantly higher (90%) than the respondents who self-financed their training or education.

The systematic and structured project management processes that automotive companies followed had helped in ensuring that the employees' roles and responsibilities were clearly identified, encouraged effective collaboration among team members, and that teams were led by managers who could safeguard them. This has led to increased job satisfaction. Of the respondents, 84.9% have their roles and responsibilities clearly defined; 79% appreciate the way their managers work with the teams to handle conflicts; and, 78% either agreed or strongly agreed on the question of job satisfaction which, in turn, had a positive relationship with retention.

Job security and developing professionalism are key factors for any employee. Of the respondents, 74% either agreed or strongly agreed on the question that there will be less job security in automotive companies in the future, and believed that gaining experience in project management will help them grow professionally; 87% either agreed or strongly agreed that having taught project management techniques had increased their employability; and, 81% believed that such experiences would help them advance within the company.

The automotive industry is product-driven and, therefore, heavily dependent on innovation. On occasion, innovation and project-based philosophies do not merge well, especially when cost and time are taken into consideration. This study shows that the problem can be addressed by a good project manager; one who is willing to provide encouragement and open communication. Effective conflict management can also help an organization's risk-takers and innovators to develop great ideas and solutions. Of the respondents, 73% either agreed or strongly agreed that their project managers encouraged open communication, and 79% agreed that they also effectively resolved conflicts.

The most obvious outcome from the survey was the fact that 91% of the respondents reported an increase in their workload. The increase in workload was directly related to the number of projects that the employees were working on. However, there are other variables that have some effect on the increase in workload. During the last five years, the domestic automotive industry has shrunk, and companies have laid off thousands of employees. As the industry reorganized and improved financially, companies failed to hire with the same pace. This led to an increase in the workload for their engineers; however, more research is being done on this topic to determine the actual root causes.

There is a specific group within these respondents, those who have supported their own training/education. From this group, 77% were dissatisfied with their job, and 88% reported that they had searched for other jobs in the last six months. However, there was no difference between this group and other respondents in relation to the value added by project management.

Conclusion

Advantages and value from project management in industries is very well documented. Project management had a late start in the automotive industry compared with military and construction management; however, it has reached maturity much quicker, while presenting new project management tools and techniques. This study concentrated on the value project management brings to one of the automotive industry's key stakeholders—the employees. The study highlighted the fact that when automotive companies gain value from project management, employees concurrently extract value, thus creating a win-win situation. Using PCA and descriptive statistics, it was concluded that value for companies may or may not be defined the same for employees. For companies, the value from project management is in the form of improved, well-structured business processes, stronger organizational culture and good leadership. Employees receive a different type of value when they are involved with projects and project management. Their value is more towards their personal satisfaction with their jobs, their loyalty towards their organization and, finally, exposure within their companies that increases their employability.

The study concentrated on automotive companies in Michigan and concluded that the majority were following formal project management processes. Automotive employees gain valuable experience from following project management within their companies, thereby increasing their chances of promotion within the company or gaining better employment elsewhere. It also improves job satisfaction, provides better relationships with management and encourages leadership. It should also be noted that employees who self-finance their training or education are more inclined to change companies and have less loyalty toward their current companies. An important finding was the fact that following

formal project management techniques has encouraged automotive employees to innovate in the product-driven industry by ensuring open communication and encouragement from trained project managers who help risk takers to innovate by effectively managing conflicts.

References

[1] Hillman, A. J., & Keim, G. D. (2001). Shareholder Value, Stakeholder Management, and Social Issues: What's the Bottom Line? *Strategic Management Journal, 22*(2), 125-139.

[2] Kerzner, H. (2004). *Advanced Project Management: Best Practices on Implementation*, (2nd ed.), John Wiley & Sons.

[3] Cooper, R. G. (2001). *Winning at new products.* Perseus Books.

[4] Midler, C., & Navarre, C. (2004). Project Management in the Automotive Industry. In Morris, Peter W.G., Pinto, J. K. (Eds.). *Wiley Guide to Managing Projects*. John Wiley & Sons.

[5] CAR Center for Automotive Research (2010). *Contribution of the automotive industry to the economies of all fifty states and the United States*, AnnArbor MI.

[6] Keenan, T. (1996). Making beautiful music with program management. *Ward's Auto World, 32*(8), 32.

[7] Arminas, D. (2001). Suppliers face extinction over lack of project skills. *Supply Management, 6*(24), 10.

[8] Ellison, D. J., Clark, K. B., Fujimoto T., & Hyun, Y. S. (1995). *Product development performance in the auto industry: 1990s Update*. International Motor vehicle Program, (Working Paper #95-066). Annual Sponsor Meeting, Toronto.

[9] Lenfle, S., & Midler. C. (2002). Innovation-based competition and the dynamics of design in upstream suppliers. *International Journal of Automotive Technology and Management*, *2*(5).

[10] Midler, C., Monnet, J. C., & Neffa, P. (2002). Globalizing the firm through projects: The Case of Renault. *International Journal of Automotive Technology & Management, 2*(1), 24-46.

[11] Niebecker, K., Eager, D., & Kubitza, K. (2008). Improving cross-company project management performance with a collaborative project scorecard. *International Journal of Managing Projects in Business, 1*(3), 368-386.

[12] Barclay, C., & Kweku-MuataOsei, B. (2010). Project performance development framework: An approach for developing performance criteria & measures for information systems (IS) projects. *International Journal of Production Economics, 124*, 272-292.

[13] Ashton, R. H. (2005). Intellectual Capital and Value Creation: A Review. *Journal of Accounting Literature, 24*, 35-134.

[14] Thomas, J., & Mullaly, M. (2008). *Researching the Value of Project Management*. Proj. Mgmt. Institute.

[15] Hurt, M., & Thomas, J. L. (2009). Building Value through sustainable project management offices. *Project Management Journal*, *40*(1), 55-72.

[16] Uffmann, J., Sihn, W., & Warnecke, H-J. (2006). A Concept for Knowledge Transfer between New Product Projects in the Automotive Industry, *CIRP Annals - Manufacturing Technology*, *55*(1), 461-464.

[17] Jung, J. Y. (2009). Operational improvement project management: Categorization and selection. *Journal of International Academy for Case Studies, 15*(4).

[18] Beaume, R., Maniak, R., & Midler, C. (2009). Crossing innovation and product projects management: A comparative analysis in the automotive industry. *International Journal of Project Management*, *27*(2), 166-174.

[19] Sihem, B. M., & Lenfle, S. (2010). Platform Re-use Lessons from the Automotive Industry. *International Journal of Operations & Production Management, 30*(1).

[20] Delaide, K. (2007). Formal and Informal Aspects of Project Management. Retrieved December 01, 2011, from http://e-articles.info/e/a/title/formal-and-informal-aspects-of-project-management

[21] Hurt, M., & Thomas, J. (2009). Building Value Through Sustainable Project Management Offices. *Project Management Journal*, *40*, 55-72.

[22] Ibbs. C. W., & Kwak, Y. H. (2000). Accessing Project Management Maturity, *Project Management Journal*, *31*(1), 32–43.

[23] Current Population Survey, Bureau of Labor Statistics, Table 18: Employed Persons by Detailed Industry, Sex, Race, and Hispanic or Latino Ethnicity, 2011, Annual Averages. Retrieved June 12, 2012 from http://www.bls.gov/cps/tables.ht

[24] Wright, M. (2007, Aug 16). Mind of the engineer. *Electronic Design Network, EDN*. Retrieved June 10, 2012 from http://www.edn.com/electronics-news/4314993/-Mind-of-the-Engineer-yields-range-of-response

Biography

MUHAMMAD SOHAIL AHMED is an Assistant Professor of Engineering Management at Eastern Michigan University. He earned his B.E. (Mechanical Engineering) degree from NED Univ., Karachi Pakistan, MS (Mechanical Engineering, 1992), MS (Manufacturing Engineering, 1996) and Ph.D. (Industrial Engineering, 1999) from Wayne State University. Research interests include Project / Knowledge / Engineering Management, and Engineering Education. He may be reached at mahmed6@emich.edu

PERFORMANCE IMPROVEMENT OF MANETS WITH LINK LIFETIME

Merlinda Drini, Queensborough Community College/CUNY; Tarek Saadawi, City College of New York

Abstract

There are many different factors in the physical layer that impact the performance evaluation of the routing protocols. Such factors consist of signal reception, path loss, fading and interference. With this in mind, a numerical approach based on Finite State Markov Chain channel model was adopted for this study in order to evaluate the performance of an ad hoc routing protocol under various radio propagation models. In this paper, the authors present a new cross-layer algorithm for joint physical and routing layers in wireless ad hoc networks by applying this to the Optimized Link State Routing (OLSR) protocol in order to demonstrate the effectiveness of the Link Lifetime (LLT) and channel quality measured by Signal to Interference and Noise Ratio (SINR) as a metric in the selection of routes. The problem of link and route stability, focusing primarily on the multipoint relay (MPR) selection method, was addressed in order to find the most optimal routes between any pair of nodes. The simulation results indicate that the network throughput is greatly improved and the delay is significantly decreased using this cross-layer mechanism when compared to the original OLSR.

Introduction

Layered networking architecture has been the key to the huge success and widespread use of the Internet, as well as the initial development of wireless systems. The success of layered architecture has been its ability to provide modularity and transparency between the layers. However, in order to support the revolution of new applications, a new era of network architectures has emerged. A major challenge has been to understand at a fundamental level how to best design and control these networks, referred to as "wireless ad hoc networks".

Since human-operated devices will more likely be used indoors, that leads to many issues related to the strength of signal fading in this environment. It has been suggested that a possible interaction might exist between various parameters of the ad hoc networks and, more precisely, between the propagation model and the routing protocol. The focus in this study was on the physical layer, which has a great impact on the performance of the system and which is responsible for the node's connectivity and overall network throughput. This is known as a cross-layer design which, unlike traditional architecture, allows for information exchange between Open System Interconnection (OSI) layers. The cross-layer design is a very promising field of investigation. The use of physical (PHY) layer information in the routing decision, which was implemented in this study, is the result of cross-layer dialogue between the PHY and the Network layers.

The quality of wireless channels among the mobile nodes is time varying, due to fading, shadowing and path loss. Given that the shortest-path metric does not take into account the physical channel variations of the wireless medium, it is desirable to select the routes with minimum cost based on some other metrics which take into account the wireless nature of the underlying physical channel. In Mobile Ad hoc Networks (MANETs) there are many other metrics to be considered: Power, Packet Loss, Maximum available bandwidth, etc. These metrics should come from a cross-layer approach in order to make the routing layer aware of the local issues of the underling layers.

The main contribution of this study is the introduction of link-quality evaluation methodology based on Signal to Interference and Noise Ratio (SINR) and Link Lifetime (LLT) enhanced adaptability of ad hoc routing in a dynamically changing topology. As an example of its applicability to various routing protocols, the usefulness of the Link Lifetime, as a new metric in the selection of routes, was demonstrated to the Optimized Link State Routing (OLSR) protocol [1]. The problem of link and route stability was addressed, focusing particularly on the multipoint relay (MPR) selection method as well as determining the optimal path for any pair of nodes in this protocol.

Related Work

Routing in MANETs (Mobile Ad Hoc Networks) is challenging due to the dynamic nature of network topology and resource constraints. To maximize the channel resource utilization and minimize the network transfer delay along the path, the shortest path with a minimum-hops scheme is often adopted.

DeCouto et al. [2] showed that routing in multi-hop wireless networks using the shortest-path metric is not a sufficient condition to construct good quality paths because minimum-hop-count routing often chooses routes that have significantly less capacity than the best paths that exist in the network. Specifically, the nodes near the center of the network carry high loads when the routing protocol uses a shortest-path route strategy.

Node mobility causes links between nodes to break frequently, thus terminating the lifetime of the routes containing those links. An alternative route has to be discovered once a link is detected as broken, incurring extra route discovery overhead and packet latency. A simple solution for reducing the frequency of this costly discovery procedure is to choose a long lifetime route carefully during the route discovery phase rather than a simple random shortest-path route scheme. Cheng & Heinzelman [3] studied the effect of node mobility in the link lifetime distribution, noting that the smaller the moving probability, p, the longer lifetime a link tends to have. When neither node is moving ($p = 0$), the link never breaks. But in wireless propagation environments, small-scale fading makes it difficult to recognize the node's moving tendency and cannot be simply ignored.

Link lifetime plays an important role in routing protocol design and performance. There has been some investigation into the estimation and predictability of link lifetimes. Bohacek et al. [4] examined many predictors in urban environments; however, such predictors would require knowledge of the location of the node, the path loss across the link and the age of the link.

Route-Lifetime Assessment–Based Routing (RABR) [5] uses an affinity parameter based on the measured rate of change of signal strength averaged over the last few samples in order to estimate the lifetime of a link. A metric combining the affinity parameter and the number of links in the route is then used to select routes for TCP traffic. However, shadow and multipath fading experienced by the received signal make the estimation of link lifetime prone to error.

Singh et al. [6] presented a cross-layer ad hoc routing approach based on link connectivity assessment in network topology and suggest a framework for proactive enhancements to the OLSR protocol. They then deployed an IEEE 802.11b-based vehicular network and demonstrated the effectiveness of link-quality assessment-based enhancements in improving the performance of inter-vehicle ad hoc routing. Every node in the network can maintain the history of averaged Signal to Noise Ratio (SNR) values to its neighbors; then, from the average rate of change of SNR, the affinity between the two nodes can be estimated. Yet, the affinity between two nodes is only a prediction of the lifetime of the link.

Interference Impact on Wireless Channels

The signal transmitted from a mobile node to others loses part of its power along the way. This happens because of the distance it travels and the terrain across which it travels. The radio wave (signal) propagation is generally modeled by the combination of large-scale and small-scale propagation models [7]. Large-scale fading is due to the distance loss and shadowing effects and changes relatively slowly. As the node moves over longer distances, the average signal strength gradually decreases. For this reason, large-scale fading is of interest because the movement tendency of the nodes enables us to discover routes which are more likely to fail. On the other hand, node movement over short distances may cause the rapid variation of the received signal strength, thus giving rise to small-scale fading. Small-scale fading can be modeled by Ricean fading (with line of sight) or Rayleigh fading (with no line of sight).

In a wireless ad hoc network, because nodes share a common channel, interference usually has a greater impact than noise [8]. In addition, thanks to in-band transmissions from nodes that are out of range but close enough to cause interference as well as crosstalk from near-band transmissions, the interference level can have large, rapidly changing values. Hence, the focus of this study was on SINR rather than SNR.

Computation of interference and noise at each receiver is a critical factor in wireless communication modeling, as this computation becomes the basis of SINR or SNR that has a strong correlation with PER (Packet Error Rate) on the channel. The power of interference and noise is calculated as the sum of all signals on the channel, other than the one being received by the radio, plus the thermal (receiver) noise. The resulting power is used as the base of SNR, which determines the probability of successful signal reception for a given packet [9].

Thus, communication between two nodes u and v is successful if the SINR at receiver v is above a certain threshold which depends on the desired transmission characteristics (e.g., channel, data rate, etc.). More formally, denoting the signal strength of a packet from node u (sender) at node v (receiver) by $Pv(u)$, a packet on the link (u,v) from node u to node v is correctly received if and only if SINR is above a certain threshold:

$$SINR = \frac{P_v(u)}{N + \Sigma_{w \in v'} P_v(w)} \geq \delta \quad (1)$$

where N is the background noise, v' is the set of nodes simultaneously transmitting, and δ is a constant which depends on the data rate, channel characteristics, modulation scheme, etc.

Since in a realistic channel the interference cannot be excluded, SINR will hereafter be referred to as SNR. Accordingly, N represents the background noise plus the total interference of all neighboring transmissions.

Modeling Wireless Channels with a Three-State Markov Model

In this study, the work by Rayleigh [10] on fading channel was considered; therefore, the received signal is the sum of signals with different phases caused by different paths, which can be modeled as a random variable. In a multipath propagation environment with additive Gaussian noise, the received SNR also has the Rayleigh distribution with the probability density function:

$$p(\gamma) = \frac{1}{\bar{\gamma}} \exp\left(-\frac{\gamma}{\bar{\gamma}}\right) \quad (2)$$

where γ is the received SNR and $\bar{\gamma}$ is the average SNR, which is physical layer dependent. Given the physical layer conditions, the average received SNR enables us to characterize the channel variation at the physical layer using the Finite State Markov Chain channel model, known as FSMC.

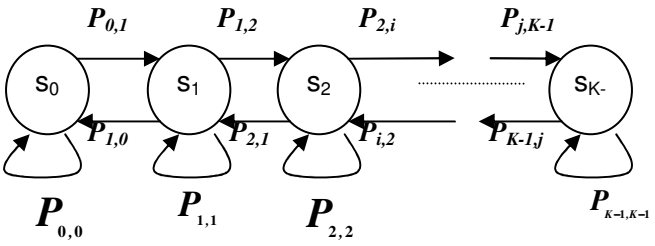

Figure 1. Graphical Representation of Finite-State Markov Chain (FSMC)

In order to build the FSMC, it was assumed that the received SNR remains at a certain level for the duration of a packet; therefore, a received packet completely falls in one state and the following packet only stays in the current state or one of the two neighboring states. As a result, the range of the SNR can be partitioned into a finite number of intervals with corresponding states [10]. The channel is said to be in state k, if SNR remains between two thresholds of average SNR: [Γk,Γk+1]. The state space of a stationary Markov chain with K states is denoted by S=s1,s2,…,sK. State space S is that of K different channel states with corresponding SNR thresholds, Γk, in increasing order [11].

$$0 = \Gamma_0 < \Gamma_1 < \Gamma_2 < \cdots < \Gamma_{K-1} < \Gamma_K = \infty \quad (3)$$

Steady-state probabilities can be calculated from the following expression:

$$\pi_{kk} = \int_{\Gamma_k}^{\Gamma_{k+1}} p(\gamma) d\gamma = \exp\left(-\frac{\Gamma_k}{\bar{\gamma}}\right) - \exp\left(-\frac{\Gamma_{k+1}}{\bar{\gamma}}\right) \quad (4)$$

Considering the mobility of the nodes, their motion of a certain speed causes the Doppler frequency, f_m, the number of times that the received signal crosses the given threshold, Γ_k, in the positive or negative direction only, is known as the level crossing rate of level Γ_k and is given by:

$$N(\Gamma_k) = \sqrt{\frac{2\pi\Gamma_k}{\bar{\gamma}}} f_m \exp\left(-\frac{\Gamma_k}{\bar{\gamma}}\right) \quad (5)$$

$$f_m = \frac{f_c v}{c} \quad (6)$$

where f_c is the carrier frequency, v speed of the node and c is the speed of light. Thus, the transition probabilities from state s_k to state s_{k+1}, $P_{k,k+1}$ can be expressed as a ratio of the level crossing rate at threshold Γ_{k+1} and the average number of signal segments per second staying in state s_k.

The transition probabilities can be approximated as

$$\begin{aligned} P_{k,k+1} &= \frac{N(\Gamma_{k+1})T_p}{\pi_{kk}}, \quad k = 1,2,...,K-1 \\ P_{k,k-1} &= \frac{N(\Gamma_k)T_p}{\pi_{kk}}, \quad k = 2,3,...,K \end{aligned} \quad (7)$$

where T_p is the packet transmission time. Packet transmission time can be obtained as a ratio of the packet size and the effective network bandwidth. Consequently, knowing the transition probabilities, probabilities of staying in the same state, can be calculated as

$$P_{kk} = \begin{cases} 1 - P_{k,k+1} - P_{k,K-1}, & if \quad 0 < k < K \\ 1 - P_{01}, & if \quad k = 0 \\ 1 - P_{K,K-1}, & if \quad k = K \end{cases} \quad (8)$$

and

$$P_C = \left\lfloor P_{ij} \right\rfloor_{(K+1)x(K+1)} \quad (9)$$

where P_c is the transition matrix of the FSMC model for the wireless channel.

For simplicity, the approach taken in this study used a three-state Markov chain model (see Figure 2), where there are two good states: "Excellent" and "Fair", and a single bad state, "Bad". It was assumed that the situation in which the success of a packet transmission in a given state would be determined by comparing the received SNR to the thresholds in each state, each of which having a certain packet error probability (PER) [12]. The transition probabilities are given as a ratio of level crossing rate at a certain SNR threshold and the number of signal segments per second, staying at the next state.

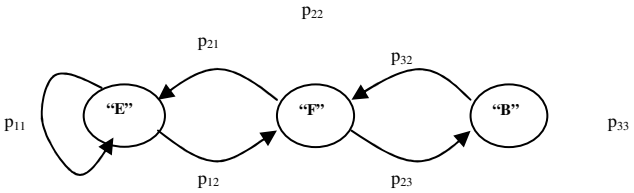

Figure 2. Three-State Markov Model

Hence, the transition probabilities, as given in Equations (7)-(9) are now given by the following matrix:

$$\boldsymbol{P} = \begin{bmatrix} \boldsymbol{p}_{11} & \boldsymbol{p}_{12} & \boldsymbol{p}_{13} \\ \boldsymbol{p}_{21} & \boldsymbol{p}_{22} & \boldsymbol{p}_{23} \\ \boldsymbol{p}_{31} & \boldsymbol{p}_{32} & \boldsymbol{p}_{33} \end{bmatrix} = \begin{bmatrix} p_{EE} & 1-p_{EE} & 0 \\ p_{FE} & p_{FF} & 1-p_{FE}-p_{EF} \\ 0 & 1-p_{BB} & p_{BB} \end{bmatrix} \quad (10)$$

Once these transition probabilities are determined, the mean sojourn time that the channel remains in either of the two good states, "Excellent" or "Fair", can be calculated:

$$T = \frac{T_p}{1-P_{GG}} \quad (11)$$

where T_p is the packet transmission time and

$$P_{GG} = P_{EE} + P_{FF} \quad (12)$$

Design of an OLSR Routing Protocol with Cross-Layer Design

To demonstrate this approach, the authors applied it to a typical routing algorithm, choosing an Optimized Link State Routing protocol (OLSR) as an example of a table-driven proactive routing protocol.

Overview of Optimized Link State Routing Protocol (OLSR)

Optimized Link State Protocol (OLSR) [1] is a proactive routing protocol, so the routes are always immediately available when needed. OLSR is an optimization version of a pure link state protocol, where the topological changes cause the flooding of the topological information to all available hosts in the network. Using Multipoint Relays (MPR) can reduce the possible overhead in the network protocol. The idea of MPR is to reduce flooding of broadcasts by reducing the same broadcast in some regions in the network. MPRs can also provide the shortest path. Reducing the time interval for the control messages transmission can also bring more reactivity to the topological changes.

OLSR uses two kinds of the control messages: HELLO and Topology Control (TC). HELLO messages are used for finding information about the link status and the host's neighbors. With the HELLO message, the MPR selector set is constructed which describes which neighbors have chosen this host to act as MPR; from this information, the host can calculate its own set of the MPRs. The HELLO messages are sent only one hop away but the TC messages are broadcast throughout the entire network.

TC messages are used for broadcasting information about their own advertised neighbors, which includes at least the MPR selector list. The TC messages are broadcast periodically and only the MPR hosts can forward the TC messages.

Neighbor/Route Discovery

A node sends a HELLO message to identify itself and to report a list of neighboring mobile nodes. From a HELLO message, the mobile node receives information about its immediate neighbors and 2-hop neighbors, and selects MPRs accordingly. A TC message originates at an MPR node announcing who has selected it as an MPR. Such messages are relayed by other MPRs throughout the entire network, enabling the remote nodes to discover the links between an MPR and its selectors. Periodic HELLO messages are used to establish neighbor links and to distribute MPRs determined by the algorithm. MPR nodes are selected nodes that have connectivity to other nodes. These nodes have two main advantages:

- Reduce the amount of flooded messages.
- Find the shortest path.

With the reduction in control messages, the OLSR can react quickly to topological changes.

OLSR with Cross-Layer Design (CLD)

In this section, the routing algorithm, which selects the route that provides a higher SNR along its hops to the destination, is presented. When a node is initially detected via a HELLO message, it is entered into the neighbor table, but it is selected as an MPR and broadcast to other nodes via HELLO messages only if the SNR to this neighbor is found to be above the SNR threshold. Since the wireless channel with a three-state Markov model was used in this study, two SNR thresholds were considered. Thus, if the SNR of the link is found to be higher than the first threshold, the link is considered "Excellent"; but, if its SNR is between two thresholds, that node is selected as the MPR according to the lifetime of the link. This neighbor is considered during routing table calculations.

The variations in signal strength (see Figure 3) affect ad hoc network protocols in a way that differs from other wired network architectures. For example, in regards to the SNR value, a link may be considered "Excellent", though not long lived. In mobile ad hoc networks, the impact of mobility on the link and route lifetimes is of major importance for the design of efficient MAC and network layer protocols [13].

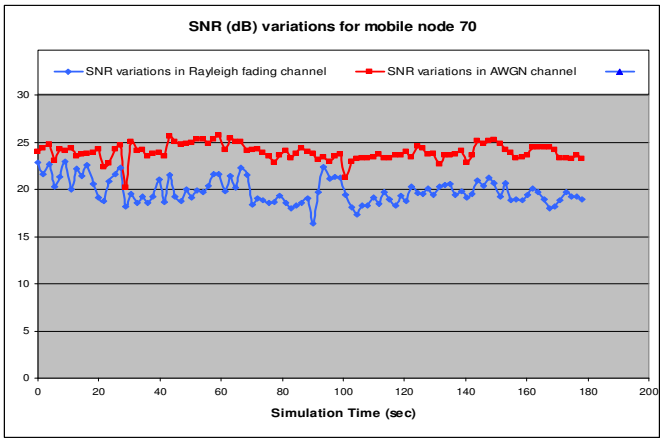

Figure 3. SNR Variations in Time for a Specific Receiver-Node 70. (NOTE: This figure was obtained from the OPNET simulator, which already has an upgraded program for calculating the SNR statistic)

In this study, a solution to this problem was proposed by introducing a special algorithm dedicated to Link-Lifetime (LLT) estimation, which is based on the use of the normalized mean sojourn time in the determination of the LLT. This value is normalized based on the maximum holding time of the routing table of the protocol. Besides this, the direction of the movement of the sending and receiving node can be determined by comparison of the previous SNR value already stored in the neighbor table and the newly received SNR values. If the existing value is lower than the one received, it can be said that the nodes are approaching each other. This mechanism is very efficient in calculating the stability of the link. Thus, in the CLD mechanism, the authors considered two constraints which together characterize the new metric: stability.

The control packets HELLO and TC are generated in a similar way. However, the HELLO packets, along with neighbor sensing, are now used to calculate the LLT based on the link SNR experienced during transmission from the neighbors. Using this information, MPRs are selected among the one-hop neighbors to reach all of the two-hop neighbors with the maximum LLT and SNR as a new metric. MPRs, in turn, transmit TC messages with link quality and LLT information to all the nodes in the network. This metric further is used as a criterion in computing the routes between a source and the destination pair.

Each node in the network periodically generates HELLO messages and transmits to all of the one-hop neighbors. However, in the HELLO message's header, two more fields are included: SNR and the speed of the source node for calculating the LLT metric. When a HELLO packet is received by a node, the SNR value is stored in the neighbor table. Besides, according to the speed of the source node and the previous SNR, the LLT of the link is computed by each node. This information is treated as the stability of the link and is recorded in the neighbor table, too.

The criteria for MPR selection in OLSR with CLD protocol are to consider the SNR level of the one-hop nodes as a link quality metric, and to select maximum lifetime links in order to increase their stability.

The MPR selection algorithm can be described as follows:

- In the empty set of MPRs, first identify all two-hop neighbors of a node *u*, which have only one neighbor in the one-hop neighbor set, and add those nodes to the MPR set. If there are multiple neighbors from node *u*, select that neighbor as the MPR, which results in the greatest stability, or the maximum SNR and LLT.
- Each node in the network that is selected as an MPR, by at least one of its neighbors transmits a TC message periodically. The TC messages from the algorithm in this study were modified to include the link quality and LLT between the MPR node and its selectors. TC messages are forwarded through the network like typical broadcast messages from the MPRs. Since only the MPRs generate the TC messages that contain link stability infor-

mation, the overhead of the transmission is reduced significantly, in contrast to the traditional OLSR protocol.

- In the topology table of the nodes, each node maintains information about the SNR and LLT obtained from the TC messages. The routing table calculation is based on this information. The routing table of a node enables it to route packets for other destinations in the network. It consists of entries such as the destination address, next-hop address and the path lifetime from the source to the destination.
- The path lifetime, moreover, is calculated as the minimum lifetime of the consisting links.

This prevents calculation of routes passing through a weak link and this information being disseminated to other nodes in the network. Thus, only nodes which are connected to neighbors with high-quality links—the highest SNR and LLT—process the control and overhead information.

As an example, let us consider a network topology extended with the two metrics which constitute the SNR and LLT of the links. The letters indicate the link status and the number along the lines indicate the LLT of the links in a successful transmission from a node to a neighbor node. The idea behind this is to select the MPRs in a way such that all the two-hop neighbors have the maximum lifetime of a path through the MPRs to the current node.

Now, show how node S selects its MPRs based on the network depicted in Figure 4. For source node, S, there are two different routes: S-2-7-10-11-16-18-D and S-3-6-12-11-15-17-D. By the traditional method, the first route will be selected. But this is not the most stable route. Let us start with the route selection on a link-by-link basis. Node S has five possible routes: S-1-8, S-2-8, S-2-7, S-3-6, S-3-7 but it selects the highest SNR and maximum lifetime route, S-3-6. To reach 6, S selects 3 as its MPR. Then, to reach 8, it selects 2 as its MPR. By following the same procedure to reach 5, 12 and 13, node 6 is selected as its MPR. To reach 8, 9 or 10, 7 is selected as its MPR. To reach 15, nodes 12 or 13 may be selected as its MPRs. But it accomplishes the best route if it selects node 12 as its MPR. Furthermore, to reach 16, node 11 or 15 may be selected as its MPR. Using the algorithm described above, node 11 is selected as its MPR. And, to reach D, node17 is selected as its MPR.

Simulation of the OLSR Protocol

Presented here are the results using the scenario investigating the performance benefits of the OLSR with CLD in wireless mobile environments. All of the nodes in the network are configured to work under an ad hoc mode. In this study, the IEEE 802.11 Wireless LAN model with the ad hoc network configuration was used.

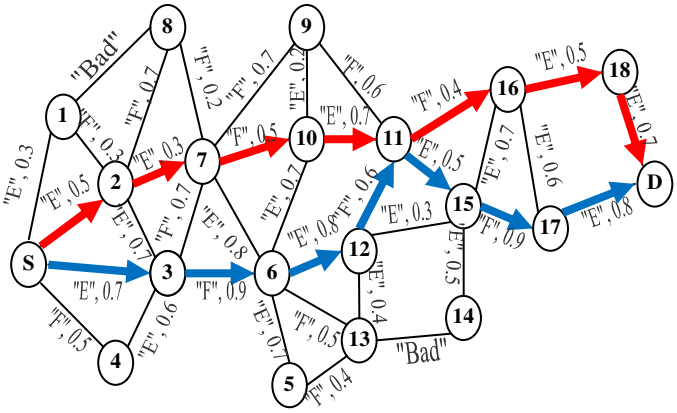

Figure 4. Route Selection in the OLSR with SNR Route Selection with SNR and LLT Metrics

A network of size 1000x1000 m^2 was chosen, but the size of the network is not restricted. The nodes in this current scenario were mobile but the position of the wireless nodes was arbitrarily chosen (see Figure 5). The mobility assigned to each node during simulation within OPNET is an important factor in the performance of the protocol. Each node is assigned a trajectory, which is generated from the traffic simulator. This will provide realistic node movement. Mobility of a mobile node generates a Doppler shift, which is a key parameter of fading channel.

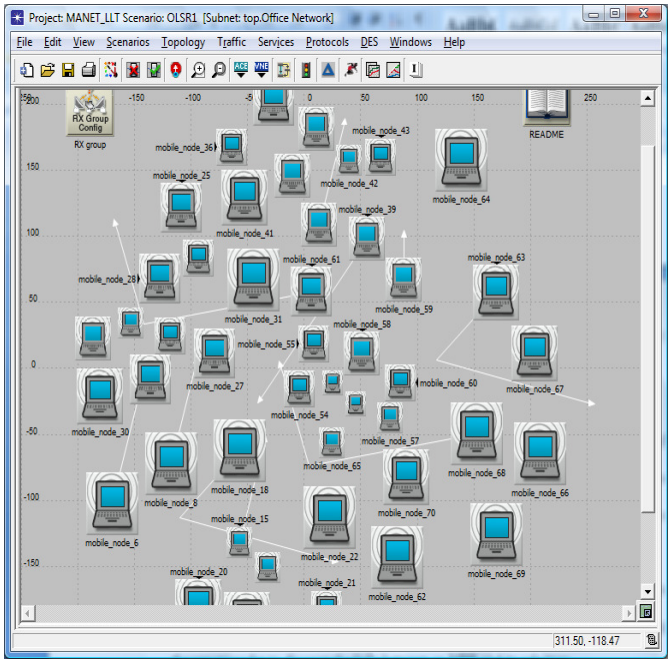

Figure 5. Simulation Scenario in OPNET

While propagation models such as fading, shadowing and path loss are not part of the radio models in simulators, they control the input given to the physical layer models and have a great impact on their performance. All other parameters of this scenario can be seen in Table 1.

Table 1. Parameter Values in the Simulations

Parameters	Value
Modulation Scheme	BPSK
Traffic rate	1 Mbps
Radio Tx Power	0.005 W
Mobility model	Random-Waypoint
Propagation model	Rayleigh fading
MAC protocol	802.11
Packet size	512 bytes
Routing protocol	OLSR
Carrier Frequency	2.4 GHz
Terrain dimensions	1000mx1000m
Simulation time	180 s
Nodes number	100
Traffic	CBR
SNR Thresholds	22[dB] / 17[dB]
Transmission Range	250 m
Speed	1-20 m/s

The simulation model in this study used OPNET Network simulation tools [14]. By default, OPNET assumes that a Gaussian channel model is being used and does not consider any fading. The Gaussian channel is a much more idealized environment for communication than a fading channel. For any SNIR of practical interest, the bit error rate (BER) in a fading channel is much higher than that of a Gaussian channel. Consequently, it is difficult to simulate some prominent wireless communication effects such as path loss, fading and shadowing in OPNET. To solve this problem, the authors added a Rayleigh fading channel model to OPNET and implemented the fading effect in the simulation by modifying the transceiver pipeline stages. Second, it was found that the OPNET Wireless Suite uses a fixed value of the path-loss exponent without considering that different environments have different path-loss exponents. In this study's enhanced wireless model, different path-loss exponents and the shadowing effect were added, again implemented as a function in pipeline stages.

Simulation results of the OLSR protocol performance (Figures 6-9) verify the physical-layer enhanced wireless models used in this study and display their application in the OPNET simulator. The remainder of this section focuses on the cross-layer enhancement of the routing protocol, taking into account only the simulation of the Rayleigh fading channel.

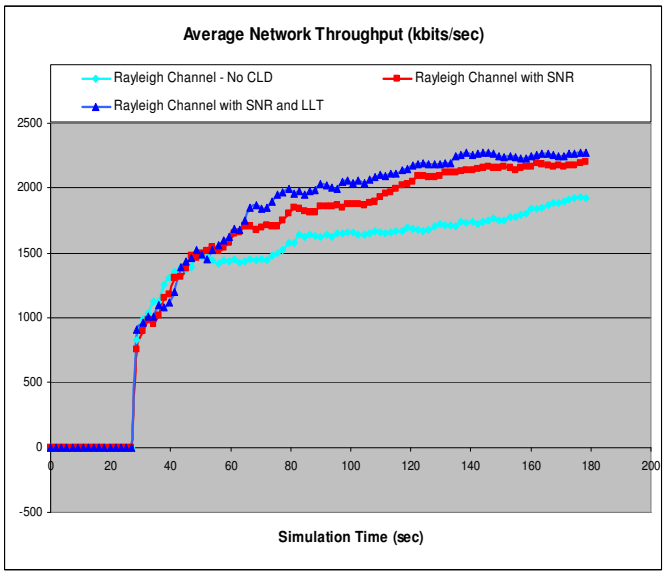

Figure 6. Network Throughput versus Simulation Time in the Rayleigh Fading Channel (NOTE: The simulation was done for a short period of time as the purpose was to see the impact of the physical layer in the higher layers; thus, this time is not enough to reach the stationary state)

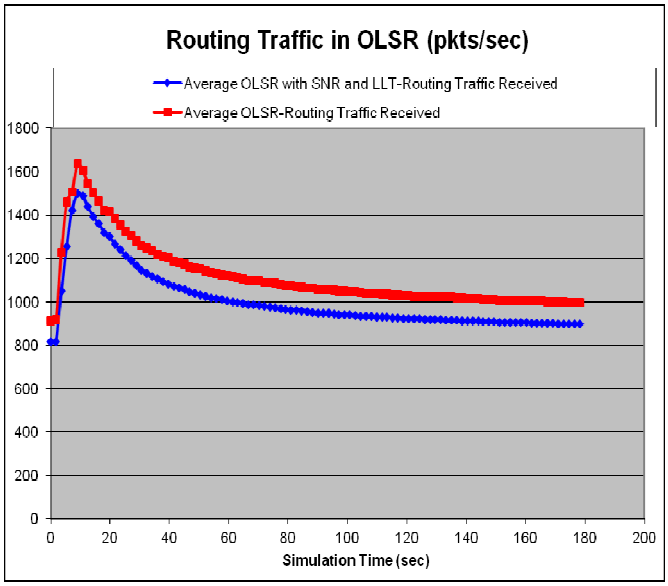

Figure 7. Routing Traffic in the OLSR and OLSR with SNR-LLT

Simulation results show that the OLSR protocol with CLD yields better performance compared to the best-effort OLSR protocol, and significantly improves throughput by using the algorithm proposed here. From Figure 6 it can be seen that the cross-layer use encourages transmission over more stable links, thereby achieving higher throughput values. On the contrary, transmission over the poor channel conditions with low LLT leads to transmissions with errors and higher routing traffic (see Figure 7). As expected, fewer losses in OLSR with CLD was seen as the metric proposed here favors minimum loss paths. In addition, the packet transmission time will be reduced, leading to a smaller average delay. The original OLSR protocol has frequent route changes, which has a negative impact on the delay performance because of the time needed for the nodes to update their routing tables (see Figure 8).

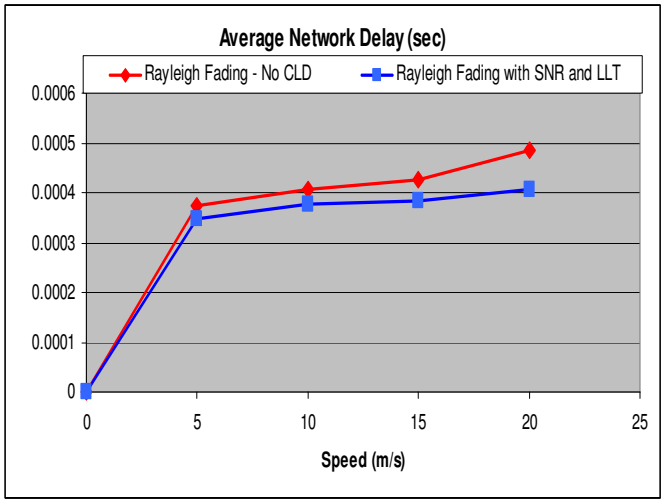

Figure 8. Average Network Delay in Seconds versus Mobility Speed (NOTE: As the delay cannot be zero, this value was not simulated for the static network)

The ability of a routing protocol to scale networks is highly dependent on its ability to control routing traffic overhead. When links are chosen with good quality and stability, fewer TC messages will be sent, which causes a lower number of MPRs to be selected (see Figure 9). The main function of the Multipoint Relay (MPR) of the Optimized Link State Routing protocol is to reduce the flooding overhead compared with classic flooding. When an OLSR protocol has fewer MPRs, the coverage of the TC broadcast traffic is narrower and adjacent nodes will be receiving less routing traffic.

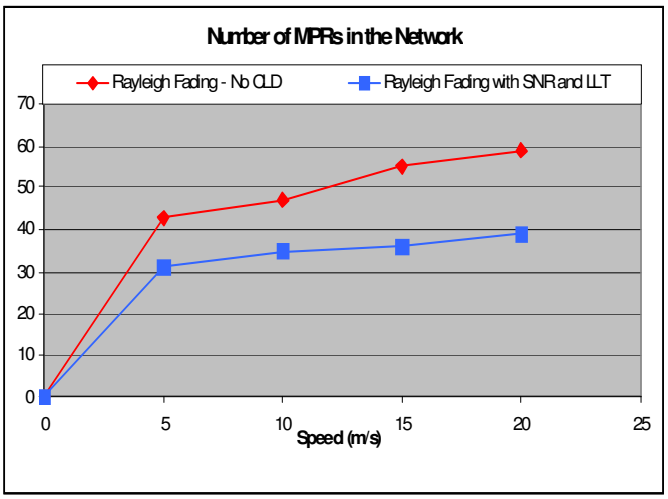

Figure 9. Number of MPRs in the Network versus Mobility Speed

Conclusion

Using the aforementioned Rayleigh fading and shadowing model, and considering interference, the authors make the following contributions:

A network architecture that supports QoS in wireless ad hoc networks using an algorithm which monitors the channel conditions during data transmission and feeds this information to the routing layer. The motivation for this study was to explore routing protocols with a cross-layer design and present the benefits of this approach with its impact on the transport layer and overall network.

This study also showed how network throughput behaves for different pathloss models. Moreover, the results indicate that the network throughput under the multipath fading and shadowing is far less than that under the free-space pathloss model, which is used in the majority of existing studies. But it can be greatly improved by using the cross-layer architecture. The goal of this study was not only to find a route from a source to a destination, but an optimal route that satisfies the end-to-end QoS requirement, in terms of quality and lifetime.

References

[1] Clausen, T., & Jacquet, P. (2003). Optimized Link State Routing Protocol. Retrieved from http://tools.ietf.org/html/draft-ietf-manet-olsr-1

[2] DeCouto, D. S. J., Aguayo, D., Chambers, B. A., & Morris, R. (2002). Performance of multi-hop wireless networks: Shortest path is not enough. *Proceedings*

of the First Workshop on Hot Topics in Networks, HotNets-I.

[3] Ishibashi, B., & Boutaba, R. (2005). Topology and Mobility Considerations in Mobile Ad Hoc Networks. *Ad Hoc Networks, 3,* 762-776.

[4] Cheng, Z., & Heinzelman, W. B. (2004). Exploring Long Lifetime Routing (LLR) in Ad Hoc Networks. *7th ACM International Symposium on Modeling, Analysis and Simulation of Wireless and Mobile Systems,* (pp. 203–210).

[5] Samar, P., & Wicker, S. B. (2006). Link Dynamics and Protocol Design in a Multihop Mobile Environment. *IEEE Transactions on Mobile Computing*, *5* (9), 1156-1172.

[6] Bohacek, S., Ilic, A., & Sridhara, V. (2005). On the Predictability of Link Lifetimes in Urban MANETs. *3rd International Symposium on Modeling and Optimization in Mobile, Ad Hoc and Wireless Networks*, (pp. 209-218). WiOpt.

[7] Agarwal, S., Ahuja, A., Singh, J. P., & Shorey, R. (2000). Route-Lifetime Assessment Based Routing (RABR) Protocol for Mobile Ad Hoc Networks, *Proceedings of the IEEE International Conference on Communications (ICC)*), *3*, 1697–1701.

[8] Singh, J. P., Bambos, N., Srinivasan, B., & Clawin, D. (2006). Cross-layer Multi-hop Wireless Routing for Inter-Vehicle Communication. *2nd International Conference on Testbeds & Research Infrastructures for the Development of Networks & Communities*, (pp. 100-101). TRIDENTCOM

[9] Rappaport, T. S. (2002). *Wireless Communications: Principles and Practice.* Prentice Hall. ISBN #0-13-042232-0.

[10] Avestimehr, A. S., Diggavi, S. N., & Tse, D. N. C. (2007). A Deterministic Model for Wireless Relay Networks and its Capacity. *Proceedings of Allerton Conference*, (pp. 6-11).

[11] Takai, M., Martin, J., & Bagrodia, R. (2001). Effects of Wireless Physical Layer Modeling in Mobile Ad Hoc Networks. *Proceedings of the 2nd ACM International Symposium on Mobile Ad Hoc Networking & Computing*, (pp. 87-94). Mobihoc

[12] Zhang, Q., & Kassam, S. A. (1999). Finite-State Markov Model for Rayleigh Fading Channels. *IEEE transactions on communications*, *47*(11), 1688-1692.

[13] Su, W., Lee, S. J., & Gerla, M. (2001). Mobility Prediction and Routing in Ad Hoc Wireless Networks. *International Journal of Network Management*, *11* (1), 3–30.

[14] Drini, M., & Saadawi, T. (2008). Modeling Wireless Channel for Ad Hoc Network Routing Protocol. *The IEEE symposium on Computers and Communications ISCC*, (pp. 549-555). Marakech Marocco.

[15] Ermel, E., & Muehlethaler, P. (2006). *Using OLSR Multipoint Relays (MPRs) to estimate node positions in a Wireless Mesh Network*. Research Report, INRIA.

[16] Villanueva-Pena, P. E., & Kunz, T. (2006). Extending Network Knowledge: Making OLSR A Quality Of Service Conducive Protocol. *Proceedings of the International Conference on Communications and Mobile Computing*, (pp. 103-108). IWCMC, Vancouver, Canada.

[17] Lenders, V., Wagner, J., & May, M. (2006). Analyzing the Impact of Mobility in Ad Hoc Networks. *International Symposium on Mobile Ad Hoc Networking & Computing*, (pp. 39–46).

[18] The OPNET simulator. (2010, April 10). Retrieved from www.opnet.com

Biographies

MERLINDA DRINI, Assistant Professor in Engineering Technology Department of Queensborough CC/ CUNY. She earned PhD in Electrical Engineering, The City University of New York, (June 2009), M. of Phil. (February 2007) and M. E. in Electrical Engineering Department, The City University of New York, City College (June 2004). Her research interests lie in the area of wireless networking, with emphasis on cross-layer design in ad-hoc networks, with focus on the interactions among PHY, MAC and Network Layers.

TAREK N. SAADAWI. Since 1980 Dr. Saadawi has been with the Electrical Engineering Department, The City University of New York, City College where he currently directs the Information Networking and Telecommunications group at CCNY. His current research interests are telecommunications networks, high-speed networks, multimedia networks, AD-HOC networks and packet radio networks. He has published extensively in the area of telecommunications networks. He is a Co-author of the book, "Fundamentals of Telecommunication Networks," John Wiley & Sons, 1994. Dr. Saadawi is a Former Chairman of IEEE Computer Society of New York City and received IEEE Region 1 Award.

PREDICTION OF CHAMBER PRESSURE FOR A MACH 4 SUPERSONIC WIND TUNNEL

Z.T. Deng, Xiaoqing Qian and Dave Pett, Alabama A&M University; Dan Rodgerson, AeroLab LLC

Abstract

A variable-Mach-number supersonic wind tunnel capable of producing up to Mach 4 with a 6"x6" test section was installed at Alabama A&M University. This wind tunnel is a blow-down type which requires the compressed air to be provided through large external tanks. The compressed air is delivered to the test section through large-diameter high-pressure pipes with control valves. The test section Mach number is controlled by a variable throat area using two solid nozzle blocks with the lower nozzle block movable in the flow direction with respect to the upper nozzle block. The air is then discharged at ambient air pressure through a vertical exhaust pipe. One of the critical operational parameters is the chamber pressure. To reach steady supersonic speeds in the test section, chamber pressure has to be high enough to push out the starting shockwaves in the tunnel. Parametric studies using computational fluid dynamics simulations were conducted for a series of chamber pressures and nozzle throat areas (area ratios). Results indicated that it is very difficult to reach Mach 3.5 to Mach 4 test conditions if chamber pressure is below 120psi. In order to obtain a shockwave-free (clean) supersonic test section with a Mach number ranging from 3.5 to 4.0, it is recommended that the optimum chamber pressure be about 170psi.

Introduction

The variable-Mach-number supersonic wind tunnel at Alabama A&M University (AAMU) is of the blow-down type. It was designed and manufactured by AEROLAB [1]. The air is compressed through an external compressor and is then stored in three large air tanks. The wind tunnel compressed air system is installed on a 1,200ft² concrete pad. The compressed-air system provides one thousand cubic feet (7,500 gal.) of dry air at 200psi. The system is designed to charge three storage/discharge tanks from atmospheric pressure (~14.7psi) to 200psi in less than one hour in order to accommodate rapid-turn-around test sequences. The tanks are capable of combined or individual discharge. Isolation valves are installed between the storage/discharge tanks and all components in the system for isolation of operation, maintenance and repair. Figure 1 shows the compressed-air supply system. The high-pressure, room-temperature air is then discharged through a large-diameter, high-pressure pipe and inlet diffuser to a mixing chamber and to create an air supply to the supersonic wind tunnel. The high-pressure air is then accelerated through a converging-diverging nozzle to provide Mach 4 speed at the inlet of the test section. The inlet of the test section is 6"x6" square. The converging-diverging nozzle upstream of the test section inlet has a variable throat area in order to provide supersonic flows with variable-test-section inlet Mach number. The air is then discharged at subsonic speeds and enters a large-diameter vertical exhaust pipe at ambient pressures. Figure 2 shows the supersonic wind tunnel system.

Figure 1. External Compressed-Air Supply System

Figure 2. Supersonic Wind Tunnel System at AAMU

The inlet valve and nozzle block are processor controlled. An electromechanical inlet valve controls inlet air pressure.

The valve automatically terminates the test run when inlet pressure falls to within 10psi of the required inlet chamber pressure. A stagnation tank containing baffle plates and turbulence-reducing screens conditions inlet air. The establishment of the critical chamber pressure is crucial to the success of the tunnel operation.

The wind tunnel employs a sliding-nozzle-block design with the lower block adjustable in position with respect to the upper block, as shown in Figure 3.

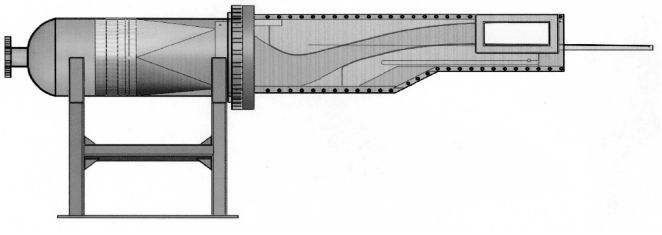

Figure 3. Moving Lower Nozzle Block

Nozzle contours are electrically adjusted through a linear actuator, as shown in Figure 4. Adjusting the lower nozzle block will change nozzle throat diameter and, in turn, change the test-volume-inlet Mach number. The sliding block design provides a continuous Mach number between 1.3 and 4.

Figure 4. Control of the Lower Nozzle Block Through a Linear Actuator

The design test Mach number ranges from 1.3 to 4.0. The wind tunnel test section and observation windows have fixed inlet dimensions of 6”W x 6”H x 18”L, as shown in Figure 5. According to isentropic theory [2], the test-volume -inlet Mach number can be determined solely based on the area ratio between nozzle exit and nozzle throat. However, the starting process of the supersonic wind tunnel requires high power to overcome the normal shock loss [3] and, in general, the higher the test Mach number, the higher the power requirement. This power requirement can be interpreted as the ratio of the necessary stagnation pressure to diffusor exit ambient pressure. With the normal shock in the test section, the theoretical compression ratio between stagnation chamber pressure and diffusor exit pressure ranges from 1 to approximately 7.5 for testing Mach numbers between 1 and 4 [3]. The probable maximum needed for starting of supersonic wind tunnel at Mach 4 is approximately 15, which is equivalent to a pressure of 220psi with respect to standard air exhaust. When flow becomes steady, the probable minimum needed for running the tunnel at Mach 4 is about 6. In practice, the parameters affecting the test-volume Mach number are throat area, chamber pressure, flow quality and starting, and back pressure [4-8]. The Mach number at the test-section inlet of the supersonic wind tunnel is locked by the area ratio once supersonic flow is established in the test section. If chamber pressure increases above the minimum required pressure, the test-section Mach number will not change. However, if the chamber pressure is low enough, the normal shockwave may not be pushed out of the test section and a clean supersonic flow may not be established at the desired area ratio. The objective of this study was to numerically predict the minimum operational chamber pressure requirement for AAMU’s Mach 4 supersonic wind tunnel, under different test-volume Mach numbers.

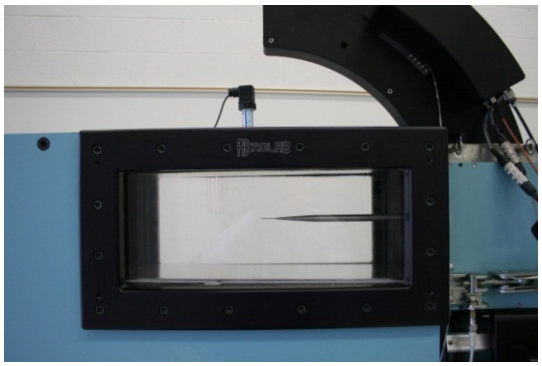

Figure 5. 6”x6”x18” Test Volume and Observation Window

Numerical Procedures

The ideal test-volume-inlet Mach number can be calculated based on isentropic theory using area ratio, as in Figure 6. It is possible to reach Mach 4 speed with an area ratio close to 11. But, with viscous effects, the ideal prediction does not provide an accurate prediction of Mach number for the supersonic wind tunnel. The full Navier-Stokes equations must be solved for the entire flow field in order to obtain realistic test-volume flow characteristics.

In the current study, computational fluid dynamics (CFD) simulations were conducted using WIND code [9]. This CFD tool solves Reynolds-Averaged Full Navier-Stokes (RANS) equations with conventional laminar or turbulent models. It was observed that the prediction of the test-volume Mach number depends on specification of down-

stream conditions for both Laminar and turbulent-flow simulation models. To select appropriate flow model and boundary conditions, a series of one-zone simulations were conducted. In these calculations, air was discharged at ambient pressures from the diffusor exit. As indicated in Figure 7(a-c), various exit boundary conditions were applied with Laminar and/or turbulent-flow assumptions. Boundary layers were very thick and flow separation inside the diffuser was obvious.

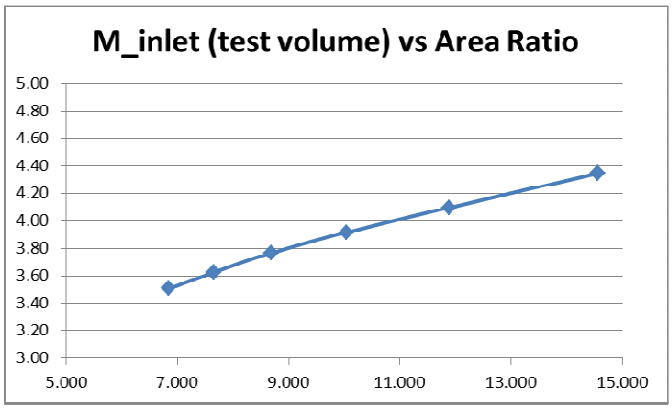

Figure 6. Ideal Design Mach Number at the Inlet of Test Volume as a Function of Area Ratio

It was observed that if downstream boundary conditions were relaxed to be pure extrapolation of pressure, a complete supersonic expansion was obtained, as indicated in Figure 7(d), even in the downstream diffuser section causing exit pressure to be near vacuum. This un-realistic condition cannot be achieved in the experiment at room condition laboratory. This suggested that conventional boundary conditions may not be accurate if the vertical exhaust-pipe configuration is neglected. A realistic vertical pipe configuration has to be considered. Multi-zone computation is needed. Apparently, the selection of a laminar model inside the diffuser section created inaccurate Mach number distributions. It was observed that the turbulent models used in the prediction play important roles in controlling wall boundary layers. A suitable turbulent model inside the wind tunnel must be selected for the simulation. Extensive simulation was performed in order to select a valid turbulent model. The turbulent models used in the prediction play important roles in controlling wall boundary layer growth. It was concluded that the Spalart turbulent model was good for the present flow simulation using the existing RANS solver.

Results and Discussion

The two-zone computational domain was created to compute air flow from the inlet of the stagnation settling chamber to the vertical exhaust pipe exit. Figure 8 shows zone 1 of the computational domain covering flows from the inlet to the diffusor exit of the wind tunnel. According to the theoretical prediction [2], if the ambient pressure is the standard 14.7psi, the operational chamber pressure should then range from 110 to 220psi in order to reach Mach 3-4 test conditions. As a result of this, a group of representative chamber pressures of 180, 160 and 120psi were selected for the CFD simulation. The pressure at the vertical exhaust pipe exit was considered to be standard air and fixed at 14.7psi. The area ratio was computed as the ratio of test-volume inlet to nozzle throat. The area ratio between test-volume inlet and control-nozzle throat were selected from 6.8 to 14.6, according to the wind tunnel configurations. The corresponding test Mach number ranged from 3.5 to 4.0. Table 1 shows the simulation parameter matrix in terms of chamber pressure and area ratio. It was extracted from relative positions between upper and lower nozzle blocks based on the CAD geometry. A combination of 18 simulation cases were conducted.

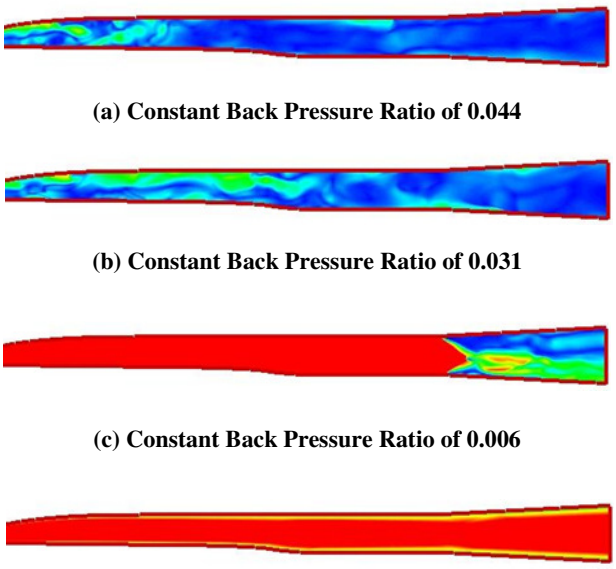

(a) Constant Back Pressure Ratio of 0.044

(b) Constant Back Pressure Ratio of 0.031

(c) Constant Back Pressure Ratio of 0.006

(d) Extrapolation Exit Boundary
(Cannot be achieved on experimental setting)

Figure 7. Effects of Downstream Conditions on the Simulation

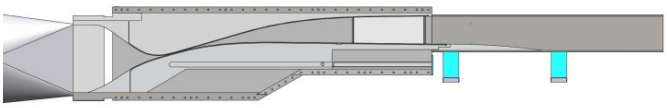

Figure 8. Sketch of the Flow Path of the AAMU Mach 4 Supersonic Wind Tunnel

Table 1. CFD Simulation Parameter Matrix

Area Ratio	Chamber Pressure (psi) / Ambient Pressure (psi)		
14.6	180 / 14.7	160 / 14.7	120 / 14.7
11.9	180 / 14.7	160 / 14.7	120 / 14.7
10.0	180 / 14.7	160 / 14.7	120 / 14.7
8.7	180 / 14.7	160 / 14.7	120 / 14.7
7.7	180 / 14.7	160 / 14.7	120 / 14.7
6.8	180 / 14.7	160 / 14.7	120 / 14.7

Figure 9 (a-f) shows the computational results at a chamber pressure of 160psi and a back pressure of 14.7psi. Six lower-nozzle block positions were used to compute the area ratio, as indicated in Table 1. At larger throat areas, the maximum Mach number in the test section reached 3.56; at the same time, shockwaves existed in the downstream diffusor, while the test volume was shock-free. As the throat area decreased, the maximum test Mach number in the test volume increased; however, the shockwave approached closer and closer to the test volume from downstream. As area ratio decreased to 8.7, the maximum Mach number reached 3.87, but shockwaves existed inside the test volume.

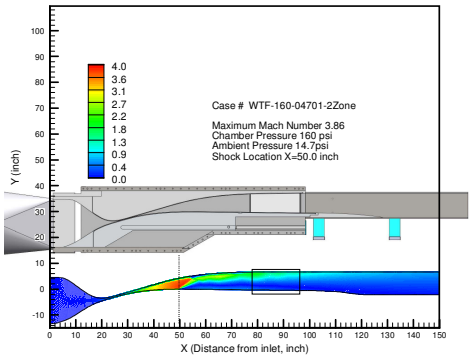

(a)

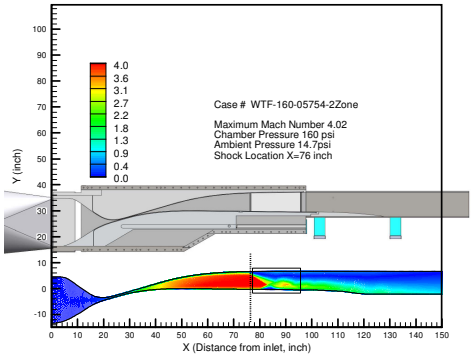

(b)

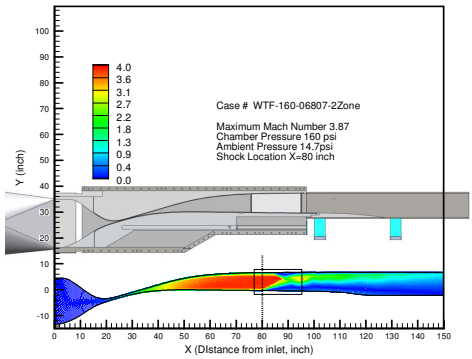

(c)

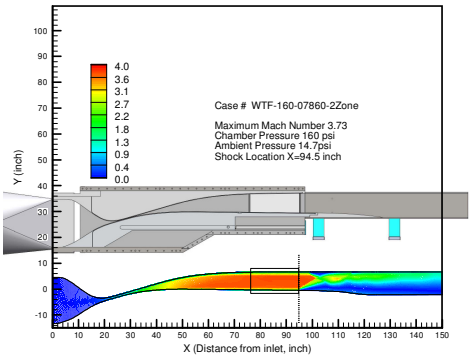

(d)

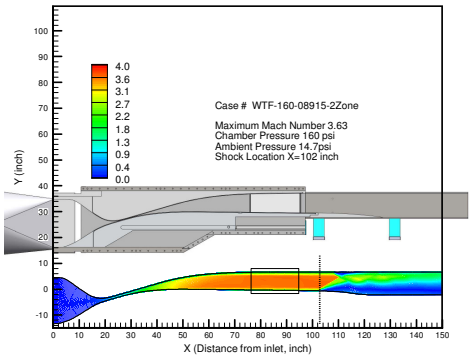

(e)

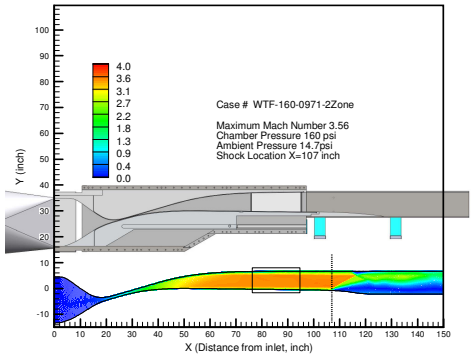

(f)

Figure 9 (a-f). Mach Number Contours and Shockwave Locations Inside the Test Volume for Case 160 / 14.7

Further reduction of area ratio created shockwaves inside the test volume. When area ratio reached 6.8, the minimum throat opening was reached and it was obvious that viscous effects become dominant and the entire test-volume Mach number was below 2.7.

Figure 10 shows the CFD simulation results for test-volume Mach number distribution and shockwave location near the test volume for the cases 120/14.7 (a1-a6) and 180/14.7 (b1-b6) for the selected area ratio. Measured from the wind tunnel design geometry CAD file, the test-section observation window started at 76 inches from the settling chamber exit. At a chamber pressure of 120psi, it was seen that shockwaves exist inside the test volume. In order to get a clean test volume, the shockwave has to be pushed out of the test volume for all area ratios. This suggests that in order to obtain Mach 3.5 to 4.0 test Mach numbers, the minimum chamber pressure should be higher than 120psi. If chamber pressure cannot be increased, then back pressure has to be lowered.

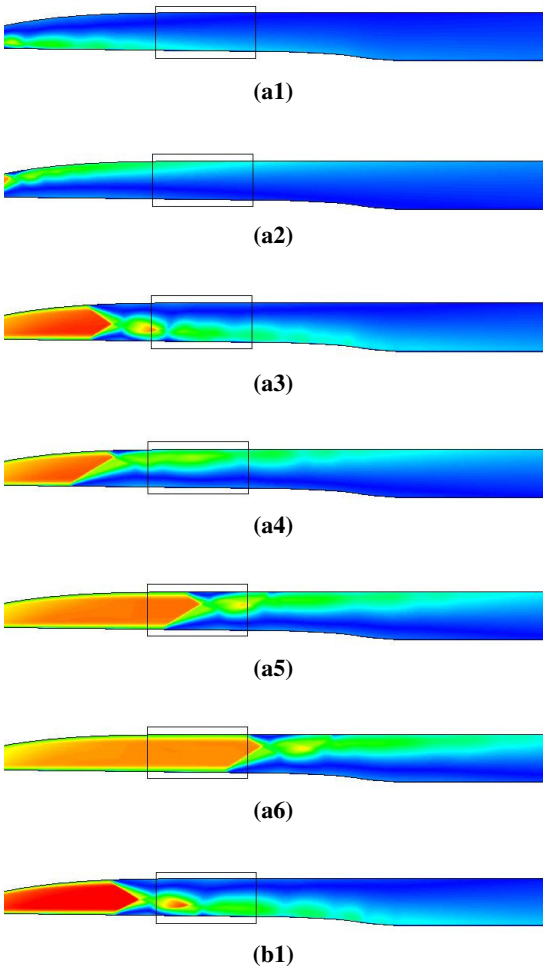

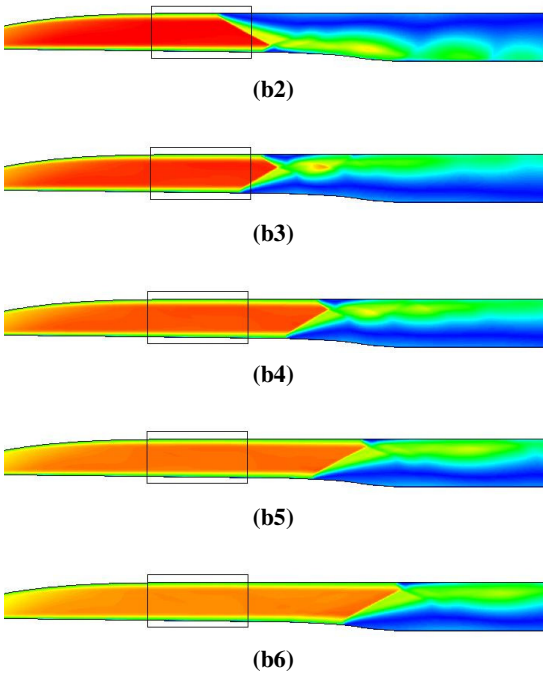

Figure 10. Mach Number Distribution and Shockwave Location Near the Test Volume: a1-a6 Pressure Ratio 120psi Chamber / 14.7psi Back; b1-b6 Pressure Ratio of 180psi Chamber / 14.7psi Back. Area Ratio Index (1) 14.6; (2) 11.9; (3) 10.0; (2) 8.7; (5) 7.7; (6) 6.8

With the wind tunnel suggested geometry, it was found that area ratio 10 (case index 3) with a chamber pressure of 180psi will comfortably provide Mach 4 test-volume conditions. Figure 11 summarizes the maximum Mach number reached for a given chamber pressure and area ratio. Figure 12 shows the shockwave locations. Results indicated that under chamber pressures of 160 and 180psi, the wind tunnel will produce clean supersonic test conditions up to Mach 3.85 at area ratios smaller than 10. To reach Mach 4 test conditions, it is necessary to raise the chamber pressure above 160psi in order to create clean supersonic test condition inside the test volume. At 180psi chamber pressure, it is possible to reach Mach 4 at an area ratio of 10. Therefore, it is recommended that the optimum chamber pressure for Mach 3.5 to 4.0 tests is approximately 170psi, if back pressure at the vertical pipe exit is 14.7psi. It is very difficult to obtain Mach 4 test conditions if chamber pressure is below 120psi.

Conclusion

CFD simulations were conducted to predict critical settling chamber pressure requirements for AAMU's Mach 4 supersonic wind tunnel. The CFD simulation adopts RANS

solver of Navier-Stokes equations with the Spalart turbulent model. Real wind-tunnel geometry was used to construct a computational domain. Results indicated that it is very difficult to reach Mach 3.5 to Mach 4 test conditions if chamber pressure is below 120psi. In order to obtain a shockwave-free (clean) supersonic test section between Mach 3.5 and 4.0, it is recommended that the optimum chamber pressure be about 170psi.

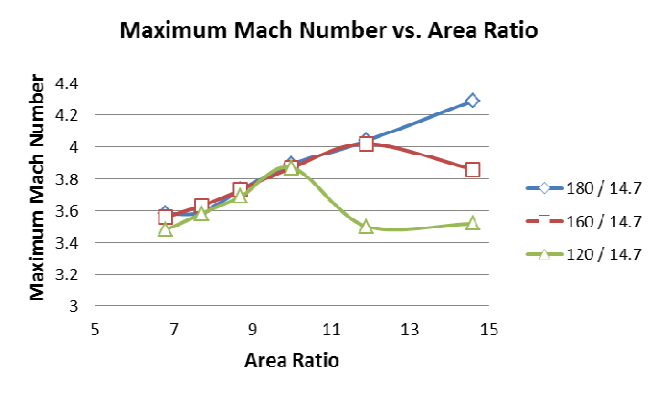

Figure 11. Computed Maximum Test Volume Mach Number as a Function of Area Ratio

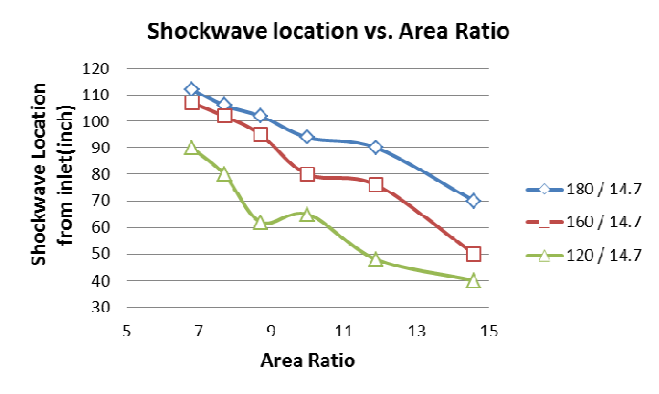

Figure 12. Computed Shockwave Location Measured from the Chamber Exit

References

[1] AeroLab. (2011, April). *6-inch Variable Mach Number Supersonic Wind Tunnel System, Operator's/ Owner's Manual*. (Volume 1.1). Alabama A&M University.

[2] Zuker, R. D., & Biblarz, O. (2002). *Fundamentals of Gas Dynamics*. (2nd ed.). John Wiley.

[3] Pope, A., & Goin, K. L. (1965). *High-Speed Wind Tunnel Testing*. John Wiley & Sons.

[4] Braun, E., Lu, F., Panicker, P., Mitchell, R., Wilson, D., et al. (2008). Supersonic Blowdown Wind Tunnel Control Using LabVIEW. *46th AIAA Aerospace Sciences Meeting and Exhibit, AIAA-2008-852*.

[5] Mittal, S., & Yadav, S. (2001). Computation of Flows in Supersonic Wind-Tunnels. *Computer Methods in Applied Mechanics and Engineering*, *191*, 611 -634.

[6] Squire, L.C. (1998). A Review of the Role of Some Small High-Speed Wind Tunnels in Aeronautical Research. *Prog. Aerospace Science*, *34*, 107-166.

[7] Rao, M., Collier, A. S., & Hand, T. (2006). Design and Manufacture of the AEDC Tunnel 9 Aerodynamic Mach 8 Nozzle. *25th AIAA Aerodynamic Measurement Technology and Ground Testing Conference, AIAA-2006-2812*.

[8] Mitchell, R., & Lu, F. (2009). Development of a Supersonic Aerodynamic Test Section Using Computational Modeling. *39th AIAA Fluid Dynamics Conference, AIAA-2009-3573*.

[9] The NPARC Alliance. (2008). *Wind-US User's Guide, version 2*. NASA Glenn Research Center & USAF Arnold Engineering Development Center.

Biographies

Z.T. DENG is a professor in Mechanical Engineering at the Alabama A&M University. Dr. Deng may be reached at zhengtao.deng@aamu.edu.

XIAOQING QIAN is a professor in Mechanical Engineering at the Alabama A&M University.

DAVE PETT is an engineer in the college of engineering, technology and physical science at Alabama A&M University.

DAN RODGERSON is the general manager of Aerolab LLC, in Laurel, Maryland.

COMPARISON OF TIME DELAY CONTROLLERS FOR A CLASS OF NETWORKED CONTROL SYSTEMS

Sri R. Kolla, Bowling Green State University

Abstract

In a networked control system (NCS), sensors, controllers and actuators are connected to the communication network as nodes instead of hardwiring them with point-to-point connections. The communication network may introduce time delays while exchanging data among devices connected to the shared network medium. These delays can degrade system performance. Traditional controllers that do not consider time delays in the design may not perform adequately when applied to the NCS. The traditional linear quadratic regulator (LQR) design with a delayed state control was shown to degrade the performance for a rotating base pendulum system with control over a wireless network. Based on this current study, it is recommended to use an LQR design that takes a class of delays into account, does not degrade performance, and illustrates the improved results for the rotating-base pendulum system with MATLAB simulations. This study also evaluated the robust stability properties of these controllers against parameter variations.

Introduction

Of late, the use of digital communication networks—such as AS-i, Devicenet, Ethernet, Foundation Fieldbus and Profibus that are commonly referred as fieldbuses—and wireless networks are becoming popular in the implementation of process control systems [1]. As shown in Figure 1, these networks allow sensors, controllers and actuators to be connected to the network as nodes instead of hardwiring the devices with point-to-point connections. Some of these devices, e.g., sensor 2 and actuator 2 in Figure 1, also use wireless communication. These networks provide several advantages such as reduced system wiring and improved flexibility and interoperability, among others. However, the communication network may induce time delays while exchanging data among devices connected to the shared network medium. These time delays can degrade system performance and even affect the stability of the control system [2].

Recently, theoretical results have been reported in the literature addressing these time delays and other aspects of networked control systems [3-16]. Gupta & Chow [11], Tipsuwan & Chow [6] and Yang [12] surveyed recent articles in the NCS area. A special issue on NCS was edited by Antsaklis & Baillieul [13]. Some researchers analyzed the effect of time delays on traditional controllers such as LQR [10], while others introduced new control designs to take the delays into account [8], [16]. Some of the analytical results gave bounds on the allowable delays that would preserve stability of the networked control systems [3-5]. Liu & Goldsmith [7] studied the effects of wireless network medium access control protocols on the performance of the networked control systems. Robust H_∞ control design for NCS was presented by Yue et al. [14]. Li et al. [15] investigated the delays associated with the use of Profibus-PA networks within control loops.

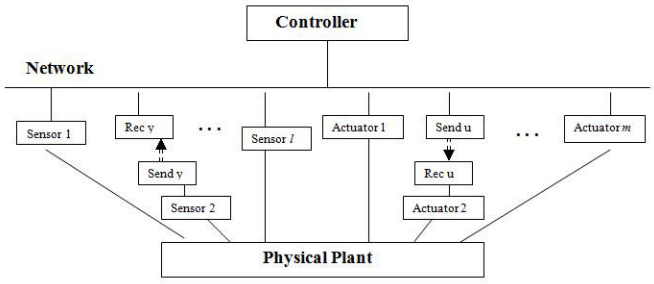

Figure 1. A Typical Networked Control System

This study compared LQR controller designs for a class of networked control systems with time delays. Presented here is a review of the traditional LQR design, followed by a look at the effect of a delayed state on this controller, as used in a wireless implementation by Ploplys et al. [10]. An alternate LQR design that takes delays into account is suggested for NCS. The performance of these two controllers is illustrated using a MATLAB simulation of a rotating-base pendulum system. Finally, the robust stability properties of these controllers are compared with the parameter variations. These robustness results are applied to the rotating-base pendulum system.

Time Delay Controllers for Networked Control Systems

Consider the discrete-time system

$$x(k+1) = Ax(k) + Bu(k) \quad (1)$$

where x is the n-dimensional state vector, A is the nxn time-invariant asymptotically stable matrix, u is the m-dimensional control vector, and B is the nxm constant matrix. It is of interest when designing controllers that the overall system be stable and meet certain performance measures.

Assuming that the system pair (A, B) is controllable, a state feedback controller to stabilize the system can be designed. This controller can be obtained in several ways [17]. Using the LQR design, the controller is given by

$$u(k) = G\,x(k) \tag{2}$$

where

$$G = -(R + BTKB)\text{-}1BTKA \tag{3}$$

and K is the positive definite solution of the algebraic discrete-time Riccati equation

$$K = Q + ATKA - ATKB(R + BTKB)\text{-}1BTKA \tag{4}$$

The matrices Q and R are weighting matrices in the performance index

$$J = \sum_{k=0}^{\infty} [x^T(k)Qx(k) + u^T(k)Ru(k)] \tag{5}$$

which can be used as a design parameter to get different stabilizing controllers. It is well known that the resulting closed-loop system

$$x(k+1) = (A + BG)\,x(k) \tag{6}$$

is stable with eigenvalues located inside the unit circle [17].

Controller 1: LQR Design using Delayed State Vector as the Input

The controller of Equation (2) assumes that there are no delays in control implementation. However, in networked control systems, this assumption may not be valid. Recently, Ploplys et al. [10] used the following modified controller with unit delay, suitable for control over wireless networks:

$$u(k) = G\,x(k\text{-}1) \tag{7}$$

The controller gain, G, in Equation (7) is the same as in Equation (3), except that the state vector in Equation (2) is delayed. The closed-loop system of Equations (1) and (7) is given by

$$\begin{bmatrix} x(k+1) \\ x(k) \end{bmatrix} = \begin{bmatrix} A & BG \\ I & 0 \end{bmatrix} \begin{bmatrix} x(k) \\ x(k-1) \end{bmatrix} \tag{8}$$

In general, the stability and performance of Equation (8) cannot be guaranteed with a controller, as given by Equation (7) [18]. For a rotating-base pendulum system, Ploplys et al. [10] showed that the dynamics of the closed-loop system—see Equation (8)—are adversely affected by the feedback delay with additional eigenvalues, though the stability is maintained, as illustrated in the following section.

Controller 2: LQR Design using Delayed State and Control Vectors as the Inputs

The following alternative implementation of the controller with unit delay is suggested for control over wireless networks [18]:

$$u(k) = GAx(k\text{-}1) + GBu(k\text{-}1) \tag{9}$$

The controller gain, G, in Equation (9) is the same as in Equation (3), except that the state vector in Equation (2) is determined from previous state and control vectors. The closed-loop system of Equations (1) and (9) is given by

$$\begin{bmatrix} x(k+1) \\ u(k+1) \end{bmatrix} = \begin{bmatrix} A & B \\ GA & GB \end{bmatrix} \begin{bmatrix} x(k) \\ u(k) \end{bmatrix} \tag{10}$$

Mita [18] performed a detailed analysis of this controller and showed that the closed-loop system matrix of Equation (10) has eigenvalues of $(A+BG)$ plus m zero eigenvalues. The stability of the closed-loop system is therefore maintained with the unit delay controller given in Equation (9). The performance index of Equation (5) is modified for this unit delay case [18]. This unit delay controller may perform better than the controller suggested by Ploplys et al. [10] for control over wireless networks, as will be illustrated in the next section.

If the time delay in the networked control system is more than one sample, the controller of Equation (9) can be extended to L sample delays given by

$$u(k) = GA^L\,x(k\text{-}L) + GA^{L\text{-}1}Bu(k\text{-}L) + \ldots + GBu(k\text{-}1) \tag{11}$$

The closed-loop system of (1) and (11) has eigenvalues of $(A+BG)$ plus mL zero eigenvalues. The stability of the closed-loop system is also maintained with the L-step delay controller Equation (11). The performance index of Equation (5) is modified for this L-step delay case as well [18].

Application to a Rotating-Base Pendulum System

Referring again to Equation (1), consider the discretized linear model of the rotating-base pendulum system—shown

in Figure 2 and described by Ploplys et al. [10]—with the following matrices:

$$A = \begin{bmatrix} 1.0008 & 0.005 & 0 & 0 \\ 0.3164 & 1.0008 & 0 & 0 \\ -0.0004 & 0 & 1 & 0.005 \\ -0.1666 & -0.0004 & 0 & 1 \end{bmatrix}, B = \begin{bmatrix} -0.0065 \\ -2.6043 \\ 0.0101 \\ 4.0210 \end{bmatrix}$$

Here, the control input, u, is the torque applied to the rotating base to move the horizontal arm through a yaw angle of ϕ. A pendulum mounted at the end of the horizontal arm freely swings about a pitch angle θ. For the state vector:

$$x = [\theta \ \dot{\theta} \ \phi \ \dot{\phi}]^T$$

Swing up and stabilization are two modes of control used to balance this system. Swing up can be obtained using different methods such as energy control [10]. The stabilization mode of the control for this system can be achieved using several methods such as LQR [10]. The effects of time delay Controllers 1 and 2, due to the delay introduced by wireless communication implementation of controllers and LQR, are illustrated in this section for the stabilization mode control with MATLAB simulation.

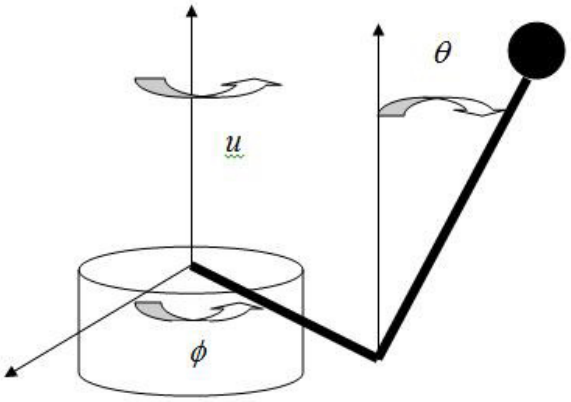

Figure 2. Structure of the Rotating Base Pendulum

For this system, Ploplys et al. [10] gave an LQR controller design of Equation (2) with

$$G = [2.094 \ 0.378 \ 0.117 \ 0.092]$$

The eigenvalues of the closed-loop system without delays are 0.414, 0.987 ± i0.0119, 0.9866. As expected, the closed-loop system was stable with all eigenvalues located inside the unit circle, although an unstable eigenvalue at 1.04 was present in the open-loop system. Figure 3 shows the initial condition response of state x_2 for the closed-loop system of Equation (6).

Ploplys et al. [10] gave the eigenvalues of the closed-loop system for Equation (8) that used Controller 1 given in Equation (7) as 0.5205 ± i0.5961, 0.987 ± i0.0119, 0.9866, 0.0, 0.0, 0.0. They further stated that the complex pair 0.5205 ± i0.5961 contributes to slower and more oscillatory state convergence when the feedback delay of Equation (7) is included and compared with the control Equation (2) that has no feedback delay. Figure 4 shows the initial condition response of state x_2 for the closed-loop system of Equation (8) which exhibits more oscillations than state x_2 for the closed-loop system of Equation (6).

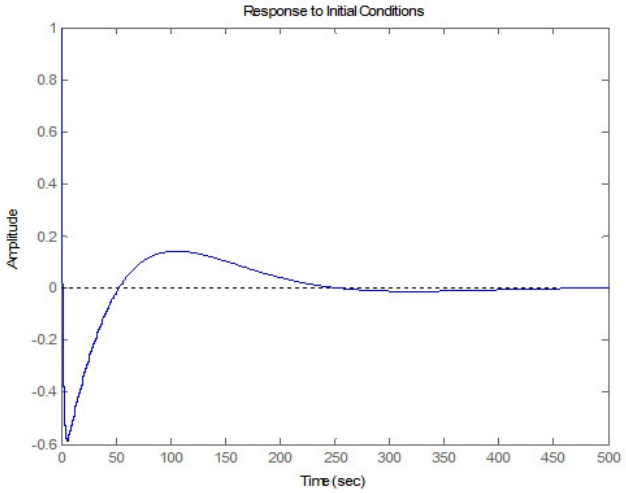

Figure 3. Initial Condition Response of State x_2 for the LQR Closed-Loop System (6) [Time scale should be multiplied by sampling time 5ms]

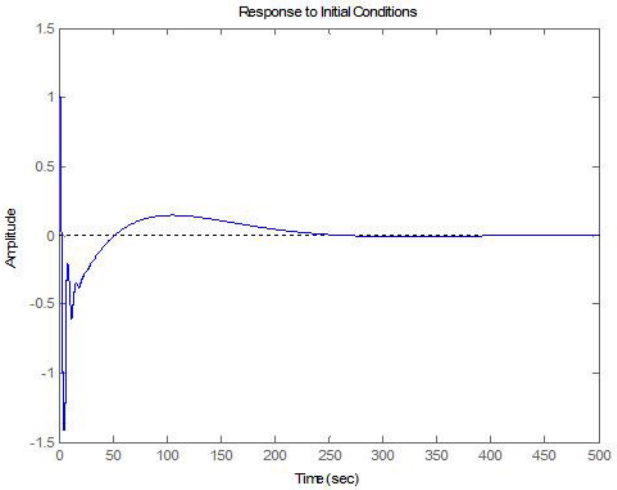

Figure 4. Initial Condition Response of State x_2 for Controller 1 Closed-Loop System (8) [Time scale should be multiplied by sampling time 5ms]

The eigenvalues of the closed-loop system of Equation (10) that uses Controller 2 given by Equation (9) are 0.414, 0.987 ± i0.0119, 0.9866, 0.0. This controller does not change the eigenvalues of the delayless controller and adds extra zero eigenvalues, thus giving better performance than Controller 1. Figure 5 shows the initial condition response of state x_2 for the closed-loop system of Equation (10). This response looks similar to the non-delay controller of Equation (2) and exhibits fewer oscillations than Controller 1 of Equation (7).

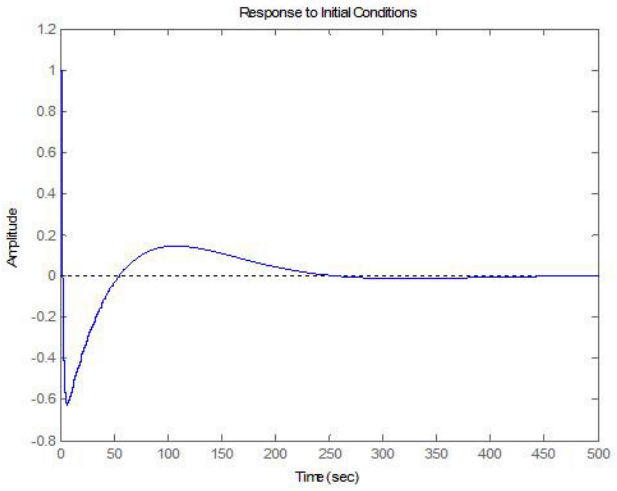

Figure 5. Initial Condition Response of State x_2 for Controller 2 Closed-Loop System (10) [Time scale should be multiplied by sampling-time 5ms]

Stability Robustness of Time-Delay Controllers for NCS

In this section, the stability robustness properties of the NCS in the presence of parameter variations in the system matrices are presented. Consider the linear discrete-time system described by

$$x(k+1) = [A_c + E]x(k) \qquad (12)$$

where x is the n-dimensional state vector, A_c is an nxn time-invariant asymptotically stable matrix, and E is a perturbation matrix. Define constants εij and ε such that

$$eij(k) \le max\,|eij(k)| = \varepsilon ij \text{ and } \varepsilon = max\,\varepsilon ij \qquad (13)$$

Let $U = [uij]$, $uij = \varepsilon ij/\varepsilon$. Note that $0 \le uij \le 1$, with $uij = 0$ if the perturbation eij of $acij$ is known to be zero. The following bound μ on ε of the E matrix that maintains the stability of the A_c matrix was presented by Kolla et al. [19]:

$$\varepsilon < \mu = -\left[\frac{\sigma_{\max}(U^T|PA_c|)_s}{\sigma_{\max}(U^T|P|U)}\right] + \sqrt{\left[\frac{\sigma_{\max}(U^T|PA_c|)_s}{\sigma_{\max}(U^T|P|U)}\right]^2 + \left[\frac{\sigma_{\min}(\overline{Q})}{\sigma_{\max}(U^T|P|U)}\right]} \qquad (14)$$

where $P > 0$ is the solution of the discrete-time Lyapunov equation $A_c{}^T PA_c - P + \overline{Q} = 0$ for any given symmetric $\overline{Q} > 0$, and $\sigma(.)$ is the singular value of (.). The notation |(.)| represents the matrix whose elements are the magnitudes of the elements of (.), and $(.)_s$ represents the symmetric part of (.). This bound can be used to study the robust stability properties in the presence of parameter variations for the closed-loop NCS with delays by taking A_c as any of the closed-loop matrices given in Equations (6), (8) or (10). These results are applied to the rotating-base pendulum system and illustrated with the following MATLAB simulation.

Application to a Rotating-Base Pendulum System

Consider the rotating-base pendulum system [10] discussed in the previous section. For this system, as described earlier, the LQR controller design of Equation (2) gives G = [2.094 0.378 0.117 0.092]. As expected, the closed-loop system is stable with all eigenvalues located inside the unit circle. For the closed-loop system of Equation (6), the stability robustness bound of Equation (14) with

$$U = \begin{bmatrix} 1 & 1 & 1 & 1 \\ 1 & 1 & 1 & 1 \\ 1 & 1 & 1 & 1 \\ 1 & 1 & 1 & 1 \end{bmatrix} \text{ and } \overline{Q} = \mathrm{I} \text{ gives } \mu = 2.1409x10^{-6}.$$

This means that the closed-loop system remains stable as long as variation in each element of A_c is less than μ.

Controller 1, given in Equation (7) provides the closed-loop system matrix in Equation (8) for NCS. For this closed-loop system, the stability robustness bound of Equation (14) with an 8x8 U matrix with all ones, and $\overline{Q} = \mathrm{I}$, gives $\mu = 7.3749x10^{-7}$. This means that the closed-loop system remains stable as long as variation in each element of A_c is less than μ. The closed-loop system with Controller 1 still has some robustness properties, though the allowable parameter variations are less than the controller without time delay due to the lower value for μ.

Controller 2, given by Equation (9) provides the closed-loop system matrix in Equation (10) for NCS. For this closed-loop system, the stability robustness bound of Equation (14) with a 5x5 U matrix with all ones, and $\overline{Q} = \mathrm{I}$, gives $\mu = 3.8557x10^{-6}$. As before, this means that the

closed-loop system remains stable as long as variation in each element of A_c is less than μ. It can be observed that the closed-loop system with Controller 2 given in Equation (10) showed better robustness properties against parameter variations than the closed-loop system with Controller 1 given in Equation (8) due to the higher value for μ.

Conclusion

In this paper, a comparison of the time-delay controller designs for a class of NCS were presented. One of these controllers (Controller 1) uses the traditional LQR state-feedback gain matrix with a unit delay state vector [10]. The performance of Controller 1 for NCS may not be satisfactory based on the eigenvalue analysis of the closed-loop system and the initial condition response, illustrated using a rotating-base pendulum system with a MATLAB simulation. It is suggested that a different LQR controller [18] with time delays (Controller 2) be used for NCS and obtain better performance based on eigenvalue analysis of the closed-loop system and initial condition response, illustrated using the rotating-base pendulum system. The stability robustness properties of both these time-delay controllers for NCS against parameter variations were studied. These controllers' robustness properties were illustrated using the rotating -base pendulum system. For this system, Controller 2 showed better robustness properties against parameter variations than Controller 1. In addition to the type of time delays considered in this paper, other issues such as information packet loss during communication in NCS and random time delays are critical, and their effect on performance needs further investigation [11-13].

References

[1] Mahalik, N. P. (Ed.) (2003). *Fieldbus Technology – Industrial Network Standards for Real-Time Distributed Control*. Berlin, Germany: Springer-Verlag.

[2] Lian, F.-L., Moyne, J. R., & Tilbury, D. M. (2001). Performance evaluation of control networks: Ethernet, ControlNet, and DeviceNet. *IEEE Control Systems Magazine*, *21*, 66-83.

[3] Zhang, W., Branicky, M. S., & Phillips, S. M. (2001). Stability of networked control systems. *IEEE Control Systems Magazine*, *21*, 84-99.

[4] Walsh, G. C., Ye, H., & Bushnell, L. (2002). Stability analysis of networked control systems. *IEEE Transactions on Control Systems Technology, 10*, 438-446.

[5] Ye, H., Walsh, G. C., & Bushnell, L. (2001). Real-time mixed-traffic wireless networks. *IEEE Transactions on Industrial Electronics*, *48*, 883-890.

[6] Tipsuwan, Y., & Chow, M.-Y. (2003). Control methodologies in networked control systems. *Control Engineering Practice*, *11*, 1099-1111.

[7] Liu, X., & Goldsmith, A. (2004). Wireless medium access control in networked control systems *Proceedings of the American Control Conference*. Boston, Massachusetts.

[8] Lian, F.-L., Moyne, J., & Tilbury, D. (2003). Modelling and optimal controller design of networked control systems with multiple delays. *International Journal of Control, 76*, 591-606.

[9] Munir, S., & Book, W. J. (2003). Control techniques and programming issues for time delayed internet based teleoperation. *ASME Journal of Dynamic Systems, Measurement, and Control, 125*, 205-214.

[10] Ploplys, N. J., Kawka, P. A., & Alleyne, A. G. (2004). Closed-loop control over wireless networks. *IEEE Control Systems Magazine*, *24*, 54-71.

[11] Gupta, R. A., & Chow, M.-Y. (2010). Networked control system: overview and research trends. *IEEE Transactions on Industrial Electronics*, *57*(7), 2527-2535.

[12] Yang, T. C. (2006). Networked control systems: a brief survey. *IEEE Proceedings – Control Theory and Applications*, *153*, 403-412.

[13] Antsaklis, P., & Baillieul, J. (Eds.) (2007). Special issue on technology of networked control systems. *Proceedings of IEEE*, *95*, 5-8.

[14] Yue, D., Han, Q.-L., & Lau, J. (2005). Network-based robust H_∞ control of systems with uncertainty. *Automatica*, *41*, 999-1007.

[15] Li, Q., Jiang, J., & Rankin, D. J. (2011). Evaluation of delays induced by Profibus PA networks. *IEEE Transactions on Instrumentation and Measurement, 60*(8), 2910-2917.

[16] Zhang, L., & Fang, H.-J. (2006). A novel controller design and evaluation for networked control systems with time-variant delays. *Journal of Franklin Institute*, *343*, 161-167.

[17] Franklin, G. F., Powell. J. D., & Workman. M. (1998). *Digital Control of Dynamic Systems*. (3rd ed.). Menlo Park, CA: Addison Wesley Longman.

[18] Mita, T (1985). Optimal digital feedback control systems counting computation time of control laws. *IEEE Transactions on Automatic Control*, *30*, 542-548.

[19] Kolla, S. R., Yedavalli, R. K., & Farison, J. B. (1989). Robust stability bounds on time-varying perturbations for state-space models of linear discrete-time systems. *International Journal of Control*, *50*, 151-159.

Biography

SRI R. KOLLA is a Professor in the Electronics and Computer Technology Program at the Bowling Green State University, Ohio, since 1993. During 2008-'09, he was a Fulbright Research Scholar at the Electrical Engineering Department, Indian Institute of Science, Bangalore. He was a Guest Researcher at the Intelligent Systems Division, National Institute of Standards and Technology, Gaithersburg, MD, 2000-'01. He was an Assistant Professor at the Pennsylvania State University, 1990-'93. He got a Ph.D. from the Electrical Engineering Department of the University of Toledo, Ohio, in 1989. His teaching and research interests are in electrical engineering/technology area with specialization in artificial intelligence, control systems, computer networks and power systems. He is a fellow of IE (India), senior member of IEEE and ISA, and a member of ASEE and ATMAE. Dr. Kolla may be reached at email: skolla@bgsu.edu, phone: +01-419-372-7507.

PERFORMANCE ANALYSIS ON MULTICAST FEEDBACK CONTROL WITH UNSYNCHRONIZED CLOCKS

Shuju Wu, Central Connecticut State University; Xiaobing Hou, Central Connecticut State University

Abstract

To ensure reliable multicast delivery, packet loss needs to be reported to the sender by sending feedback messages. Feedback implosion problems arise when too many multicast group members generate and send duplicate feedback messages which overwhelm the sender processing capability or cause network congestion near the multicast sender. Proposed feedback control mechanisms use timers, representative or network layer support to reduce the number of feedback messages. Comparative studies show that representative schemes with timers provide better feedback suppression performance where the timer length is determined by assuming synchronized clocks among the group members. However, synchronized clocks may not be available network-wide and there is a systematic synchronization bias when link delays between the time client and the time server are asymmetric. This paper extends the study of previous representative schemes and analyzes their performance when unsynchronized clocks are used. A simulation study was performed in order to verify the effectiveness of suppression, and the number and the location of representatives were observed based on dynamic network situations. The analysis and simulation results showed that the representative schemes with deterministic timers maintain good feedback suppression performance even if the clocks of multicast group members are unsynchronized.

Introduction

Communications using multicasting, be it IP- or overlay-based, attain efficiency over using unicasts by building an efficient multicast tree. However, faults in the Internet result in performance areas because group members share a multicast tree. Members in a performance area suffer from the same packet loss and, if the loss needs to be reported, duplicate feedback messages are sent by group members, which can overwhelm the sender processing capability and cause network congestion. This is called feedback implosion. For example, in Figure 1(a), router 1 keeps dropping data packets due to network congestion causing all of the group members in the same performance area behind it to suffer the same losses. The consequence is that all of the affected members will send the same feedback message and cause new congestion close to the source, as shown in Figure 1(b).

The Internet is dynamic and unpredictable in nature. Dynamic events such as changing node failures, link failures or network congestion can cause packet loss or faults. Faults resulting from network congestion in the Internet could last a long time and cause end-to-end performance degradation without a total loss of connection. This in turn generates a large number of feedback messages. Experiments on the MBone [1] show that even for a small multicast group of 11 members, each member experiences a very long consecutive loss of up to a few minutes, a loss that occurs in almost every trace. According to C'aceres et al. [2], link loss rates in a MBone group of 8 members are measured in one-hour long intervals and shown to vary between 2% and 35%. On a specific link, loss rates higher than 15% happen frequently and often last about 10 minutes. Also, from the results of Internet measurements [3-4], it is not unusual to find long-lasting, high-loss periods between Internet nodes, although the average loss rate over a day could be low. When such faults happen in a multicast tree and are close to the multicast source, the size of the performance cluster will be large which adversely affects most of the group members.

Feedback implosion is one of the issues that hinder the large-scale Internet implementation of IP multicast. Overlay multicast does not suffer this problem as the tree consists of unicast connections; rather, how to construct an efficient multicast tree using unicast connections is the key issue [5]. Many Internet communications can utilize multicast but are loss intolerant. Examples of such applications include video server replication and data dissemination (news, stock market quotes, collaborations, software distributions, etc.), in both wired and wireless networks [6-7]. Feedback implosion problems can impede the scalability and large-scale implementation of such applications. Therefore, feedback control is important for multicast communications.

Current feedback control mechanisms can be characterized by their use of timers, hierarchies or representatives. Timer-based mechanisms [8-10] require each member to wait a period of time, either random or deterministic, before it sends feedback. If a member receives another member's feedback before the timer expires, its feedback is suppressed. Hierarchy-based mechanisms [11-14] organize the group members into a domain hierarchy and restrict feedback messages within the local domain. Representative-based schemes [15-16] use representatives, members that

can send feedback messages immediately, to suppress the other members' feedback.

It is well recognized that random timer-based approaches are simpler but less responsive and suppressive. The reason is that every feedback is delayed for a random period of time resulting in random suppression performance. Hierarchy-based schemes are more complex due to hierarchy management and utilize random timers. Using representatives to send immediate feedbacks improves the response and suppression performance. Wu et al. [17] have shown that feedback control schemes using representatives and deterministic timers provide superior overall performance.

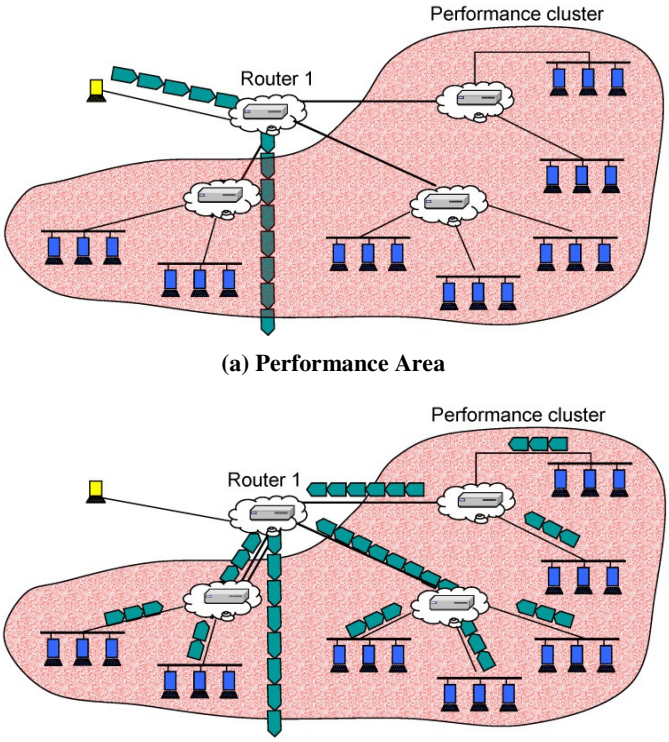

(a) Performance Area

(b) Feedback implosion

Figure 1. Example of Feedback Implosion

Wu et al. further assumed that all of the group members have synchronized clocks to calculate the timer length. There are two concerns in assuming synchronized clocks. First, nowadays, many of the Internet end-hosts (used by end users) do not have the synchronized time service. Even though service and protocol such as Network Time Protocol NTP [18] is available, the end hosts may not be configured or have an NTP server to access. Second, in reality, there is a systematic synchronization bias when link delays between the time client and the time server are asymmetric. Since the feedback suppression timer length itself is related to network link delays, such a bias could severely affect suppression performance.

This study extends the work of Wu et al. by analyzing the feedback control performance when unsynchronized clocks are used. Simulation study is performed to verify the effectiveness of suppression in which the number and location of representatives are observed based on dynamic network fault situations.

The Representative-based Multicast Feedback Control Scheme

The work by Wu et al. used representatives and deterministic timers calculated on perfectly synchronized clocks for feedback control purposes. The proposed scheme is called Loss Pattern matched Area Based Feedback Control (LPABFC). The comparative study in the paper by Wu et al. [17] shows that LPABFC provides better performance than the other representative schemes such as REP [15] by adaptively changing the number of representatives and the locations of the representatives based on network fault situations. The REP scheme uses a constant number of representatives, which means that if the number of performance clusters is larger than the number of representatives, some clusters will have no representative to provide immediate feedback. A sensible solution is to dynamically identify the performance clusters and allow each cluster to have its own representative.

Here a few issues arise: first, how to accurately and dynamically identify and group the members into clusters without sacrificing simplicity; second, the number of representatives should be neither constant nor limited by a maximum number—ideally, it should be equal to the current number of performance clusters; third, before a representative is assigned to a cluster, suppression is still needed among the cluster members to prevent feedback implosion; fourth, operations by group members should be minimized—therefore, the members should not be involved in representative selection and management; fifth, interactions and cooperation among members normally incur overhead and increase the complexity—therefore, they should be minimized, too.

Unlike previous schemes that focus on timer selection, LPABFC tries to identify performance areas according to current fault conditions by performing loss pattern matching. Figure 2 shows the general model of feedback suppression in LPABFC. Each area has a representative (AR) that multicasts feedback messages without delay. Every receiver stores an n-bit bitmap indicating its receiving status of the

most recent n data packets. For the purpose of loss pattern matching, the representative attaches its own n-bit loss pattern in the feedback message, so every group member keeps the loss pattern for each representative and updates it upon receiving a new one. Let LP_i be the loss pattern of receiver i, R be the receiver set, and $S\{LP_i; LP_j\}$ be the number of bits that have the same value in the bitmap corresponding to the same data packet. Receiver j is the closest matched receiver to receiver i if:

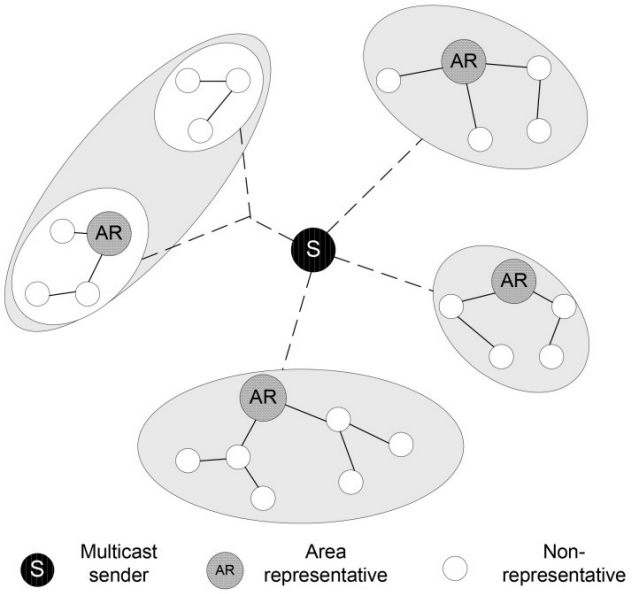

Figure 2. The Area-based Feedback Control Model

$$S\{LP_i, LP_j\} > S\{LP_i, LP_k\}, \forall k \in R, k \neq i, j$$

A receiver selects the closest matched representative as its representative. This way, representative selection is more accurate and stable, so feedback suppression is improved. The loss pattern can also provide local congestion information for multicast congestion control.

In LPABFC, timers are used by the non-representative members, called representees. The timer of a representee serves two purposes: it should be long enough to allow the AR's feedback to suppress the representee's feedback, and before a new cluster has a representative, the timer should be able to provide a certain degree of suppression among the representees. To meet these conditions, each representee calculates the length of its timer as follows. A representative attaches a time-stamp, t_{rep}—the receiving time of the DATA packet that triggers the feedback—in its feedback message. Suppose that at time $t_{feedback}$ this feedback arrives at a representee, which received the same DATA packet at t_{member}. The timer length, d, of the representee is then:

if $t_{member} < t_{rep}$,

$$d = t_{feedback} - t_{member}$$

otherwise,

$$d = t_{feedback} - t_{rep}$$

This way, deterministic suppression exists not only between the AR and representees, but also among the representees when an AR cannot represent the loss. This is because the timer length is decided by the one-way delay between the representative and representees. A representee having smaller one-way delay can suppress the other representees that have larger one-way delays. Since network dynamics may cause d to change from time to time, a representee actually keeps m most recent measurements of d to each representative, and uses the largest one of them.

The value of d includes the delay between a representative and a representee. Therefore, the timer lengths of the representees are differentiated by their delays to a representative. The timer length of a representee with shorter delay to a representative is smaller than that of a representee with a larger delay. Therefore, if a new packet loss occurs, which is not representable by the current AR, the member that is closest to the AR will timeout first and suppress further members. This decreases the chance of feedback implosion before a new representative is selected.

In LPABFC, group members are assumed to use synchronized clocks to calculate the timer length. Synchronized clocks are easy to implement in simulations and the results from work by Wu & Banerjee [16] have proved the effective performance of LPABFC. However, considering real-life Internet implementation, many of the Internet end hosts nowadays still do not have the synchronized time service. Even though service and protocol such as Network Time Protocol NTP [17] is available, the end hosts may not be configured or have an NTP server to access. Second, in reality, there is a systematic synchronization bias when link delays between the time client and the time server are asymmetric. Since the feedback suppression timer length itself is related to network link delays, such a bias could severely affect suppression performance. Therefore, it is important to validate the effectiveness of LPABFC in an unsynchronized clock environment.

Using Unsynchronized Clocks in LPABFC

In this section, an analysis and discussion is presented on suppression performance when Round Trip Time (RTT)

between a representative and a representee is used to calculate the timer length without assuming synchronized clocks and symmetric link delays. First, different scenarios are analyzed to see whether the representative can suppress the representees, and then deterministic suppression among the representees is discussed.

The analysis assumes that a representee knows its RTT to the AR. How to measure the RTT is introduced at the end of this section. A representee sets its timer length to $s \cdot RTT$ with $s > 1.0$ in order to ensure suppression by the representative.

Figure 3 shows the location scenarios of the multicast source, S, the area representative, R, an intermediate member, m, and a representee, 1, used in the following analysis. Figure 3(a) shows the logical connection between the multicast source *S*, a representative *R* and a general representee 1. Figures 3(b-e) show the possible real relative positions between representative R and member 1.

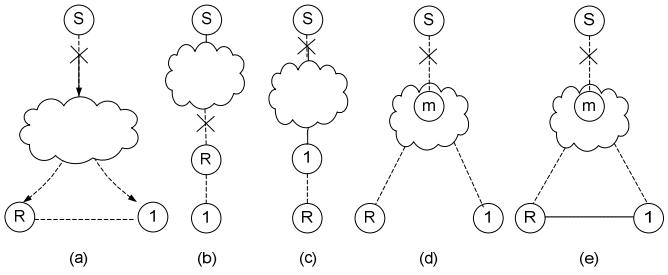

Figure 3. Suppression between a Representative and the Representees in Different Location Scenarios
(a) Logical Connections between Group Members Loss Affects Both Representative *R* and Member 1
(b) Real Location Same Branch Representative at the Upper Level
(c) Real Location Same Branch Representative at the Lower Level
(d) & (e) Real Location—The Representative and Representees in Different Branches

Suppression between the AR and the Representees

Referring to Figure 3(a)—note that this is not a real network topology—when a packet is lost by both representative *R* and representee 1, the feedback of *R* can suppress that of representee 1 if it arrives before 1's timer expires. Let:

d_{ij} = one-way delay between member *i* and member *j*
$RTT_{ij} = d_{ij} + d_{ji}$, round trip time between *i* and *j*
$T_{Ri} = d_{SR} + d_{Ri}$, time for feedback of *R* to arrive *i*
$T_i = d_{Si} + s \cdot RTT_{iR}$, time for representee *i* to send feedback
$T_{ij} = T_i + d_{ij}$, time for feedback of representee *i* to arrive *j*

For R to suppress representee 1, the following condition must be satisfied:

$$T_1 - T_{R1} = d_{S1} + s \cdot d_{1R} + (s-1) \cdot d_{R1} - d_{SR} > 0 \quad (1)$$

Since a representative or a representee could be anywhere in the network topology, the following studies consider different location scenarios in order to analyze whether a representative can effectively suppress the representees if RTT is used to calculate the timer length.

Same Branch Representative at the Upper Level:

In Figure 3(b), the representative *R* and the representee are in the same multicast tree branch, but *R* is closer to the source and, therefore, always detects packet loss earlier. Since $d_{S1} = d_{SR} + d_{R1}$, Equation (1) becomes:

$$\begin{aligned} T_1 - T_{R1} &= d_{SR} + d_{R1} + s \cdot d_{1R} + (s-1) \cdot d_{R1} - d_{SR} \\ &= s \cdot (d_{R1} + d_{1R}) = s \cdot RTT_{1R} > 0 \end{aligned} \quad (2)$$

This means that a representative can always suppress those lower-level representees.

Same Branch, Representative at the lower Level:

In Figure 3(c), the representative *R* and representee 1 are in the same tree branch, but *R* always detects packet loss later than the representee. Since $d_{SR} = d_{S1} + d_{1R}$, Equation (1) becomes:

$$\begin{aligned} T_1 - T_{R1} &= d_{S1} + s \cdot d_{1R} + (s-1) \cdot d_{R1} - (d_{S1} + d_{1R}) \\ &= (s-1) \cdot (d_{R1} + d_{1R}) = (s-1) \cdot RTT_{1R} > 0 \end{aligned} \quad (3)$$

Equation (3) shows that a representative can always suppress those upper-level representees in the same branch.

Different Branches:

When the representative and the representee are located in different multicast tree branches, two scenarios exist as shown in Figures 3(d) and 3(e). In Figure 3(d), the feedback of *R* travels some links in the multicast tree before arriving at representee 1. In Figure 3(e), however, the feedback of *R* does not pass the links in the multicast.

In the case of Figure 3(d), Equation (1) becomes:

$$\begin{aligned} T_1 - T_{R1} &= d_{Sm} + d_{m1} + s \cdot d_{1R} + (s-1) \cdot d_{R1} - (d_{Sm} + d_{mR}) \\ &= s \cdot RTT_{1R} - RTT_{Rm} > 0 \end{aligned} \quad (4)$$

Since RTT_{1R} is larger than RTT_{Rm} and s is larger than 1, Equation (4) shows that representative R can always suppress representee 1.

In the case of Figure 3(e), Equation (1) becomes:

$$T_1 - T_{R1} = d_{m1} + s \cdot d_{1R} + (s-1) \cdot d_{R1} - d_{mR} \quad (5)$$

According to Equation (5), whether representative R can suppress member 1 is decided by the one-way delays among members R, m and 1. When d_{mR} is over large compared to d_{m1}, there is a possibility that the representative R cannot suppress the representee.

From the above analysis, it can be seen that, in most cases, a representative can suppress the representees in its area if RTT is used to calculate the timer length. Although, in the case of Figure 3(e), a representative may not be able to suppress a representee, two solutions exist. First, in LPABFC, such a representative could be an inferior initial selection (e.g., dynamic membership) far away from the fault location, in which case the representative selection algorithm will react accordingly. Second, a representee can adjust its timer to prevent further early timeouts if R continues to be appointed as the representative by the source.

Suppression among Representees

In the previous section, suppression between a representative and a representee if a packet loss affects both of them was presented. When packet loss only affects representees, deterministic suppression is desirable so that the number of timeout feedback messages is small. In this section, the authors analyze whether using RTT to calculate the timer length provides this property. Similar to the previous analysis, different location scenarios are used.

Figure 4(a) shows the logical connections between the multicast source S, a representative R and representees 1 and 2. Assume a packet loss only affects members 1 and 2. To decrease the number of feedbacks, the timeout feedback of one representee should arrive at another representee before its timer expires. In other words, member 1 can suppress member 2 if:

$$T_{12} - T_2 < 0$$

which is equivalent to

$$(d_{S1} - d_{S2}) + s \cdot (RTT_{1R} - RTT_{2R}) + d_{12} < 0 \quad (6)$$

The following scenario considers different location scenarios for analyzing how the above condition affects feedback suppression among representees.

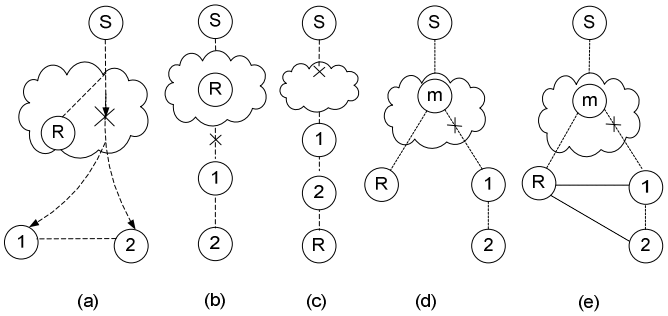

Figure 4. Suppression among Representees
(a) Logical Connections between Group Members where the Loss Affects Two Representees: Members 1 and 2
(b) Real Location
Same Branch Representative at the Upper Level
(c) Real location
Same Branch Representative at the Lower Level
(d) & (e) Real Location, Different Branches

Same Branch Representative at the Upper Level:

In Figure 4(b), representees 1 and 2 are in the same multicast tree branch. Since $d_{S2} = d_{S1} + d_{12}$, Equation (6) becomes:

$$T_{12} - T_2 = -s \cdot (d_{12} + d_{21}) < 0 \quad (7)$$

This means that an upper-level representee can always suppress those lower-level representees.

Same Branch Representative at the Lower Level:

This case is shown in Figure 4(c). In fact, in this case, packet loss also affects the representative which can suppress both member 1 and member 2. There is no timeout feedback in this case.

Different Branches:

When the representative and the representees are located in different multicast tree branches, two scenarios exist, as shown in Figures 4(d) and 4(e). In Figure 4(d), the feedback of R always travels some links in the multicast tree before arriving at representees 1 and 2. In Figure 4(e), however, representees 1 and 2 receive feedback messages from R from different paths and their RTTs to R are independent.

For the case of Figure 4(d), the result is same as Equation (7) and representee 1 can still suppress representee 2. In the case of Figure 4(e), the suppression between member 1 and member 2 depends on their RTTs to representative R. According to Equation (6), member 1 can suppress member 2 if:

$$T_{12} - T_2 = s \cdot (RTT_{1R} - RTT_{2R}) < 0 \quad (8)$$

Similarly, member 2 can suppress member 1 if:

$$T_{21} - T_1 = (d_{S2} - d_{S1}) + s \cdot (RTT_{2R} - RTT_{1R}) + d_{21} < 0 \quad (9)$$

which is equivalent to:

$$2 \cdot d_{21} + s \cdot RTT_{2R} < RTT_{1R} \quad (10)$$

From Equations (8)-(10), it can be seen that the only condition for no suppression between two representees is when $RTT_{2R} < RTT_{1R} < 2 \cdot d_{21} + s \cdot RTT_{2R}$.

Similar to using a synchronized clock, deterministic suppression among the representees exists in most cases. It should be noted that there is no guarantee of a single timeout feedback message, either by using the synchronized clock or by measuring the RTT.

RTT Measurement and Timer Adjustment

To measure the RTT, a member could unicast probe messages infrequently to the representative. When the representative sends feedback, it puts the time information (aggregated for all of the members that have probed it during that period) in the feedback. Then, the representees can calculate their RTTs after receiving the feedback.

In the case of synchronized clocks, representative R can always suppress representee 1 because both d_{SR} and d_{R1} are considered in the timer length calculation, thus the timer length is long enough for suppression. However, when using RTT to calculate the timer length, d_{SR} is not considered and the representative may not be able to suppress the representees, as in the case of Figure 3(e). In this case, the representee needs to adjust its timer length. For this purpose, if a representee timeouts (at t_1) before the feedback of its area representative arrives (at t_2), it should increase its RTT by at least $t_2 - t_1$ to avoid further early timeouts.

Simulation Results

Timer selection affects the responsiveness of the feedback and location of the selected representative because the member with the smallest timer will send out a feedback message first and could be selected as a representative. This section introduces the simulation results that show how the area representatives are selected and managed based on the number of network faults and dynamics. Unsynchronized clocks are used to measure RTTs between members. The results show that using unsynchronized clocks in LPABFC still achieves effective representative selection, which is similar to the original scheme that uses synchronized clocks.

The simulation study is implemented with Network Simulator-2 (ns-2) [19] with random transit-stub-type network topology generated by GT-ITM [20]. The transit-stub graph model is widely used in network simulation research to model today's Internet. The transit domains represent the backbone networks and the stub domains represent the edge networks. The new ns-3 is not used due to its incompatibility with GT-ITM. Since the synchronized-clock approach in LPABFC was studied in ns-2 and GT-ITM, to be consistent, this study was carried out in the same simulation environment.

The study on the representative management is carried in a 100-node transit-stub network topology. Packet loss is randomly introduced on the transit-stub links. The length of a loss period is uniformly selected between 20 seconds and 40 seconds, and the length of a loss-free period is uniformly selected from between 30 seconds and 60 seconds.

Figure 5 shows how the number of representatives changes according to loss conditions from simulation times of 0 to 200. It can be seen that during the first half of the time, the number of representatives increases as new losses appear on different links; then, it fluctuates as the old loss periods terminate and new loss periods start.

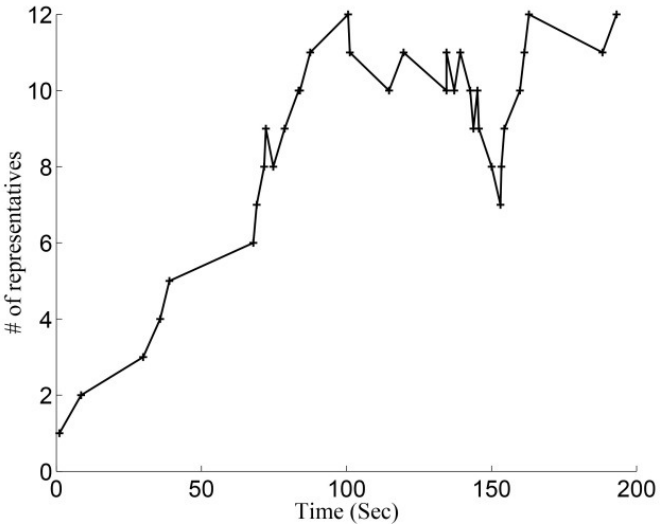

Figure 5. The Number of Representatives versus Simulation Time

The number of clusters, the members in a cluster, and the creation and merge of the cluster is shown in the following graphs and are based on the simulation time when such an even occurs.

- Simulation time of 1.290: Figure 6 shows the network topology. The multicast sender is in red and the other group members are in blue. The group density is 75%; i.e., about 75 nodes become the multicast group members. Node 17 is selected as the representative at simulation time 1.290 and there is only one area including all of the group members.

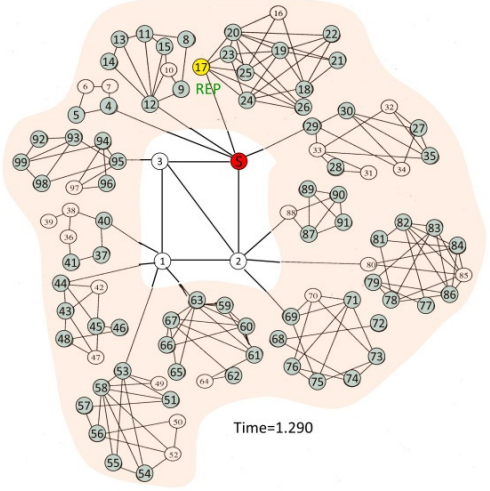

Figure 6. Representative Management at a Time of 1.290

- Simulation time of 8.654: Figure 7 shows that at time 8.654, node 40 is added as a new representative and a new area is formed accordingly. The rest of the nodes still choose REP 17 as the AR. Therefore, two areas exist. After this time, area number continues to increase when new loss occurs, and nodes 84, 63, 95 and 12 become representatives.

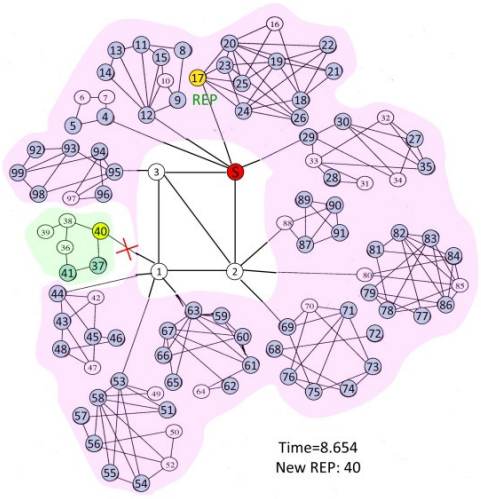

Figure 7. Representative Management at a Time of 8.654

- Simulation times of 39.099 and 68.024: It can be seen in Figures 8 and 9 that new areas are formed at times 39.099 and 68.024, respectively, in which nodes 95 and 12 are selected as ARs. In addition, $link_{1\text{-}40}$ is recovered from packet loss but node 40 remains as a representative that will be deleted if it does not send feedback for a sufficiently long time.

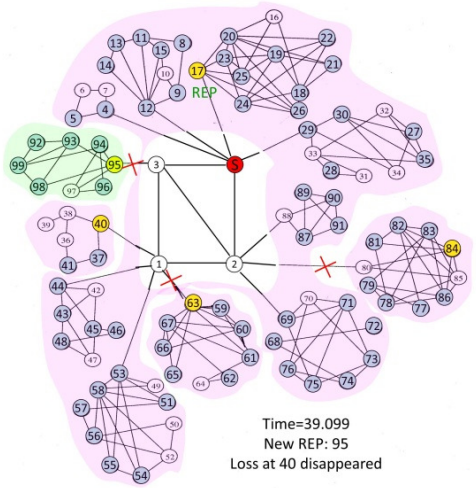

Figure 8. Representative Management at a Time of 39.099

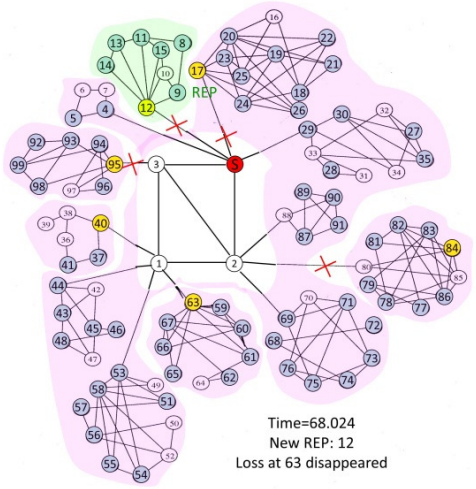

Figure 9. Representative Management at a Time of 68.024

- Simulation time of 78.687: Figure 10 shows three things at time 78.687. First, representative 40 is deleted by the sender, and its area merges with another area represented by node 63. Second, four new clusters are added with nodes 4, 29, 53 and 90 being the representative. Third, the loss on $link_{s\text{-}17}$ and $link_{3\text{-}95}$ terminates.

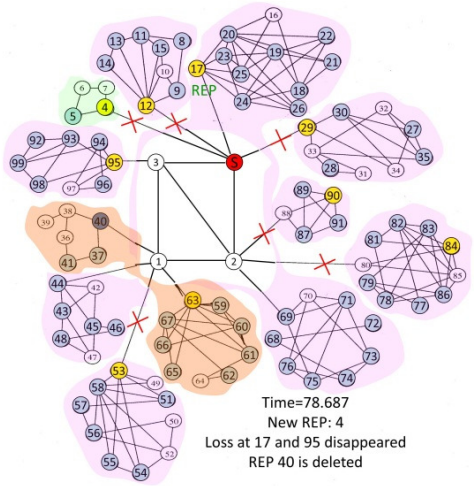

Figure 10. Representative Management at a Time of 78.687

- Simulation time of 83.994: In Figure11, loss happens on $link_{1\text{-}40}$ again and results in a new area. In addition, by monitoring the loss detection time, node 87 finds that it detects packet loss earlier than its AR, node 90. Therefore, it requests that node 90 be replaced and becomes the new representative.

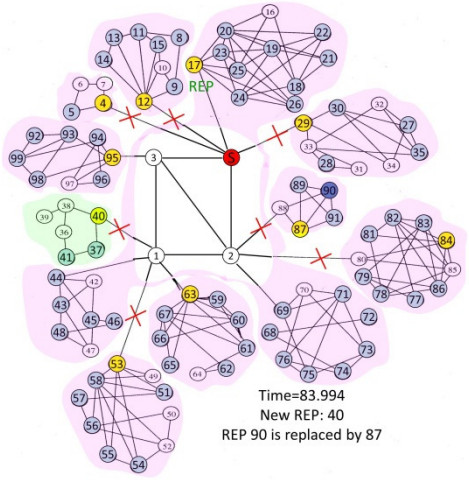

Figure 11. Representative Management at a Time of 83.994

From the above simulation results and analysis, it can be seen that the number of representatives and areas in LPABFC still adaptively changes according to the dynamic network conditions and the scheme selects the appropriate members to be the representatives.

Conclusion

Next-generation networks will support a much higher data transmission rate than current networks and provide more advanced services. In particular, the demand for Internet group communications such as live media broadcasting, content distributions and group collaborations has grown rapidly with the increase in commercial usage of the Internet. IP multicasting has to overcome some critical problems in order to be safely deployed on the Internet, and one of them is feedback implosion.

Previous studies show that LPABFC provides effective feedback implosion control. This study extends the previous studies and analyzed feedback control performance when unsynchronized clocks are used in timer calculations. The analytical and simulation results show that effective feedback suppression is retained with unsynchronized clocks, and the number and location of representatives are managed based on dynamic network fault situations.

For future studies, LPABFC can be extended to multicast congestion control because the representatives provide responsive feedback. It will also be studied in wireless communications which, by nature, supports multicast and broadcast. One example is cellular networks where handoff, i.e., user switches between cells or networks [21], must be taken into consideration. Another example is wireless mesh networks [22], where fewer available resources, such as power and computation capability, could be a concern.

References

[1] Yajnik, M., Kurose, J., & Towsley, D. (1996). Packet Loss Correlation in the mbone Multicast Network. *Proceeding of IEEE Global Conference on Communications*.

[2] C´aceres, R., Adams, A., Bu, T., Duffield, N., Horowitz, J., Friedman, T. et al. (2000). The Use of End-to-End Multicast Measurements for Characterizing Internal Network Behavior. *IEEE Communications*, *38*(5).

[3] Network Research Group. Retrieved August 21, 2012 from http://www.wand.net.nz/. Original site retrieved June 2006, from http://watt.nlanr.net/.

[4] Labovitz, C., Ahuja, A., Bose, A., & Jahanian, F. (2000). Delayed Internet Routing Convergence. *Proceeding of ACM SIGCOMM*.

[5] Hou, X., & Wu, S. (2011). On the Performance of an Application Layer Multicast Protocol. *International Journal of Modern Engineering*, *12*(1), 20-28.

[6] Yu, Y., & Ni, L. (2011). Survey of Reliable and Efficient MAC Layer Multicast Protocols in MANETs. *Second International Conference on Mechanic Automation and Control Engineering (MACE).*

[7] Vella, J., & Zammit, S. (2012). A Survey of Multicasting over Wireless Access Networks. *Communica-*

tions Surveys & Tutorials, PP(99), 1-36.
[8] Grossglauser, M. (1997). Optimal Deterministic Timeouts for Reliable Scalable Multicast. *IEEE Journal on Selected Areas of Communications*, *15*(3), 422 -433.
[9] Nonnenmacher, J., & Biersack, E. W. (1999). Scalable Feedback for Large Groups. *IEEE/ACM Transactions on Networking*, *7*(3), 375-386.
[10] Floyd, C., Jacobson, V., Liu, C., McCanne, S., & Zhang, L. (1997). A Reliable Multicast Framework for Light-weight Sessions and Application Level Framing. *IEEE/ACM Transactions on Networking*, *5* (6), 784-803.
[11] Burget, R., Komosny, D., & Ganeshan, K. (2012). Topology Aware Feedback Transmission for Real-time Control Protocol. *Journal of Network and Computer Application, 35*(2), 723-730.
[12] Holbrook, H. W., Singhal, S. K., & Cheriton, D. R. (1995). Log-based Receiver-reliable Multicast for Distributed Interactive Simulation. *Proceedings of the Conference on Applications, Technologies, Architectures, and Protocols for Computer Communication,* (pp. 328-341).
[13] Xiao, Z., & Birman, K. P. (2001). A Randomized Error Recovery Algorithm for Reliable Multicast. *Proceedings of IEEE INFOCOM*.
[14] Paul, S., Sabnani, K. K., Lin, J. C., & Bhattacharyya, S. (1997). Reliable Multicast Transport Protocol (RMTP). *IEEE Journal on Selected Areas of Communications*, *15*(3), 407-421.
[15] DeLucia, D., & Obraczka, K. (1997). Multicast Feedback Suppression Using Representatives. *Proceedings of IEEE INFOCOM*.
[16] Wu, S., & Banerjee, S. (2002). Multicast Feedback Control Using Loss-Pattern Matching. *Proceedings of the IEEE International Conference on Communications*, (pp. 1253-1258).
[17] Wu, S., Banerjee, S., & Hou, X. (2006). Performance Evaluation and Comparison of Multicast Feedback Control Mechanisms. *SIMULATION: Transactions of the Society for Modeling and Simulation International, 82*(5), 345-362.
[18] Mills, D. (1996). Simple Network Time Protocol (SNTP) Version 4 for IPv4, IPv6 and OSI. *RFC2030*.
[19] The Network Simulator - ns-2. Retrieved September 5, 2012, from http://www.isi.edu/nsnam/ns/.
[20] GT-ITM: Georgia Tech Internetwork Topology Models. Retrieved September 20, 2012, from http:// www.cc.gatech.edu/fac/Ellen.Zegura/graphs.html.
[21] Arabmakki, N., Rashad, S., & Krijestorac, S. (2012). A Comparison of Different Vertical Handoff Algorithms between WLAN and Cellular. *International Journal of Research and Innovation*, *4*(1), 5-12.
[22] Zhu, J., & Pecen, R. (2009). A Wireless Mesh Network Based Automatic Utility Data Collection System. *International Journal of Modern Engineering*, *10*(1), 29-34.

Biographies

SHUJU WU is currently an Associate Professor at the Computer Electronics and Graphics Technology Department at Central Connecticut State University. She received her Ph.D. degree in Information Science from the University of Pittsburgh in 2004. Dr. Wu's teaching and research interests include computer communications and networks, multimedia systems, performance modeling and evaluation, and network applications. Dr. Wu may be reached at swu@ccsu.edu.

XIAOBING HOU is currently an Assistant Professor at the Computer Electronics and Graphics Technology Department at Central Connecticut State University. He received his Ph.D. degree in Information Science from the University of Pittsburgh in 2006. Dr. Hou's teaching and research interests are in the areas of computer networking and information security. He is a member of IEEE and ACM. Dr. Hou may be reached at xhou@ccsu.edu.

INSTRUCTIONS FOR AUTHORS: MANUSCRIPT REQUIREMENTS

The INTERNATIONAL JOURNAL OF MODERN ENGINEERING is an online/print publication, designed for Engineering, Engineering Technology, and Industrial Technology professionals. All submissions to this journal, submission of manuscripts, peer-reviews of submitted documents, requested editing changes, notification of acceptance or rejection, and final publication of accepted manuscripts will be handled electronically. The only exception is the submission of separate high-quality image files that are too large to send electronically.

All manuscript submissions must be prepared in Microsoft Word (.doc or .docx) and contain all figures, images and/or pictures embedded where you want them and appropriately captioned. Also, for all accepted manuscripts, each figure, image or picture that was imported into your Word document must be saved individually as a **300dpi or higher JPEG (.jpg)** file and submitted separately; your manuscript and figure numbers must be used in the title of the file (e.g., **M12-S-18 Figure 4**); that means one additional file for each image imported into your manuscript. These 300dpi images do NOT need to be embedded in your manuscript. For tables or graphs created directly in Word, you do not need to submit them as separate files.

Included below is a summary of the formatting instructions. You should, however, review the sample Word document of our website for details on how to correctly format your manuscript. The editorial staff reserves the right to edit and reformat any submitted document in order to meet publication standards of the journal.

The references included in the References section of your manuscript must follow APA-formatting guidelines. In order to help you, the sample Word document also includes numerous examples of how to format a variety of scenarios. Keep in mind that an incorrectly formatted manuscript will be returned to you, a delay that may cause it (if accepted) to be moved to a subsequent issue of the journal.

1. **Word Document Page Setup**: Two columns with ¼" spacing between columns; Top of page = ¾"; Bottom of page = 1" (from the top of the footer to bottom of page); Left margin = ¾"; Right margin = ¾".

2. **Paper Title**: Centered at the top of the first page with a 22-point Times New Roman (Bold), Small-Caps font.

3. **Page Breaks**: Do not use page breaks.

4. **Body Fonts**: Use 10-point Times New Roman (TNR) for body text throughout (1/8" paragraph indention); 9-point TNR for author names/affiliations under the paper title; 16-point TNR for major section titles; 14-point TNR for minor section titles; 9-point TNR BOLD for caption titles for tables and figures; other font sizes as noted in the sample document.

5. **In-text Referencing**: List and number each reference when referring to them in the body of your document (e.g., [1]). The first entry must be [1] followed by [2], [3], etc., continuing in numerical order to the final entry in your References section. Again, see the sample Word document for specifics. Do not use the End-Page Reference utility in Microsoft Word. You must manually place references in the body of the text.

6. **Tables and Figures**: Center all tables and figures. Captions for tables must be above the table, while captions for figures are below; all captions are left-justified.

7. **Page Limit**: Manuscripts should not be more than 15 pages (single-spaced, 2-column format).

8. **Page Numbering**: Do not use page numbers.

9. **Publication Charges:** Manuscripts accepted for publication are subject to mandatory publication charges.

10. **Copyright Agreement:** Review the **copyright transfer agreement**.

11. **Submissions:** All manuscripts and associated files must be submitted electronically; the only exception would be if you wish to submit a CD with the individual files for your high-quality images, as noted above.

    MANUSCRIPTS should be submitted to Dr. Philip D. Weinsier, manuscript editor, at philipw@bgsu.edu along with a copy to editor@ijme.us.

    FILES containing your high-quality images should ONLY be submitted to philipw@bgsu.edu.

THE LEADING INTERNATIONAL JOURNAL OF ENGINEERING TECHNOLOGY

www.tiij.org

www.iajc.org

THE TECHNOLOGY INTERFACE INTERNATIONAL JOURNAL

ABOUT TIIJ:

- TIIJ is an official journal of the International Association of Journal and Conferences (IAJC).
- TIIJ is a high-quality, independent journal steered by a distinguished board of directors and supported by an international review board representing many well-known universities, colleges, and corporations in the U.S. and abroad.
- TIIJ generally publishes research related to applied mathematics, science, and engineering technology.

OTHER IJAC JOURNALS:

- The International Journal of Modern Engineering (IJME)
  For more information visit www.ijme.us
- The International Journal of Engineering Research and Innovation (IJERI)
  For more information visit www.ijeri.org

TIIJ SUBMISSIONS:

- Manuscripts should be sent electronically to the manuscript editor, Dr. Philip Weinsier, at philipw@bgsu.edu.

  For submission guidelines visit www.tiij.org/submission.htm

TO JOIN THE REVIEW BOARD:

- Contact the chair of the International Review Board, Dr. Philip Weinsier, at philipw@bgsu.edu.

  For more information visit www.tiij.org/editorial.htm

INDEXING ORGANIZATIONS:

- TIIJ is now indexed by EBSCO, one of the world's largest and most prestigious indexing organizations. The journal is also under review by Thomson Reuters ISI and DOAJ.

Contact us:

Philip D. Weinsier, Ed.D.

Editor-in-Chief
Bowling Green State University-Firelands
One University Drive
Huron, OH 44839
Office: (419) 372-0628
Email: philipw@bgsu.edu

www.ijme.us

www.ijeri.org

IJME NOW SEEKS SPONSORS

IJME IS THE OFFICAL AND FLAGSHIP JOURNAL OF THE INTERNATIONAL ASSOCATION OF JOURNALS AND CONFERENCE (IAJC)

www.iajc.org

The International Journal of Modern Engineering (IJME) is a highly-selective, peer-reviewed journal covering topics that appeal to a broad readership of various branches of engineering and related technologies. IJME is steered by the IAJC distinguished board of directors and is supported by an international review board consisting of prominent individuals representing many well-known universities, colleges, and corporations in the United States and abroad.

IJME Contact Information

General questions or inquiries about sponsorship of the journal should be directed to:

Mark Rajai, Ph.D.
Editor-in-Chief
Office: (818) 677-2167
Email: editor@ijme.us
Department of Manufacturing Systems Engineering & Management
California State University-Northridge
18111 Nordhoff St.
Northridge, CA 91330